PONTIFICIA UNIVERSIDAD CATOLICA DE CHILE

ESCUELA DE INGENIERIA

DEVELOPMENT OF REINFORCED AND CELL-LADEN VASCULAR GRAFTS STRUCTURALLY INSPIRED BY HUMAN CORONARY ARTERY

TAMARA L. AKENTJEW

Thesis submitted to the Office of Research and Graduate Studies in partial fulfillment of the requirements for the Degree of Master of Science in Engineering

Advisor:

LORETO VALENZUELA

Santiago de Chile, (June, 2017)

PONTIFICIA UNIVERSIDAD CATOLICA DE CHILE
ESCUELA DE INGENIERIA

DEVELOPMENT OF REINFORCED AND CELL-LADEN VASCULAR GRAFTS STRUCTURALLY INSPIRED BY HUMAN CORONARY ARTERY

TAMARA LISSETTE AKENTJEW FAURE

Members of the Committee:

LORETO VALENZUELA

TOMÁS EGAÑA

JUAN PABLO ACEVEDO

JORGE GIRONÁS

Thesis submitted to the Office of Research and Graduate Studies in partial fulfillment of the requirements for the Degree of Master of Science in Engineering

Santiago de Chile, (June, 2017)

To my family.

AKNOWLEDGEMENT

I want to thank all the people who have taught me and supported me in the development of this thesis. I am deeply grateful to my thesis supervisor Loreto Valenzuela, who not only taught me and supported me academically, but was my inspiration to continue my career as a biomedicine engineer. Thank you for welcoming me as your student despite all the problems involved in doing my thesis with a company, for the great patience, understanding and kind guidance. To my tutor Juan Pablo Acevedo, who opened me the doors to tissue engineering. Thanks for trusting fully in my abilities and for allowing me to innovate to finally achieve the results of this thesis, it is a pleasure working with you. To the Bioengineering group; Camila, Matías, Enrique, Claudia, Alessandro, Fabián, Cristián and Pham and to all the Cells for Cells team for teaching me how to work in laboratory, for transmitting me your experience, for your eternal patience, for sharing your equipment with me and for the millions of moments that you gave me and made my stay in the laboratory much more fun. Especially, thanks Matías for helping me with the writing, which substantially improved my thesis. To Valentina, Min, Graciela, Rai and the members of the Loreto Valenzuela's Biopolymer research group for their precious feedback, for helping me to grow as a scientist and for making me always feel welcomed despite I was working in another lab. Additionally, I want to thank Felipe, one of the smartest people I know, who generously helped me with the image processing and modelling of a lot of experiments, for his wise advice and always believing in me.

I want to thank my family, without them this would not have been possible. Thank you Mom and Dad for teaching me to be a strong, persevering woman, to never give up and to follow my dreams trying always to be a good person. To my brothers Nico y Nano and my sister-in-law Gaby for being always supportive, for helping and listening to me when I needed and for loving me unconditionally. To Tita, Tata and Didia, who have always been examples of life and effort, for the values that they have instilled in me and for the infinite love they have always given to me. Finally, my friends, especially Wally and Jesu, thank you for encouraging me in every step of my life, for your kind support and for being the best friends in the world. I love you all.

TABLE OF CONTENTS

LIST OF TABLES

LIST OF FIGURES

NOMENCLATURE

BM-MSC: Bone marrow mesenchymal stem cells

CNC: Computer numerical control

DMEM: Dulbecco's modified eagle's medium

EC: Endothelial cells

ECM: Extracellular matrix

FBS: Fetal bovine serum

GEAL: Bovine gelatin methacrylamide and sodium alginate

GelBMa: Bovine gelatin methacrylamide

GelMa: Gelatin methacrylamide

HF-SMC: Hair follicle smooth muscle cells

HUVEC: Human umbilical vein endothelial cells

ITA: Internal thoracic artery

LAD: Left anterior descending artery

LDL: Low density lipoprotein

PBS: Phosphate buffered saline

PCL: Poly-ε-caprolactone

PEG: Polyethylene glycol

PEUU: Poly(ester urethane) urea

PFTE: Polytetrafluoroethylene

PGA: Polyglycolide

PGS: Poly(glycerol sebacate)

PI: Photoinitiator

PLLA: Poly-L-lactide

PU: Polyurethane

RC: Right coronary

SBS: Solution blow spinning

SIS: Small intestine submucosa

SMC: Smooth muscle cells

SPEU: Poly(ester urethane)

TEVG: Tissue engineering vascular graft

TPP: Triphenyl phosphate

UC-MSC: Umbilical cord mesenchymal stem cells

UV: Ultraviolet

VEGF: Vascular endothelial growth factor

RESUMEN

Las enfermedades cardiovasculares son la primera causa de muerte en el mundo, en dónde la que predomina es la enfermedad de la arteria coronaria. Aunque los injertos autólogos permanecen como la mejor alternativa para la revascularización coronaria, su aplicación es limitada por problemas vasculares pre-existentes, operaciones previas y vasos sanguíneos de baja calidad, entre otros. Uno de los desafíos es desarrollar un injerto vascular capaz de mostrar un buen desempeño biológico, mecánico y una larga duración luego de ser implantado. Para esto es necesario entender profundamente la estructura, componentes, propiedades biológicas y mecánicas de las arterias. Actualmente, no existe ningún injerto vascular que sea capaz de cumplir con todos los requerimientos, en especial compliancia y no-trombogenicidad. Inspirados en la estructura de la arteria coronaria, un nuevo método de fabricación fue desarrollado para fabricar injertos vasculares con estos requerimientos. Estos injertos son estructuras tubulares multicapas y celularizadas fueron fabricadas utilizando una combinación de las técnicas de *dipping-spinning* y *solution blow spinning* controlados por un robot. Por un lado, para reforzar mecánicamente los injertos vasculares se distribuyeron fibras de policaprolactona imitando las fibras de colágeno en las arterias coronarias. Por otro lado, se encapsularon células en capas de hidrogel de gelatina-alginato intercaladas con las capas de fibras para potenciar su función biológica. Los injertos vasculares fabricados en este trabajo muestran un comportamiento mecánico dentro de los rangos de las arterias coronarias y tienen compliancia estadísticamente similar a las arterias coronarias a la presión fisiológica. Finalmente, se incorporaron células las cuales fueron distribuidas homogéneamente en todo injerto vascular, mostrando proliferación en cultivo *in vitro*. Estos resultados demuestran que se pueden producir injertos vasculares con propiedades biológicas y mecánicas similares a las arterias coronarias con este método de fabricación automatizable inspirado en la estructura de estas arterias.

Palabras claves: injertos vasculares, dipping-spinning, solution blow spinning, propiedades mecánicas, arteria coronaria, vasos sanguíneos de bajo calibre

ABSTRACT

Cardiovascular diseases are the world leading cause of death, with coronary artery disease as the predominant one. Although autologous vessels remain as the best coronary revascularization alternative, its application is limited by pre-existing vascular problems, previous operations, and low quality of vessels, among others. One challenge is to develop vascular grafts capable of showing good biological and mechanical performance and long patency once implanted. For this, it is necessary to deeply understand artery structure, components, and biological and mechanical properties. None of the currently existing vascular grafts has been able to fulfill all the requirements, especially compliance and non-thrombogenicity. Inspired by the human coronary artery structure, a new manufacturing method was developed to fabricate vascular grafts with these requirements. A combination of dipping-spinning and solution blow spinning techniques, controlled by a robot device was used to manufacture cellularized multilayer tubular structures. To mechanically reinforce the vascular grafts polycaprolactone fibers were distributed resembling collagen fibers in coronary arteries. Gelatin-alginate hydrogel layers with cell encapsulated were intercalated with fiber layers to enhance the biological function. Furthermore, middle and outer layer compositions, wavy and oriented distribution of fibers were separately optimized mimicking media and adventitia layers respectively to achieve similar mechanical properties. Composition was successfully optimized to have a stress-strain curve close to the media and adventitia curves. Vascular grafts fabricated in this work showed mechanical behavior within the coronary arteries's ranges and statistically similar compliance to coronary arteries at physiological pressure. Finally, cells were incorporated and distributed homogeneously throughout the vascular graft, showing proliferation at *in vitro* culture. These results demonstrate that vascular grafts with similar biological and mechanical properties to coronary arteries can be produced by automatable manufacturing method inspired in the artery structure.

Key words: Vascular graft, dipping-spinning, solution blow spinning, mechanical properties, coronary artery, small diameter blood vessel

1. INTRODUCTION

1.1 Cardiovascular diseases

Cardiovascular diseases are a group of problems that affect the circulatory system, i.e, the heart, vascular of the brain, and other blood vessels. Most of these problems are caused by the atherosclerosis, a complex disease caused by a plaque build-up on the inner walls of arteries over many years. This plaque is generated by the deposition of fat, cholesterol, calcium and other substances found in the blood. This deposition produces an irregular lumen surface, hardening and narrowing of the arteries causing a limited flow of blood rich in nutrients and oxygen to the organs and tissues in the body. Moreover, this plaque can rupture and trigger the formation of a blood clot that can end up in heart attack or stroke. Cardiovascular diseases caused by atherosclerosis are: ischemic heart disease or coronary artery disease; cerebrovascular disease; and diseases of the aorta, and other arteries including hypertension and peripheral vascular diseases. Other cardiovascular diseases comprise: congenital heart diseases, rheumatic heart diseases, cardiomyopathies, and cardiac arrhythmias.

The key risk factors that promote atherosclerosis and therefore, cardiovascular diseases, are the behavioral, metabolic and other factors (Li, 2015). On the one hand, tobacco use, physical inactivity, unhealthy diet and harmful use of alcohol are the prevalent behavioral factors. On the other hand, raised blood pressure (hypertension), raised blood sugar (diabetes), raised blood lipid (cholesterol) and overweight and obesity are the metabolic factors. Finally, the other factors correspond to genetic disposition, poverty and low educational status, advancing age, gender and physiological factors.

Cardiovascular diseases were the cause of death of 17.7 million people in the 2015, accounting for 31% of global death and ranking as the leading cause of death all over the world (WHO, 2017a). Low and middle-income countries represent more than three quarters of the global deaths corresponding to this disease, showing a strong socioeconomic factor (WHO, 2017a). The current and

future aging of the world population will result in a significant increase global cardiovascular deaths (Mathers et al. 2006) and will reach 24.2 million in 2030 (WHO, 2017b).

In the Americas the mortality rate of cardiovascular diseases was 37% in 2013 (PAHO, 2014a), being the first cause of death and disability in both men and women. The premature mortality probability, between 30 and 60 years old, is of 6.5% in America, being higher for men than for women (PAHO, 2014b). Guyana (55, 27%), Venezuela (44.21%), Trinidad and Tobago (41.33%), and Brazil (40.63%) and Paraguay (37.67%) are the countries with the highest number of deaths because of cardiovascular diseases (PAHO/WHO, 2016; de Souza et al., 2012).

As well as the rest of the world, cardiovascular diseases are the main cause of death in Chile. The mortality rate was of 27.53% in 2012 (MINSAL, 2014), even though, Chile is one of the Latin Americas countries with the lowest death rates (de Souza et al., 2012). High incidence of behavioral risk factors are observed, such as: a 27.1% of people are multidimensional sedentary and 88.6% have free-time sedentary activities, one of the highest obesity rates corresponding to a 25.1% of the population, and a tobacco consumption of 42% of the population (Lanas et al., 2013). All of these factors have a negative influence on cardiovascular diseases.

There is a growing interest in addressing the cardiovascular disease problem because it is not only a health issue, but also, a major economic burden (World Heart Federation, 2017). In 2010, the total cost of cardiovascular diseases corresponds to US$863 billion, which include the cost of care, their proximate risk factors and the lost in productivity owing to either premature death or significantly disabling disease (Bloom et al., 2011). Furthermore, it is projected that cardiovascular disease costs could rise by 22% with an estimated of US$1,044 billion by 2030 (Bloom et al., 2011). In particular, the total cost in Chile is US$1.4

billion each year, which correspond to a 4.2% of total health spending (World Heart Federation, 2016).

Coronary artery disease, also called ischemic heart disease is the most common cardiovascular disease. It consists in the hardening and narrowing of arteries that supply blood to the heart. Coronary narrowing restricts the flow of blood rich in oxygen and nutrients to the heart, and could lead into heart tissue starvation. Also, the plaque could rupture, which can occlude the total flow of blood, triggering a heart attack or sudden cardiac death. An estimated of 7.6 million of people die each year due this disease in the world, corresponding to a 13% of the total deaths (WHO, 2017a). The world total cost due to coronary artery disease was US$24,167 on 2010 and it is expected to rise up to US$32,339 by 2030 (Bloom et al., 2011).

Coronary artery disease is also the predominant form of cardiovascular diseases in the Americas, with a mortality rate of 35% in 2012 (PAHO/WHO, 2016; de Souza et al., 2012). Moreover, in Chile, the mortality rate due to coronary artery disease was 33% in 2012 (PAHO/WHO, 2016). The risk factors associated with coronary artery disease are mainly smoking, high levels of certain fats and cholesterol in the blood, high blood pressure, and high levels of sugar in the blood due to insulin resistance or diabetes. High rates of obesity, sedentary lifestyle, and tobacco and alcohol consumption in Chile promotes high risk factors for coronary artery disease in the Chilean population.

In order to understand the diseases and possible solutions of the coronary arteries, in the next section of this work the structure and function of the arteries will be studied.

1.2 Artery Structure

Artery structure can be studied in a macroscopic view and in a microscopic view. In one hand, arteries are a multilayered structure and each layer has a different

function. In the other hand, the artery wall is composed of two elastic fibers and cells that characterize the mechanical and biological properties.

1.2.1 Macrosructure

Structurally, blood vessels are tubes of the circulatory system that are in charge of directing the blood to the organs and tissues of the body. The blood vessels are divided into arteries, capillaries and veins. First, the arteries are responsible for transporting blood rich in oxygen and nutrients from the heart to the organs and tissues of the body. Then, the capillaries enable the exchange of water and chemicals between the blood and tissues. Finally, the veins carry blood from the capillaries back to the heart. In general, each vessel consists in three concentric layers: intima, media and adventitia (Figure 1-1). Composition of each vessel depends on its function, for example, the adventitia is the thickest layer for veins, while in arteries the media layer is the thickest one (Henrikson & Mazurkiewics, 1997). In the case of arteries, they correspond to the high-pressure portion of the circulatory system. Arteries have to resist and adjust to the varying peaks of pressures between the heart contraction (systolic pressure) and heart expansion and refill (diastolic pressure). The pulse pressure is a result of the increase in arterial pressure during systole and diastole. Structure plays a fundamental role in the biological and mechanical function of arteries. Each artery layer has a different composition and function (Wagenseil & Mecham, 2009).

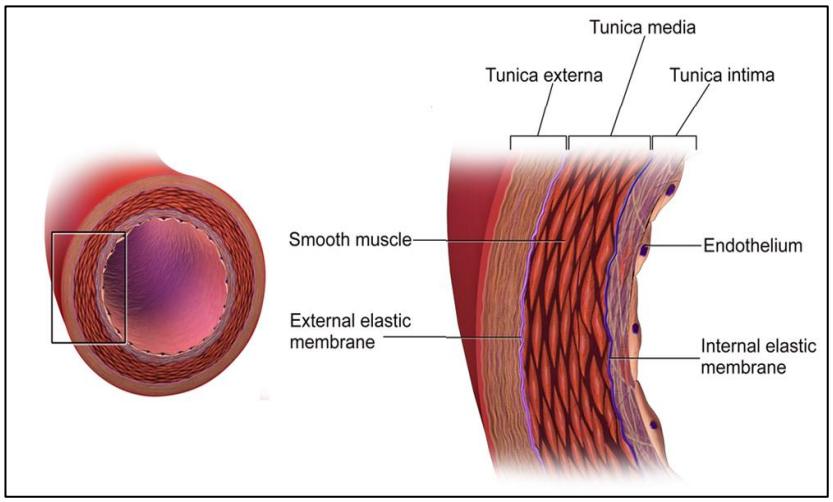

Figure 1-1: Layered structure of arteries. (Blausen.com staff, 2014)

a) Intima

The tunica intima or intima layer is the innermost lining of arteries. It is composed by a monolayer of endothelial cells (ECs) oriented towards the vessel lumen and in direct contact with the blood. In this way, the intima layer provides a blood-compatible and luminal interface to the artery.

The endothelial monolayer has important functions beyond simply providing a lumen lining to arteries. Firstly, endothelial cells prevent thrombosis and thrombolysis by different anticoagulant and antiplatelet mechanisms; therefor it plays a crucial role in providing the proper haemostatic balance (Rajendran et al., 2013). This layer has a central role in the regulation of coagulation by regulating the expression of binding sites for anti-coagulant and pro-coagulant factors on the cell surface (Rajendran et al., 2013). Secondly, endothelial cells can sense the shear stress over their surface due to blood flow and signal this information to the surrounding cells. In this way, the blood vessel can adapt its wall thickness and diameter to suit the blood flow (Alberts, 2002). Thirdly, when the vascular wall is damaged, a rapid recruitment of platelets and leukocytes at the injured sites is mediated by the release of components previously elaborated by the endothelium (Rajendran et al., 2013). Fourthly, this layer can regulate the vascular tone and

growth by releasing contraction inducing factors and a source of inhibitors and promoters (Rajendran et al., 2013). Finally, the endothelial cells promote the cell proliferation and angiogenesis by secreting vascular endothelial growth factor (VEGF) and other growth factors related with vessel maturation (Rajendran et al., 2013). Endothelial dysfunction could lead to hypertension, coronary artery disease, and chronic heart failure, among others (Rajendran et al., 2013).

b) Media

Tunica media is the middle layer of arteries. It is composed of layer of smooth muscle cells (SMCs), elastic connective tissue and collagen, which together provide mechanical structure, resistance and at the same time, serve as a vasomotor tone for muscular arteries such as coronary ones. Elastin layers divide the media into concentric layers of smooth muscle cells reinforced with elastin and collagen fibers.

This artery layer has a substantial biological role in limiting neointimal growth (Hare and Chaparro, 2008). The neointimal grows only when the lamina that lies between the intima and media, an elastic lamina, is fractured and the media is damaged (Schwartz, 1994). On the other hand, the media plays a critical role in regulating the blood pressure and proper circulation by causing changes in the luminal diameter depending on the body needs at any given moment. Smooth muscle cells are capable of causing vasoconstriction or vasodilation with the regulation of the autonomic nervous system and chemicals.

c) Adventitia

Tunica externa or adventitia is the outer layer of arteries. Fibroblast, perivascular nerves and collagen rich connective tissue are the main components of this layer. However, this layer also contains blood and lymphatic vessels and progenitor and immune cells, making the adventitia the most heterogeneous and complex layer (Stenmark, et al. 2013). Dense and wavy collagen fibers generate an interwoven

network with elastin fibers and fibroblast that protect and reinforce the vessel (Chen et al., 2011).

The adventitia has three main functions: blood irrigation, mechanics and physiologic control (Fischer, 2008). The arteries are also composed of tissue that requires constant irrigation of oxygen and nutrients, which is given by small vessels arranged in the adventitia layer, called *vasa vasorum*. Like the arteries, the *vasa vasorum* has a sensible control system to contract and relax according to the moment needs (Fischer, 2008). Artery nutrition is important to prevent development of atherosclerosis (Fischer, 2008).

1.2.2 Microstructure

In a microstructure point of view, the artery layers are mainly composed by elastin and collagen fibers (50 to 75% of the total dry defatted weight of arteries), and cells (Fischer and Llaurado, 1966).

a) Elastin

Elastin is an elastic protein of the connective tissue or extracellular matrix. It is found in highly elastic tissues distributed in the form of fibers or concentric layers, and also is found in extensible tissues in smaller quantity and thinner fibrils. Some of the tissues containing elastin are: skin, lungs, bladder, elastic cartilages and ligaments. Additionally, it is the main component of extracellular matrix of arteries (Li et al., 1998).

The elastic fiber found in this type of tissue consists of an amorphous component and a fibrillary component. The amorphous component comprises crosslinked elastin. In contrast, the fibrillar component is mainly microfibrils. Both are characterized by high content of amino acids such as glycine, valine, alanine, and proline.

The distribution of elastic fiber in dynamically elastic tissues implies a central biomechanical role (Kielty et al., 2002). Elastin is known to enable the tissue to return to its natural size after being stretched or contracted. Furthermore, elastin

plays a fundamental function in arteries, especially in large elastic arteries such as the aorta. Elastin is responsible for the vascular wall response at low or medium pressures, since they activate at low stress and deformation (Figure 1-2). It is for this reason that elastin serves as a medium for the propagation of the wave that helps the blood flow. Studies have determined that elastin also has a regulatory function during the artery development, controlling proliferation of smooth muscle and stabilizing arterial structure (Li et al., 1998).

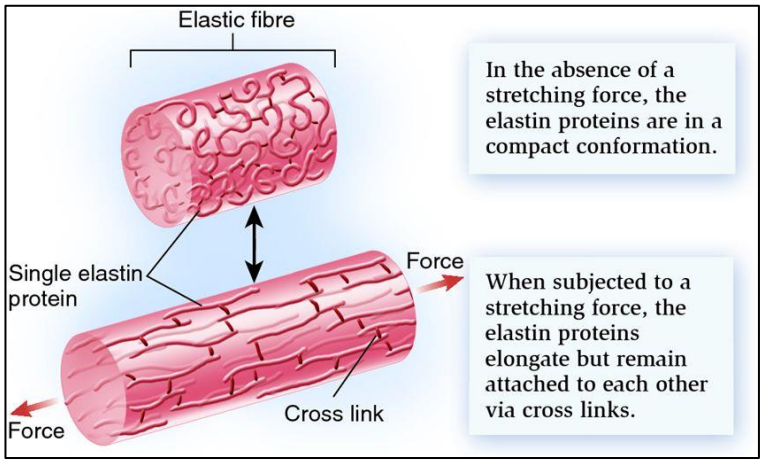

Figure 1-2: Elastic fibers in arteries (Elastic fibers are made of elastin, 2012)

b) Collagen

Collagen is the most abundant fibrous protein in mammals (Shoulders & Raines, 2009). It is a molecule composed of three polypeptide chains characterized by containing one or more regions where one glycine is repeated each three amino acids (Shoulders & Raines, 2009; Lodish et al., 2000). These chains are in a triple helix form, which is stabilized by hydrogen bonds between the chains (Shoulders & Raines, 2009. The collagen helixes are grouped together to form collagen fibers (Figure 1-3).

Currently, 28 different types of collagen are known in humans. These are grouped into collagen subfamilies. Fibrillar collagen is the most interesting in terms of biomechanics. Type I collagen is widely found in skin, tendons, bones, cornea, lungs and vasculature, often in association with collagen IV. Type II is essentially

limited to cartilage and can be found in association with collagen IV. Finally, type III is found in relatively elastic tissues such as embryonic skin, lung and blood vessels.

Collagen has structural and mechanical functions in almost all tissues. Collagen fibers have much more strength and resistance than elastin. The rigidity of rich collagen-tissues is not only because the characteristics of collagen molecule, but fundamentally by the alignment of its microfibers (Claes, 2010). If the distribution of the orientation of collagen fibers is anisotropic, the tissue will also exhibit anisotropic functional properties. Therefore, the alignment between the fiber orientation and the stress direction is critical (Ottani et al., 2001). The collagen reinforces and strengthens the arteries. It is responsible for the vascular response at pressures higher than the physiological, since the fibers first aligned and oriented during the deformation process and then they apply resistance.

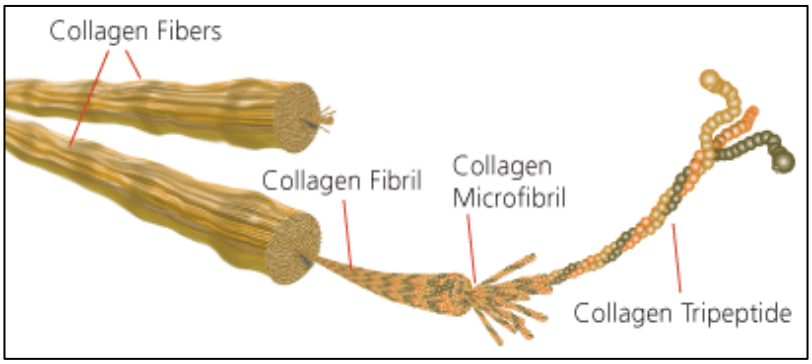

Figure 1-3: Collagen fibers structure (Collagen, n.d.)

1.2.3 Coronary Circulation

Coronary circulation is the supply of blood rich in nutrients and oxygen through blood vessels to the heart muscle (Figure 1-4). Two arteries originate at the beginning of the aorta called: right coronary artery and left coronary artery. The right coronary artery distributes blood to the right atrium, portions of both ventricles and the heart conduction system. To supply the posterior portion of the interventricular septum and portions of both ventricles the right coronary artery

gives rise to the posterior descending artery. The left coronary artery distributes blood to the interventricular septum and left atrium and ventricle. Another branch arises from the left coronary artery and is called left anterior descending artery (LAD), which give rise to numerous small branches. The coronary arteries represent the only source of blood supply to the myocardium and are classified as "end circulation"; these reasons are why the blockage of these vessels is so critical.

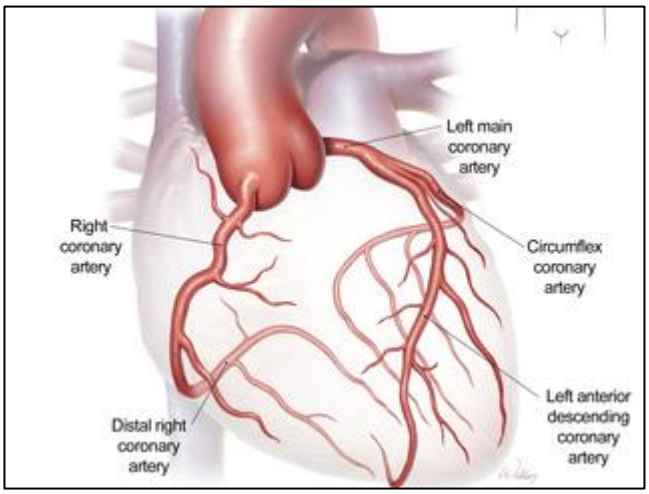

Figure 1-4: Coronary arteries in the heart. (Weldon, n.d.)

1.3 Artery diseases

Three pathologies, directly related with each other, are the main coronary diseases: arteriosclerosis, atherosclerosis and thrombosis. Figure 1-5 illustrates the three pathologies.

1.3.1 Arteriosclerosis

Arteriosclerosis is when the blood vessels that carry oxygen and nutrients to the organs and tissues, in this case, coronary arteries, become thicker and stiffer, restricting the blood flow. This can lead to hardening and narrowing of arteries.

1.3.2 Atherosclerosis

Atherosclerosis is a specific type of arteriosclerosis due to chronic inflammatory process that occurs when the endothelium of arteries is exposed to high levels of

low-density lipoprotein (LDL) cholesterol and other substances that trigger the permeabilization of the endothelium to lymphocytes and monocytes. With a series of reactions, the LDL cholesterol is attracted into deep layers of the vessel wall and smooth muscle cells migrate from the media layer in combination with the inflammation process. Later a fibrous cap consisting of smooth muscle and collagen is formed generating lesions called atheromatous plaques. These irregularities in the lumen allow cells and lipids to accumulate and form a plaque in the inner wall. An advanced atherosclerosis leads to an abnormal narrowing of arteries, limiting the blood flow into the heart tissues, known as stenosis. Even more, the advance in the inflammatory process provoke a thinning and fissuring of the endothelial surface of the plaque which can rupture and result in the formation of a thrombus.

1.3.3 Thrombosis

Thrombosis is the occlusion of a blood vessel due to formation of a blood clot or thrombus inside a vessel, in this case the coronary artery. On one hand, when the endothelium is injured, a blood clot is form from platelets and fibrin to prevent blood loss. On the other hand, a thrombus can be produced by a plaque that breaks free and travels through the vessel. If a thrombus is large enough to reduce significantly or even block the blood flow to the heart, this result in an angina or a heart attack.

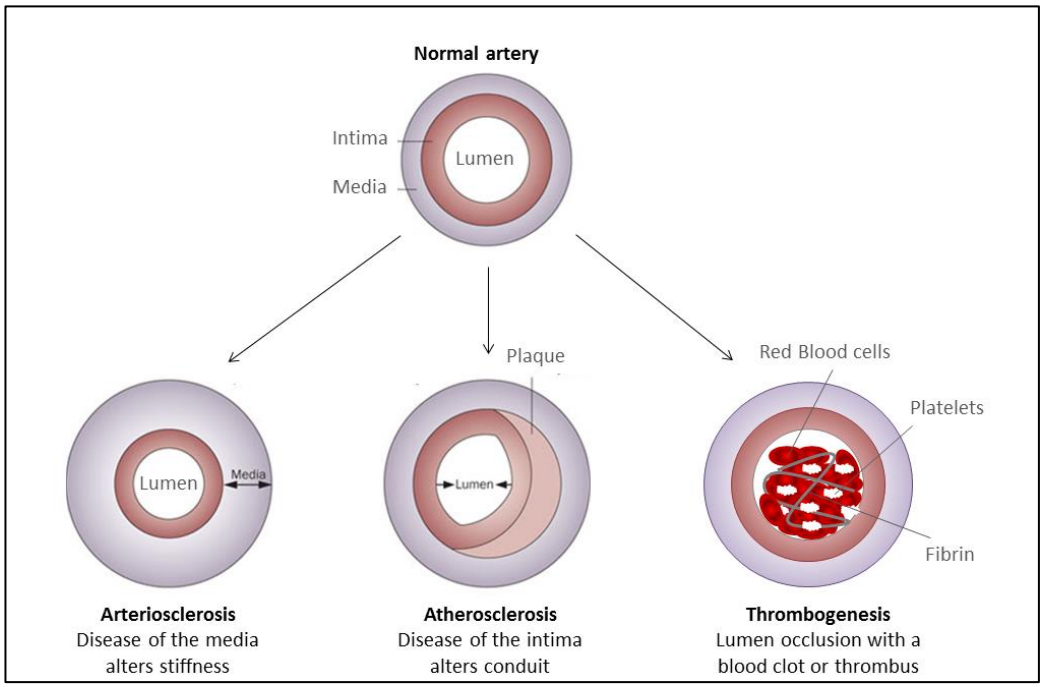

Figure 1-5: Pathologies related to coronary artery disease. Adapted from (Safar et al., 2010)

Although coronary artery disease cannot be completely cured, when not too severe, it can be managed with a combination of lifestyle changes and drugs to manage the symptoms and reduce the risk of heart attack. Lifestyle changes include quit smoking, eating healthy food, exercising regularly, losing excess weight, and reducing stress. On the other hand, various drugs such as aspirin, cholesterol modifying drugs, beta-blockers, and nitroglycerin can be used in the treatment of coronary artery disease.

1.3 Current Coronary Revascularization Procedures

Sometimes the coronary artery is too narrowed or a thrombus completely blocks the blood flow to a part of the heart, causing damage to the heart muscle. This is called heart attack and the symptom to identify it is chest pain or angina that can expand to the shoulder, arm or neck. In this situation, more aggressive treatment is needed. Invasive surgical procedures have been done to restore the arterial blood flow such as angioplasty and stent placement, atherectomy or bypass surgery.

1.3.1 Percutaneous coronary interventions

Angioplasty is a surgical procedure that aims to open or widen the narrowed section of coronary arteries. For this purpose, a thin and soft tube (catheter) is inserted by the groin or wrist. The catheter is guided through the blood vessels to the site of occlusion or narrowing. Once in site, a guide wire pass through the obstruction, and non-surgical treatments using balloon, stenting or atherectomy are used to open narrowed arteries and restore blood flow to the heart.

a) Balloon angioplasty

Balloon angioplasty is when a balloon is tipped in the catheter and passed over the guide wire into the narrowed section. Then, the balloon is inflated to flatten the plaque against the wall of the artery. Finally, the guide wire, balloon and catheter are withdrawn (Figure 1-6a). Balloon angioplasty has a primary success rate of 90% in patients with angina and no previous myocardial infraction and of 64% in patients with a previous myocardial infraction (Perry et al., 1998).

b) Stent

Most of the times, after balloon angioplasty, a stent is implanted. Stents are metal devices in shape of a small mesh tube that are inserted with the help of a catheter. Once is placed in the narrowed artery, the balloon expands and adapts the stent to the walls of the artery (Figure 1-6b). In this way, the stent remains in the artery permanently, holding it open and preventing it from closing again. Different types of stents have been developed such as bare-metal stents, drug-eluting stents, bioabsorbable stent and dual-therapy stent (combine the drug-eluting and bioabsorbable) (Garg & Serruys, 2010; Foerst et al., 2013).

c) Atherectomy

When severe calcifications are found and only a wire can cross the site of stenosis, but not a balloon, an atherectomy procedure is performed. It consists on a guide wire, similar to the angioplasty except that the catheter has a cutting device or a drill that removes the plaque and reduces calcified deposits to tiny fragments of

debris, which can easily pass through the blood vessels and be absorbed by the body (Figure 1.6c). (Hinohara et al., 1991; Wasiak et al., 2012) This procedure can be combined with the implantation of a stent (Adamian et al., 2001; Hoffmann et al., 1998,; Bramucci et al., 1998).

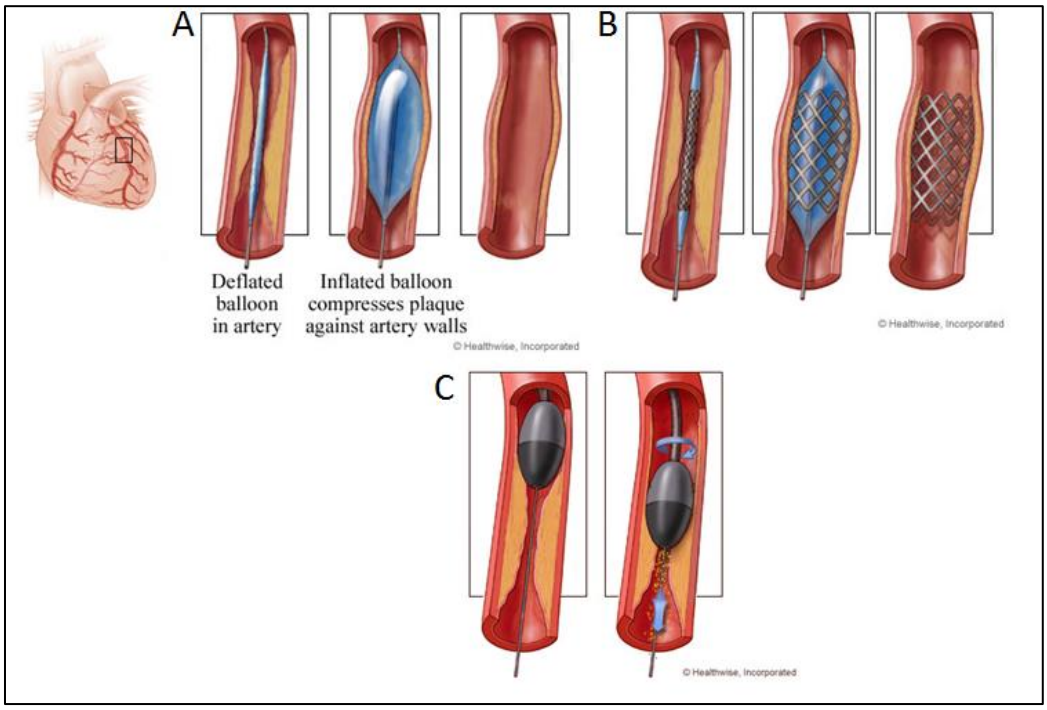

Figure 1-6: Percutaneous coronary interventions.. (A) Balloon angioplasty (Healthwise Staff, 2015a). (B) Stent implantation angioplasty (Healthwise Staff, 2015b). (C) Rotational atherectomy (Holroyd Heart Centre, 2016).

In many cases, usually within 6 months done the percutaneous coronary intervention (Grech, 2003), a gradual stenosis can be developed in the same site and therefore the artery renarrows. This phenomenon is called restenosis and it is the main lack of long-term clinical success of angioplasty and stent procedures. Post-angioplasty restenosis and in-stent restenosis is diagnosed when the luminal diameter decreases by more than a 50% with respect to the diameter after the procedure (Hamid and Coltart et al., 2007). A high incidence of restenosis is associated with balloon angioplasty ranging from 25 to 50% (Hamid and Coltart et al., 2007). On the other hand, stents have in average a 10% lower incidence of

restenosis than balloon angioplasty (Mitra and Agrawa, 2006). Furthermore, a 15.4% (Holmes et al., 2004) to 25.7% (Mohan and Dhall, 2010) of reduction in restenosis rate have been shown with the incorporation of drug-eluting stents.

1.3.2 Coronary artery bypass surgery

The coronary artery bypass surgery is a surgical heart procedure that aims to replace the narrowed or occlude artery with another vessel. For this, during surgery a healthy vessel from another part of the body is taken and surgically connected the blocked coronary artery above and below the occlusion site (Figure 1-7). In this way, oxygen and nutrient-rich blood flow is restored by creating a new path to the heart muscle. Saphenous vein and left internal mammary artery are the most common grafts used for coronary bypass. There are two usual surgeries. The first one is attaching a great saphenous vein between the major branch of the aorta and the obstructed artery immediately after the obstruction. The second one is diverting the left internal mammary artery to the left anterior descending branch of the main left coronary artery (Figure 1-7b).

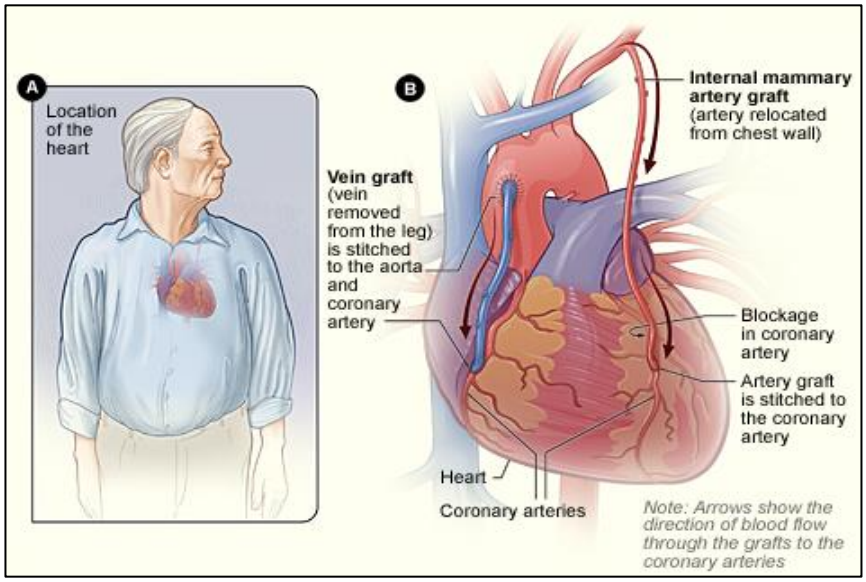

Figure 1-7: Coronary Artery Bypass Surgery. (A) Location of the heart. (B) How vein saphenous vein and internal mammary artery bypass grafts are attached to the heart. (National Heart, Lung, and Blood Instutute, 2012)

In the United States, percutaneous coronary interventions are more common than coronary artery bypass. Stents have become the leading solution at the moment with the drug-eluting stents being widely preferred (Figure 1-8)

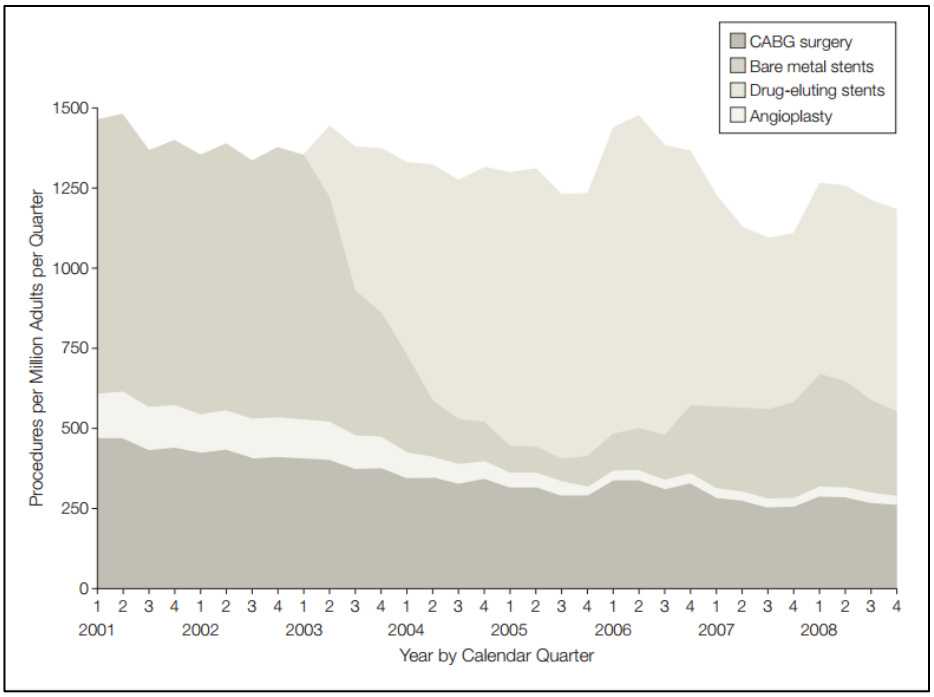

Figure 1-8: Revascularization procedure rates for coronary artery bypass grafts surgery (CABG surgery), bare metal stents, drug-eluting stents and angioplasty per million adults per quarter between 2001 and 2008 in the United States. (Epstein et al., 2011)

The procedure of choice depends on the situation of each patient. The major advantages of percutaneous coronary interventions are the relative ease of use and avoiding general anesthesia, thoracotomy, extracorporeal circulation, complications of the central nervous system, and prolonged convalescence. But it develops early restenosis and has the inability to solve many occluded arteries or extensive atherosclerotic disease (Smith et al., 2001). Coronary bypass surgery has the advantage of exceeding the 90% of graft patency rate in 10 years, which demonstrates its greater durability and allows more complete revascularization (Smith et al., 2001). For these reasons, the coronary bypass surgery is more

compelling when severe situations are presented, such as a big extension of coronary atherosclerosis or multivessel coronary artery disease (Smith et al., 2001).

1.5 Mechanical properties of coronary arteries

To understand the mechanical properties of arteries it is fundamental to know which are the mechanical solicitations in the body that make arteries behave in that way.

Arteries in their natural state within the body are subjected to constant and varying charges or solicitations that produce their special mechanical properties. First, blood flows through arteries at a rate that range from 18 to 161 mL/min (Hundley et al., 1996). This blood flow generates an internal pressure – the physiological pressure – which ranges from 80 to 120 mmHg and reaches its maximum value at the left ventricle exit. Finally, because they are attached to other organs or tissues, the arteries are in constant axial strain. In the case of coronary arteries, values of *in vivo* axial strain are between 5% (Holzapfel et al., 2005) and 10% (van Andel et al., 2003).

Mechanical properties of arteries depend on both active (smooth muscle cells) and passive (elastin and collagen fibers) components (Montini-Ballarin et al., 2016). As explained above, smooth muscle cells enable the vasoconstriction and vasodilation of arteries depending on body blood circulation needs. However, elastin and collagen fibers clearly define the cyclic mechanical behavior and play a major role in the mechanical properties of arteries. The mechanical response of arterial tissue is defined as anisotropic, hyperelastic and nonlinear.

The arteries are composed of fibrous tissue, which from a mechanical point of view is very special. In the vascular wall, elastic and collagen fibers are mostly oriented and aligned. This type of tissue is much stronger in the direction of the fiber than perpendicular to it. This result in an anisotropic behavior, i.e., its mechanical response varies depending on the direction in which it is examined.

The differences in the mechanical properties and distribution of both fibrillar components allow the arteries to have a hyperelastic and non-linear behavior. This type of behavior is characterized by a J-shaped curve when subjected to stress (Figure 1-9). As mentioned above, at low or physiological pressures the response is provided by elastin fibers in each layer. When the pressure increases beyond the resistance of the stretching elastin, then the collagen fibers start to align and orient, which result in a higher stiffness and the last linear section of the J-shape curve (Claes et al., 2010; Roach & Burton, 1957).

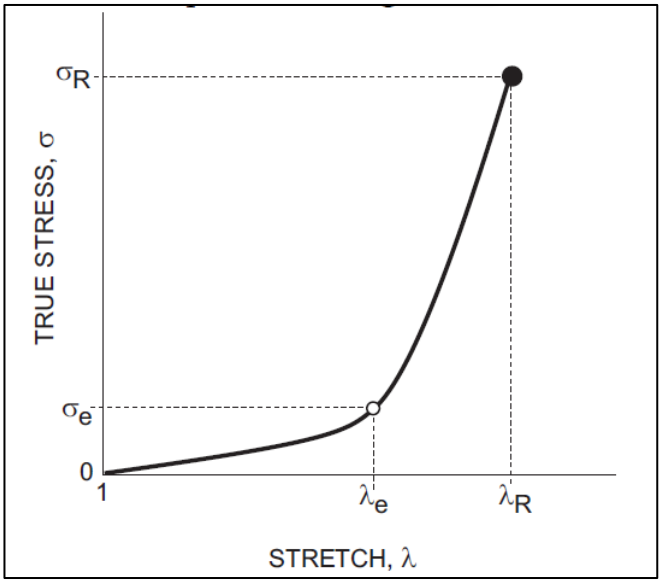

Figure 1-9: J-shaped stress-stretch curve of a coronary artery and mechanical parameters. The stress and stretch at the breaking point are σ_R and λ_R respectively. The stress and stretch at the transition point or "elbow" between the compliant (elastin fibers) and stiff (collagen) regions are are σ_e and λ_e respectively. (Claes et al, 2010)

The stiffer and late response of collagen fibers when subjected to stresses is explained by the arrangement of these fibers in the vascular wall. These fibers are composed of more resistant material than elastin ones and are aligned in a specific direction for each layer, which results in a stiffer behavior. On the other hand, collagen fibers are found in a wavy form in arteries (Figure 1-10) (Chen et al.,

2011). In this undulated state, under low pressure, fibers deforms only until completely stretched or extended. Then, by increasing the pressure and once in an extended state it can sustain significantly higher stresses. In this way, the fibers stretch gradually and their resistance to tension increases as the artery is deformed.

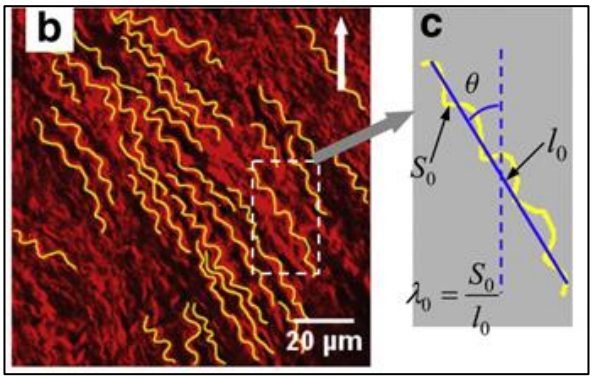

Figure 1-10: Wavy, aligned and oriented collagen fibers from an adventitia layer. (Chen et al., 2011)

In addition, the collagen and fibers are disposed in the form of intercalated layers of different fiber orientations (Figure 1-11). In this way, the fibers are distributed homogeneously throughout the entire artery wall.

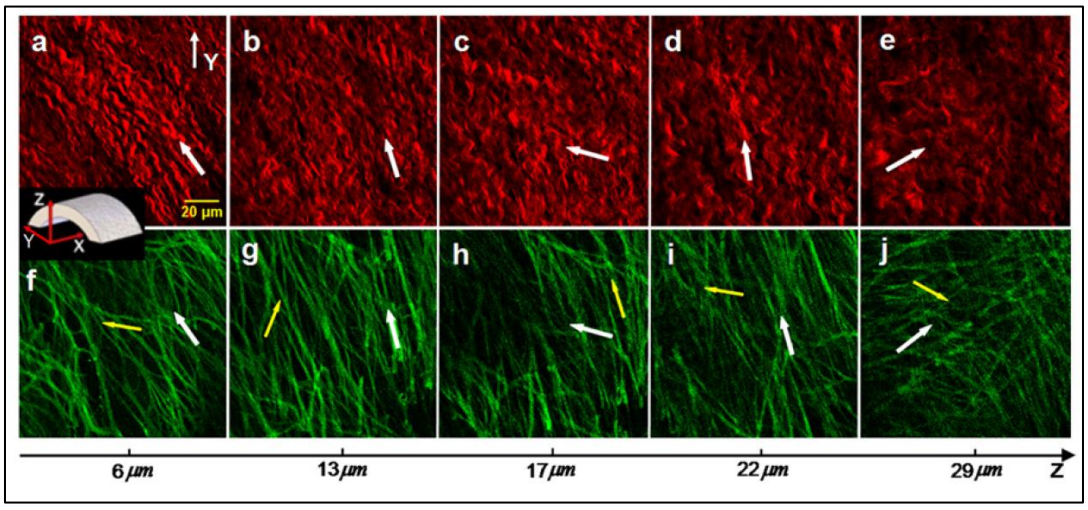

Figure 1-11: Fibers orientation and layered structures. Images *a-e* are five collagen layers at different depth Z. Images *f-j* are five elastin layers at the exactly same

depths. White arrow is the main orientation of fibers in each layer (Chen et al., 2011).

J-shaped mechanical response, strength and compliance are some of the important attributes that arteries have. This type of mechanical properties can be obtained by different mechanical tests. The most common way of characterizing the type of response of materials as tissues is performing a tensile test, while to obtain the compliance of arteries, a pressurization test is used.

1.5.1 Stress-Strain response of coronary arteries

To improve understanding of the mechanisms that involve the procedures used to treat the coronary artery disease is fundamental to first understand the behavior of coronary arteries. Studies have performed uniaxial test to human coronary arteries and each of their layers. Also a constitutive model has been created to describe the mechanical response of the artery tissue.

A comparison between human and porcine coronary arteries was done by van Andel and collaborators. The samples (ages between 61 to 85 years) were tested in axial and circumferential direction with an axial prestretch of 10% for human and 30% for porcine (Figure 1-12) (van Andel et al., 2003).

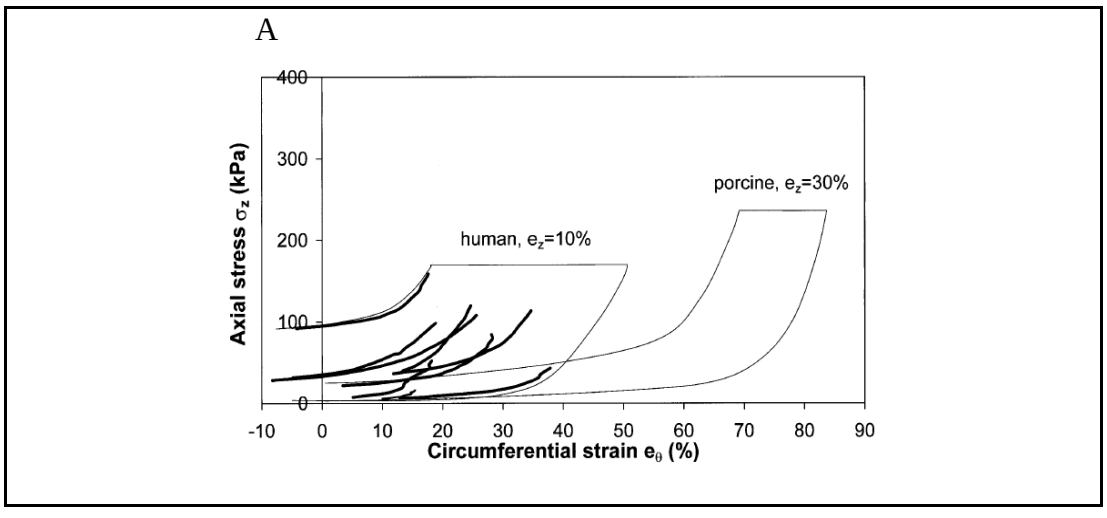

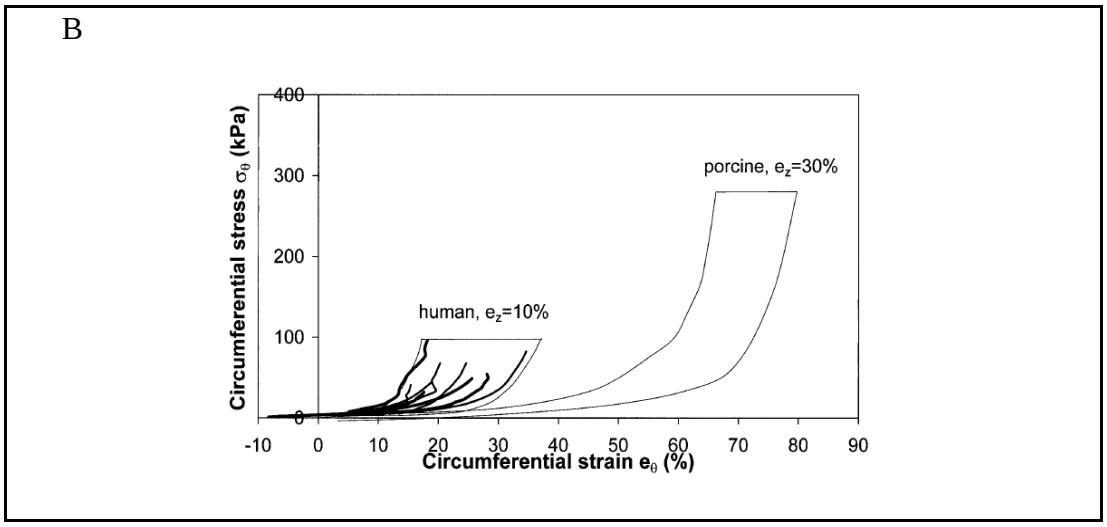

Figure 1-12: Stress-strain curves of human and porcine coronary arteries. (A) Axial direction. (B) Circumferential direction. (van Andel et al., 2003)

Claes and collaborators demonstrate that the age has a decreasing effect in the circumferential tensile strength and a tendency to work in a stress increasingly similar to elbow stress. To achieve this, tensile test of whole samples from human right (RC) and left anterior descending (LAD) coronary arteries between 23 and 83 years were performed (Claes et al., 2010). Moreover, in the doctoral thesis of Claes, tensile test until rupture were performed to human coronary (Fig 1.13), radial and mammary arteries in order to have more information of arterial mechanical behavior (Claes, 2010).

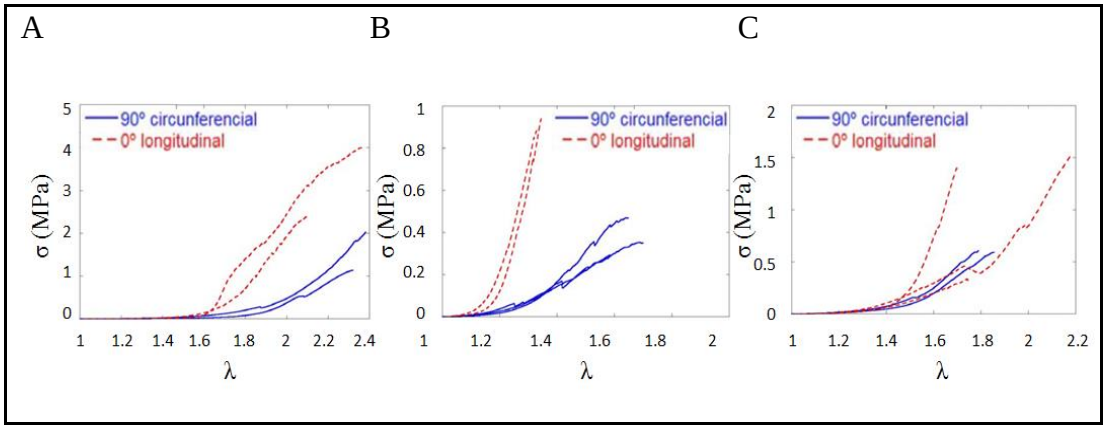

Figure 1-13: Stress-strain curves of human left coronary arteries. (A) Sample 1. (B) Sample 2. (C) Sample 3. (Claes et al., 2010)

In the three studies exposed here, coronary arteries stress-strain curves show anisotropic and non-linear J-shaped behavior for both directions, confirming the blood vessels characteristics. Additionally, a stiffer response is obtained in the longitudinal direction.

The work of Holzapfel et al (2005) will now be analyzed in more detail. They performed uniaxial test to intima, media and adventitia layer separately (Figure 1-14). Anisotropic and nonlinear mechanical response was exhibit by the tree layer tissues. The strain-stress curves intima, media and adventitia layers are clearly different between each other. All the tissues show an initial compliant behavior but then stiffens, which can be approximated as arteries are composed of a soft material with embedded collagen fibers.

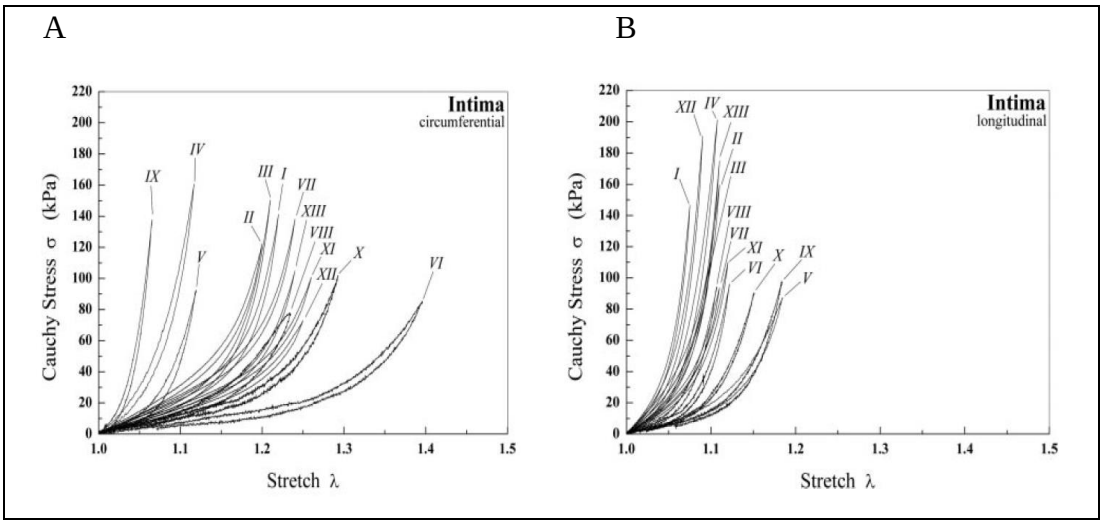

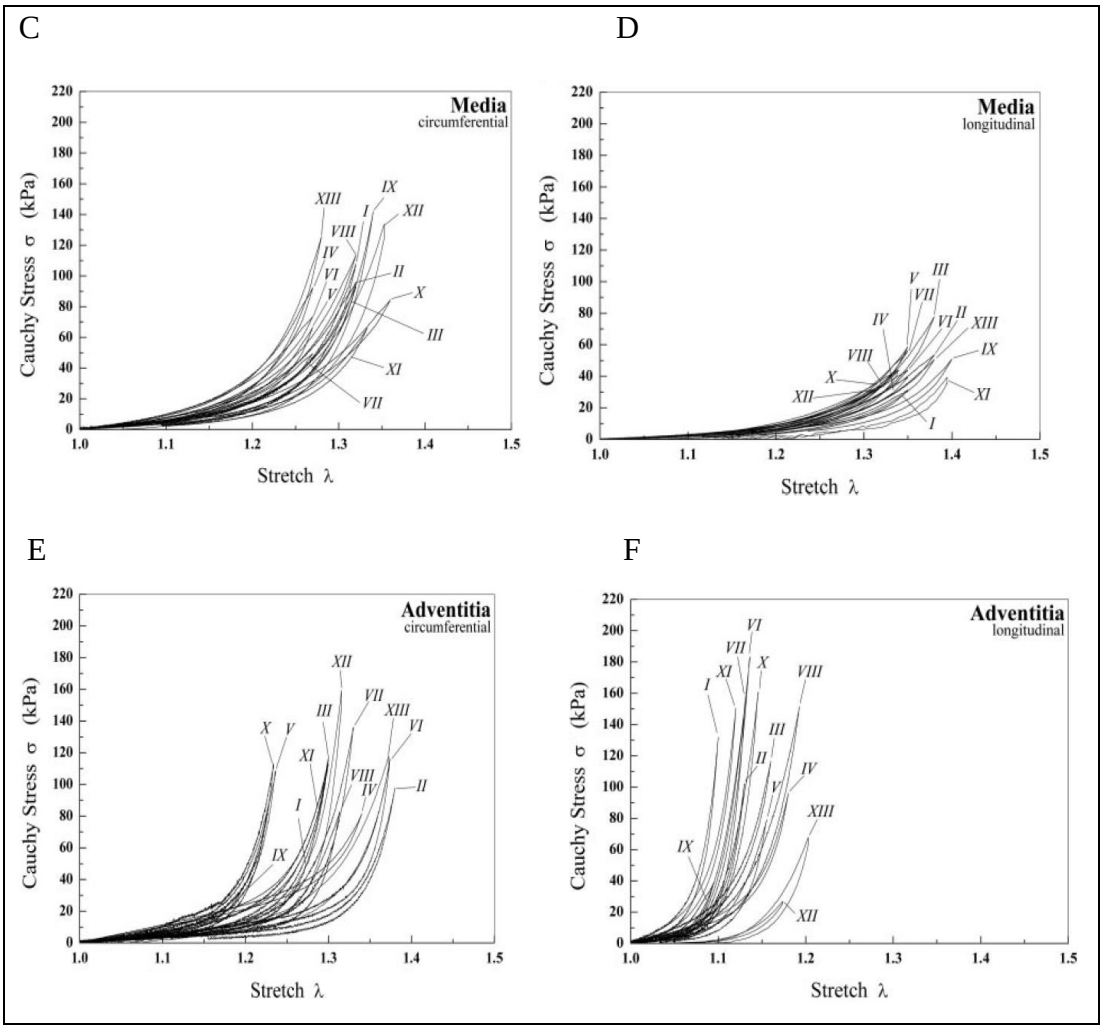

Figure 1-14: Stress-strain curves of human left coronary arteries layers. (A) Intima circumferential. (B) Intima longitudinal. (C) Media circumferential. (D) Media longitudinal. (E) Adventitia circumferential. (F) Adventitia longitudinal. (Holzapfel et al., 2005)

Holzapfel et al. (2005) developed a constitutive model to describe the anisotropic and nonlinear mechanical response of each layer of the human coronary artery. The average parameters of intima, media and adventitia were obtained from the experimental data. The parameters represent the average stiffness in the low loading domain μ (elastin and non-collagen fibers), the average stiffness in the high loading domain represented by k_1 y k_2 (collagen fibers) and a dimensionless parameter that ranges between 0 and 1 as anisotropy measure (ρ) (Table 1-1).

Table 1-1: Average constitutive parameters for intima, media and adventitia. (Holzapfel et al., 2005)

Artery Layer	μ (KPa)	k_1 (KPa)	k_2	P
Intima	27.90 ± 10.59	263.66 ± 490.95	170.88 ± 125.47	0.51 ± 0.14
Media	1.27 ± 0.63	21.60 ± 7.12	8.21 ± 3.27	0.25 ± 0.09
Adventitia	7.56 ± 4.66	38.57 ± 32.53	85.03 ± 58.94	0.55 ± 0.18

Additionally, they determined the angle of fiber reinforcement with respect to the circumferential direction by adjusting the constitutive model to the experimental data. The angle of reinforcement for intima is 60.3 ± 18.2°, for media is 20.61 ± 5.5° and for adventitia is 67.0 ± 8.5° (Holzapfel et al., 2005). It should be noted that although these angles do not necessarily represent the exact structural orientation of the fibers in each layer, it is used as a phenomenological variable that represents the direction of most strength of the tissue.

Finally, with the constitutive parameters and fiber angle mean values, the stress-stretch model response was plotted for the arterial layers in both, circumferential and longitudinal directions (Figure 1-15). This study demonstrates the change in the mechanical properties through the wall thickness and integrates this in the model. Moreover, the constitutive parameters provide information about the characteristics of human coronary arteries that can be used in applications of biomedical engineering.

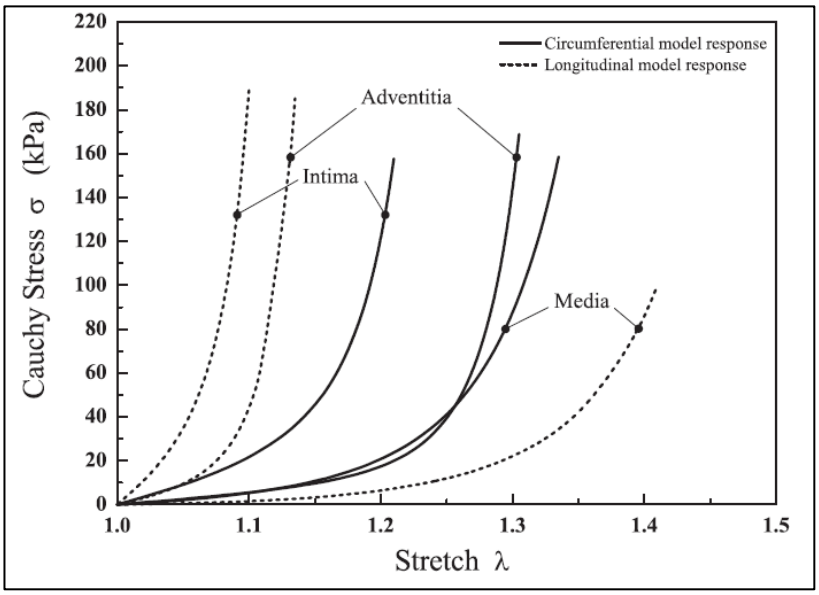

Figure 1-15: Stress-stretch model response representing the mean of all mechanical data of intima, media and adventitia in circumferential and longitudinal directions. (Holzapfel et al., 2005)

As well as coronary arteries, each layer stress-strain curves shows anisotropic and non-linear J-shaped behavior in both directions. From experimental data and constitutive parameters it can be concluded that intima layer is the stiffer one and the media is the softer layer. Additionally, a stiffer response is obtained in the longitudinal direction for intima and adventitia. An opposite behavior is observed for the media layer. This phenomenon is related to the fiber angle representing the collagen fiber organization in the tissue, which is the main and almost entire responsible for the resistance to stretch in high loading domain (Holzapfel et al., 2005).

1.5.2 Compliance of human coronary artery

The compliance is one of the most important characteristics of arteries. It is the ability of the vessel to distend and increase of lumen volume due to an increase of transmural pressure and to recoil toward its original dimension when pressure decreases. Problems of compliance such as diminish or mismatch can lead to

thrombosis or other cardiovascular diseases (Abbot et al, 1987, Weston et al 1996, Salacinski et al 2001).

As well as stress-stretch curves, van Andel et al., (2003) compared the compliance between human and porcine coronary arteries. For this, a pressurization test was made for different axial prestretch (10%, 20% and 25% for human and 30%, 40% and 50% for porcine) where the smallest value of prestretch is the approximate in situ length of the artery (van Andel et al., 2003) (Figure 1-16 A-B). In addition, Claes (2010) also studied the compliance of human coronary arteries in her doctoral thesis at different axial prestretches by a pressurization test (Figure 1-16 C-D)

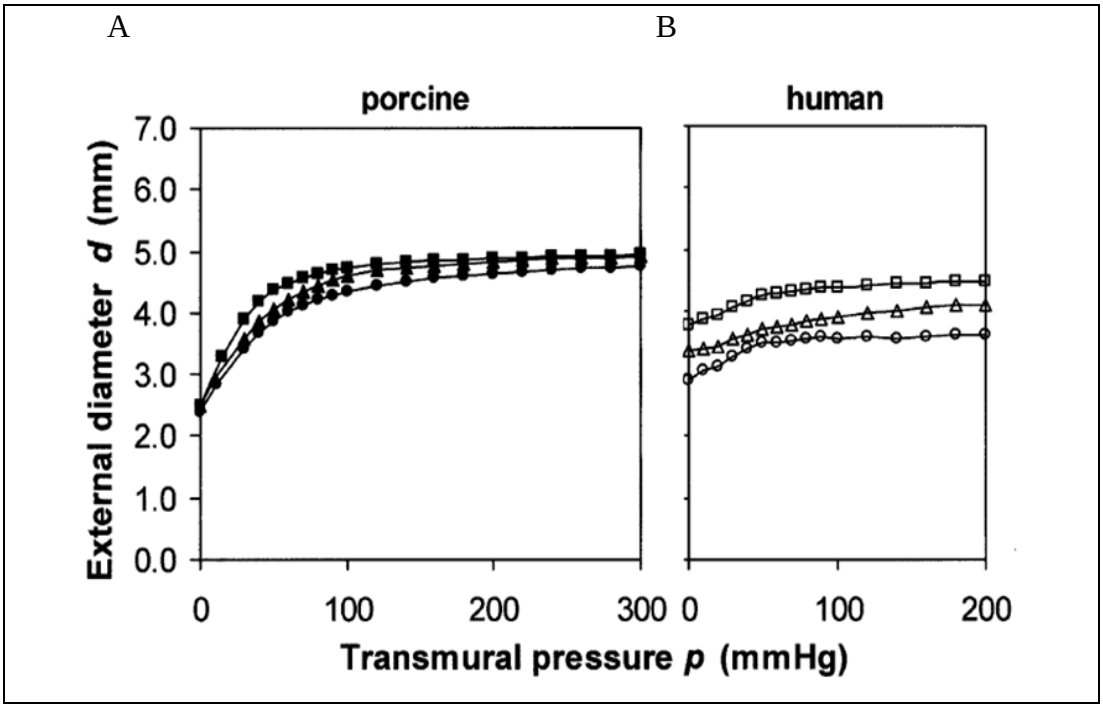

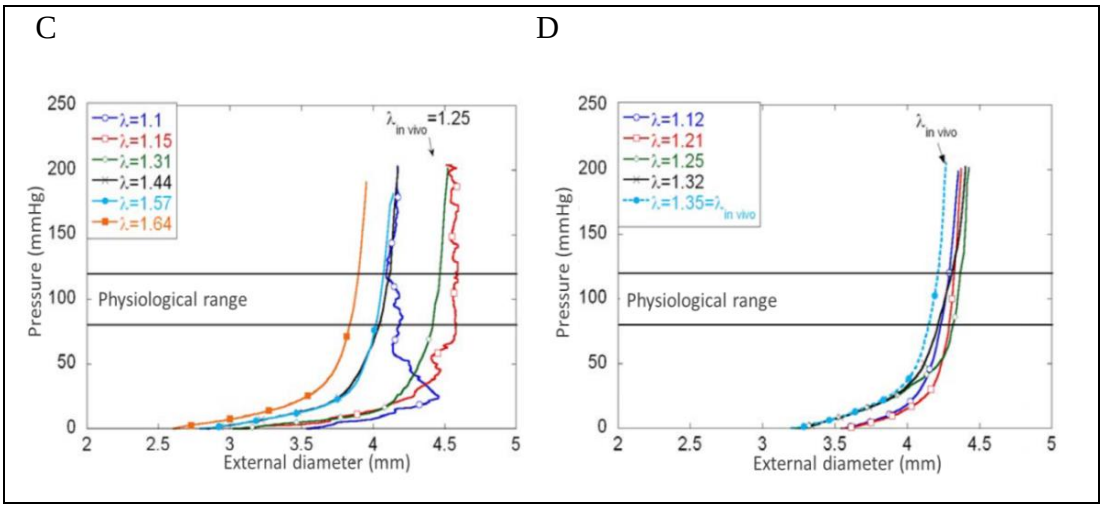

Figure 1-16: Pressure-diameter curves of (A) porcine (solid box e_z = 30%; solid triangle e_z = 40%; solid circle e_z = 50%), (B) human coronary arteries (open box e_z = 10%; open triangle e_z = 20%; open circle e_z = 25%) (van Andel et al., 2003), (C) human left descending coronary arteries sample 1. (D) Sample 2 (Claes, 2010).

In order to compare human coronary artery compliance values with the results of this thesis, values of coronary artery compliance were calculated at different ranges of pressures and axial prestretch. Experimental data from pressurization test of human coronary arteries previously described from van Andel et al., (2003) and Claes (2010) was recollected and compliance values were calculated according to standard ISO 7198 (ANSI/AAMI/ 2010) and using following equation:

$$\%C = \frac{(R_{P_2} - R_{P_1})/R_{P_1}}{P_2 - P_1} * 10^4 \qquad (1)$$

where P_1 and P_2 correspond to the lower and higher range of pressure values in mmHg, and R_{P1} and R_{P2} are the external radiuses generated at those pressures respectively (Association for the Advancement of Medical Instrumentation, 2004).

The human coronary artery compliance was calculated at three values of axial prestretch (10%; 20%; 25%) and three different ranges of pressure (50-90 mmHg; 80-120 mmHg; 110-150 mmHg).

Table 1-2: Human coronary artery compliance (%C) (10^{-2} mmHg) at different axial prestretch and pressures ranges. Adapted from (van Andel et al., 2003 and Claes, 2010)

	Pressure ranges		
Axial prestretch	50 - 90 mmHg	80 - 120 mmHg	110 – 150 mmHg
10%	6.3 ± 1.27	3.5 ± 0.04	2.5 ± 0.43
20%	7.3 ± 2.16	3.6 ± 2.69	2.5 ± 2.1
25%	7.1 ± 0.17	2.7 ± 0.37	1.2 ± 0.65

From the Table 1-2 we can observe that the compliance values decrease at higher pressures and also at higher axial prestretch. This is consistent with the fiber response in the artery wall studied before. At high pressure or subjected to high stress, the fibers are extended and will oppose more resistance, so this results in a smaller diameter change as the pressure change. The key value is the compliance at *in vivo* conditions, between 80 and 120 mmHg and with 10% of axial prestretch. Nevertheless, an important limitation is the low sample quantity used to calculate these values (n=3). For this reason, big standard deviations are shown especially for 20% of axial prestretch.

1.6 Previous studies for coronary artery replacement using vascular grafts

Several vascular grafts have been developed as a treatment for coronary artery disease. These vascular grafts are used to replace the occluded artery and are implanted in a bypass surgery. However, many of them have failed due to their low patency associated with thrombosis, intimal hyperplasia, atherosclerosis or

infection (Pashneh-Tala et al., 2016). To avoid these problems there are a set of requirements with respect to their design.

1.6.1 Requirements for a successful coronary artery vascular graft

Pashneh-Tala and collaborators (2016) have defined a number of design criteria that tissue engineering vascular graft (TEVG) must satisfy to be fit for purpose. First, because is a conduit supporting blood flow, TEGV must withstand the permanent pressure exerted by the blood flow (80 – 120 mmHg) without bursting or deforming permanently generating an aneurysm. Second, the vascular graft must possess suitable compliance, close to 3.5 ± 0.04% per 100 mmHg in physiological conditions, in order not to create high tensions near the anastomosis or flow problems associated with low patency (i.e. thrombosis). Third, similar geometry is fundamental, which does not induce undesirable flow characteristics that lead to graft failure. For coronary artery grafts must be tubular, internal diameter between 1.9 and 2.7 mm (Dodge 1992) and wall thickness from 0.55 to 1 mm (Perry, 2013). Fourth, the grafts should be non-cytotoxic and should not generate a negative immune response; indeed, it is preferable to be made of bioactive materials that induce proliferation and support cells. Fifth, must be suitable for implantation and therefore must resist being handled, manipulated and sutured. Sixth, must be able to be mass-produced in a range of dimension, quality controlled, stored and shipped at an economically viable cost. And last, must have the ability to grow, remodel and repair *in vivo*.

1.6.2 Vascular grafts types

Due to the need for vascular replacement, different techniques have been developed in order to fabricate vascular grafts such as synthetic, autologous, tissue engineering, decellulalized natural matrices, self-assembly cell sheets and scaffold based vascular grafts. Here we explain these techniques and finally summary the requirements that each technique fulfill.

a) Synthetic vascular grafts

Synthetic grafts have been a widely used solution in the replacement of blood vessels. Materials such polytetrafluoroethylene (PTFE) or polyester (Dacron®) are non-cytotoxic and resistant materials. In addition, the use of synthetic polymers has the flexibility to be able to manufacture grafts of any dimension at an economically viable cost and with scaling possibility. These reasons have allowed synthetic vascular grafts be widely used for large (> 8 mm), such as aortoiliac replacement with a 90% of patency, or medium diameter (6 – 8 mm) blood vessels replacement (Ercolani et al. 2013; Pashneh-Tala et al., 2016). However, for coronary arteries and other small diameter blood vessels (< 6mm) synthetic grafts have poor long patency (Pashneh-Tala et al., 2016).

Studies of PTFE vascular grafts as a replacement of coronary artery have shown a patency rate of approximately 60% after one year of the coronary artery bypass surgery and decline to 32% after two years (Pashneh-Tala et al., 2016). Low patency of synthetic vascular grafts is associated with the non-sufficient mechanical strength and non-resistance to hyperplasia and aneurysm formation, compliance mismatch (Catto et al, 2015; Abbott, 1987) and thrombogenic lumen surface (Byrom & Bannon, 2013; Sullivan & Brockband, 2000).

b) Autologous vascular graft

The autologous vascular grafts remain the best alternative and gold standard for coronary artery disease treatment. Vessels such as internal thoracic artery (ITA), radial artery, internal mammary artery and saphenous vein are used as autograft vessel. Saphenous vein is the most frequently used vessel in coronary artery bypass surgery, although internal thoracic artery and radial arteries are associated with superior patency (Pashneh-Tala et al., 2016). The main reason for the use of saphenous vein is the limited availability and more severe complications during artery harvesting.

Although is the best alternative for coronary artery replacement, autologous grafting has disadvantages. First, it requires double surgery: harvest of the autologous vessel surgery and bypass surgery. This can cause higher recovery costs and considerable morbidity associated with autologous harvesting. Second, although vessels have a similar structure and therefore similar mechanical properties, autologous vessels do not possess exactly the same dimensions and compliance, which diminish their patency. Finally, many times their application is limited by pre-existing vascular diseases, previous organ harvesting, amputations, limited length, and low quality (Hess et al., 2014).

c) Tissue engineered vascular grafts

Tissue engineering comes up as a new alternative that seeks to replicate the biological and mechanical properties of native vessel tissue inspired on the structure of blood vessels. Different techniques of tissue engineering have been developed in order to manufacture vascular grafts such as decellularization (Amensag et al., 2012, Cho, et al. 2005), self-assembled cell sheets (Kelm et al., 2010, Bourget et al., 2012), and scaffold–based methods (Niklason et al., 1999, Boccafoschi et al., 2007, Thomas, et al. 2013).

The advantage of tissue engineering over synthetic and autologous grafts is that it comprises the major characteristics of both. On the one hand, it allows the manufacture of grafts with similar dimensions to the vessel to be replaced. And on the other hand, it may incorporate the biological component allowing cell proliferation and tissue remodeling.

i) Decellulalized natural matrices

The decellularization of natural matrices consists on harvest blood vessels from humans or animals, or even another tissue, and removes the cells to leave the extracellular matrix alone. This matrix can be seeded with cells or used without cells. In this way it takes advantage of the structure and mechanical properties of natural tissues while avoiding the adverse immunological reactions of allogenic

alternatives. For the decellularization, chemical and biological agents, and physical methods are used. These agents are intended to maintain the tissue mechanical properties (Figure 1-17) (Pashneh-Tala et al., 2012).

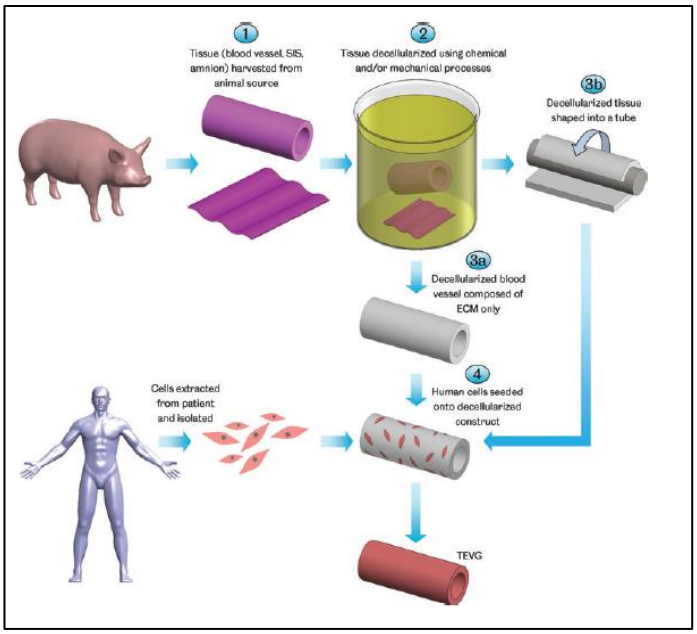

Figure 1-17: Decellularization technique for the production of vascular grafts. (Pashneh-Tala et al., 2012)

Vascular grafts for the replacement of small diameter arteries have been developed with this technique. Grafts from decellularized human amniotic membrane post-seeded with human vascular SMCs and ECs were produced with mechanical behavior and J-shape response similar to human carotid arteries (Amensag et al., 2012). In another study, decellularized canine carotid non-seeded and seeded with bone marrow cells arteries where implanted demonstrating the potential of bone marrow cells to regenerate vascular tissues and improve patency in tissue engineered small diameter vascular grafts (Cho et al., 2005). Finally, a small intestine submucosa (SIS) matrix, decellularized porcine small intestinal submucosa, seeded with hair follicle smooth muscle cells (HF-SMC) showed compliance similar to native ovine carotid artery, but a lower tensile strength (Peng et al., 2010).

Because the matrix descellularization results in the native extracellular matrix of the tissue requirements such as pressure withstand, resistance to implantation, similar compliance, non-cytotoxicity and *in vivo* remodeling are fulfilled. With this technique vascular grafts can also be made with equivalent dimension to the required vessel. However, decellularization and post-seeding processes require a lot of time and reagents, for example fabrication of seeded canine carotid artery vascular grafts takes a 7 days (Cho et al., 2005) and human amniotic membrane takes from 20 to 40 days (Amensag et al., 2012). High fabrication time and reagents leads to an increase in the cost of production.

ii) Self-assembly cell sheets

Self-assembly cell sheets vascular graft generally consists on the development of a sheet of cells that is subsequently rolled over a rod forming a tubular structure with the required dimensions. This type of graft does not have a support matrix or scaffold and can be produced by tissue engineering, microtissue aggregation or cell printing (Pashneh-Tala et al., 2012) (Figure 1-18)

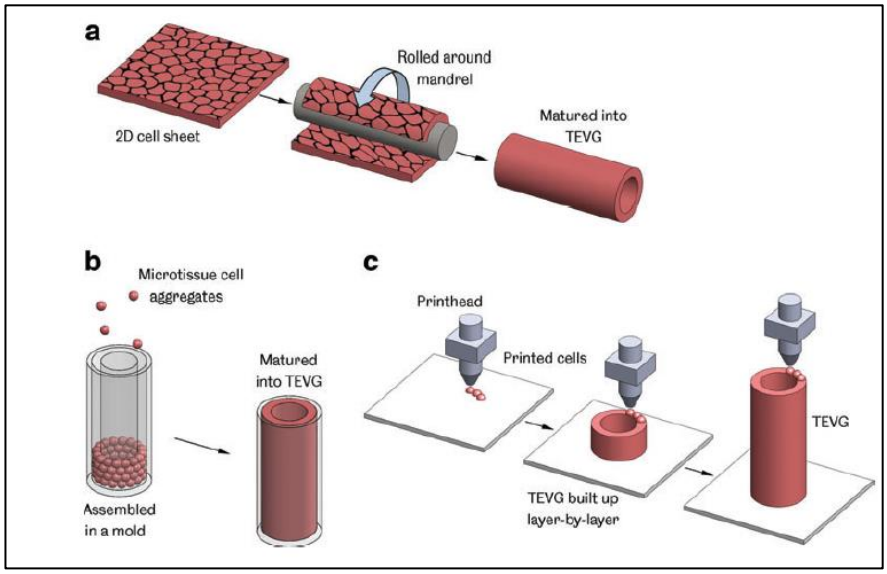

Figure 1-18: Self-assembly cell sheet technique for the production of vascular grafts. (Pashneh-Tala et al., 2012)

Although not possessing extracellular matrix, vascular grafts have been developed with this methodology with resistance to blood pressure (McAlister et al., 2009) and resistant to handling and sutured during the implantation process (Wystrychowski et al., 2014). However, there have been cases of failure due to infection, thrombosis or stenosis (Wystrychowski et al., 2014).

Their main disadvantage is the manufacturing time. Vascular grafts with high patency rate require 28 weeks for their fabrication (L'Heureux et al., 2006), while reducing manufacturing time impairs the mechanical integrity of (Pashneh-Tala et al., 2012).

iii) Scaffold based vascular grafts

Scaffold based vascular grafts consist on a template and support for cells in order to obtain complex three-dimensional structures. This technique is widely used with numerous polymers and various manufacturing methods. Polymers to assemble the extracellular matrix can be synthetic, natural or a combination of both.

Synthetic constructs have been extensively produced and submitted to clinical trials. Synthetic polymers such as poly-ε-caprolactone (PCL), poly-L-lactide (PLLA), polyglycolide (PGA) and poly(glycerol sebacate) (PGS) have been used alone or in combination, to construct vascular with different dimensions and characteristics. These polymers have the advantages of being biodegradable, generally demonstrate tailorable mechanical properties with high reproducibility, and can be produced in large quantities. However, a J-shaped response like blood vessels is hard to achieve with synthetic polymers because they present an inverse curvature i.e. at higher load less stiffness (Montini-Ballarin et al., 2016). Multiples attempts have been made to obtain a J-shaped response by manufacturing scaffolds in different ways. Good results have been obtained by making material lattices of microstructures horseshoe with elastomers (Jang et al., 2015; Ma et al., 2016). However, this manufacturing process does not allow rapid manufacture and co-deposition of cells. Finding a way to get a scaffold with J-shaped response remains

a major challenge in soft tissue engineering. This is a relevant factor for this thesis and will be explained in more detail in Chapter 4.

Natural polymers mostly used for scaffolds are fibrin, elastin, hyaluroran, silk, fibroin and collagen. Vascular grafts produced with these polymers do not activate chronic inflammation or toxicity, and therefore show a great biological performance. In addition, J-shaped mechanical response has been observed in vascular grafts made from natural polymers. Nevertheless, natural polymers are difficult to obtain, do not exhibit high reproducibility, and generally cannot withstand the needed pressure because of their low strength (Montini-Ballarin et al., 2016).

Producing vascular grafts with biological and mechanical performances similar to blood vessels has been one of the main objectives of tissue engineering and has led to design different manufacturing strategies. Some studies have reported the production of grafts with J-shaped stress-strain curves comparable with the native tissue behavior. A tubular construct made of interleaved wrapped previously seeded with ECs, SMCs and fibroblast PGA and PCL sheets was preconditioned for two weeks in dynamic culture with a bioreactor for achieving elastin production and robust vessels with elastic and similar stress-strain response to bovine arteries (Iwasaki et al., 2008). *In vivo* remodeling after 90 days on implantation and similar burst pressure to Lewis rat aortas were observed in an acellular electrospun PGS and PCL vascular grafts. However, suture retention was lower than native aortas (Wu et al., 2012). Corrugated vascular grafts fabricated with polyurethane (PU) and PGA in order to mimic corrugated laminae of blood vessels. This constucts have a J-shape response and showed mechanical behavior similar to natural porcine carotid artery (Rapoport et al. 2012).

Only a few studies have developed vascular grafts for the replacement of human coronary arteries and compared their mechanical response. Acellular electrospun vascular grafts made of poly(ester urethane) (SPEU) and PLLA to mimic elastin and collagen respectively shower a j-shape response, compliance, strength and

burst pressure values in the same order of natural coronary arteries (Montini-Ballarin et al., 2016). A combination of rolled poly(ester urethane) urea (PEUU) electrospun mesh used to mimic the collagen fibers, and bonded together by layers of polyethylene glycol-fibrin (PEG-fibrin) hydrogel resembling elastin fibers with mouse smooth muscle progenitor cells seeded and encapsulated has been used to fabricate tubular constructs with high tensile strength, high suture retention strength and j-shaped mechanical response comparable to native coronary arteries (McMahon et al. 2011). Vascular grafts fabricated with electrospun PEUUmeshes and electrosprayed with rat vascular SMCs were cultured in a spinner flask for 3 days also presented J-shaped mechanical response, compliance, burst strength and suture retention similar to human coronary arteries (Stankus et al. 2007). Table 1-3 shows a summary of the requirements that have been achieved for each manufacturing technique.

Table 1-3: Summary requirement check-list of coronary vascular grafts

	Withstand blood pressure	Similar compliance	Similar dimensions	Non cytotoxic	Resist implantation	Economically viable cost	Remodel *in vivo*
Synthetic grafts	✓	✗	✓	✓	✓	✓	✗
Autologous grafts	✓	✗	✗	✓	✓	✓	✓
Decelullarized natural matrices	✓	✓	✓	✓	✓	✗	✓
Self-assembly cell sheets grafts	✓	No studies	✓	✓	✓	✗	✓
Scaffold based grafts	✓	✓	✓	✓	✓	✓	✓

2 HYPOTHESIS AND AIMS

Vascular grafts for coronary artery replacement have been developed. However, those works do not demonstrate a clear close similarity with the mechanical behavior of arteries. Furthermore, none of the approaches combine the mimicking of the three-layer structure of arteries, the collagen fiber orientation, and undulated form of each layer and distribution of cells through the graft in order to resemble both mechanical properties and biological function.

The hypothesis of this thesis is that the vascular grafts produced by mimicking the artery structure present mechanical properties similar to human coronary arteries and cell proliferation.

The main objective of this thesis is to develop a vascular graft by mimicking the artery structure that present biological and mechanical properties similar to human coronary arteries in order to be a better alternative for the replacement of diseased vessels in the coronary artery bypass surgery. Specifically, a different approach is used to improve the vascular graft mechanical behavior inspired in the structure of coronary arteries. This approach consists in adjusting the layers separately mimicking the wavy form and different layer orientation of collagen fibers, the intercalated layer structure of artery wall and cell distribution in order to produce a mechanically improved vascular graft just combining the three adjusted layers.

For this purpose, the specific objectives are:

1) Determine the fabrication methodology and materials to produce biocompatible and resistant vascular grafts
2) Determine the fabrication parameters of hydrogel layer and fiber deposition in order to obtain a bioactive cell support and fibers that mimic the collagen fiber orientation in artery wall
3) Improve the mechanical properties of middle and outer layers by adjusting the stress-strain curve to human coronary media and adventitia artery layers
4) Manufacture a vascular graft combining the adjusted middle and outer layers

5) Characterize the mechanical properties of vascular grafts and compare to data from human coronary arteries
6) Evaluate the cell proliferation and distribution in vascular grafts in order to verify the biological component.

3. WORK STRUCTURE

Chapter 1 introduces the coronary artery disease and its current solutions such as angioplasty and coronary bypass surgery. In order to study the mechanical properties of coronary arteries, a review of the arterial structure, its main components and the mechanical properties studied are included. Finally, the vascular grafts requirements for success and the different tissue engineering methods used to fabricate them are explained with their advantages and disadvantages.

Chapter 2 presents the main objective of this thesis and the approach used to achieve it. The main objective is dismembered in six specific objectives.

Chapter 4 describes the vascular grafts manufacturing methodology of this work. First, the robot device used to automatize the fabrication process is described, which was previously designed and assembled in the laboratory of Cells for Cells (Dr. Juan Pablo Acevedo). Second, the techniques used to fabricate the different layers of the graft are explained, then the selected materials and their characteristics are described and finally the tests results used to determine the fabrication parameters are presented. It should be noted that everything shown in this chapter is work done for this thesis with the exception of the design and assembly of the robot device, which was performed in advance as part of the author's professional internship in Cells for Cells..

Chapter 5 presents the manuscript submitted to the Journal Nature Communications with the work done in this thesis. It consists on the development of vascular grafts using dipping-spinning and solution blow spinning techniques. First, it is presented the work summary, introduction and motivation. Next, the materials and methodology of layer and vascular graft manufacture is presented and the procedures followed in the mechanical and biological characterization are explained. Then, the results are described and finally the conclusions of the work are outlined.

Chapter 6 highlights the conclusions and contributions of this work and it presents some interesting research and work for the future.

4. VASCULAR GRAFTS FABRICATION TECHNIQUE

Vascular grafts developed in this thesis were fabricated with a combination of dipping-spinning and solution blow spinning (SBS) techniques using a robot device. In this way, biological and mechanical components were incorporated using hydrogel layers with encapsulated cells by dipping-spinning and depositing spun fibers with SBS respectively.

4.1 Robot device

Previously in Dr. Acevedo' laboratory, a CNC machine was designed and constructed to control elevation, drop and rotation of a plastic rod (Figure 4-1) (Wilkens et al., 2016). This robot consists in four NEMA 16 stepper motors (SM-42BYG011-25, Mercury Motor, China) that control the movement of the platforms. The first and second motors allow the elevation and drop movement of the rod. While the first one maintains the working position (Figure 4-1b) the second motor controls the rod dipping (Figure 4-1d). A third motor is used for a rotational movement of the rod (Figure 4-1d). Finally, a fourth motor is used to move and change the solutions where the rod is immersed with the dipping movement (Figure 4-1a).

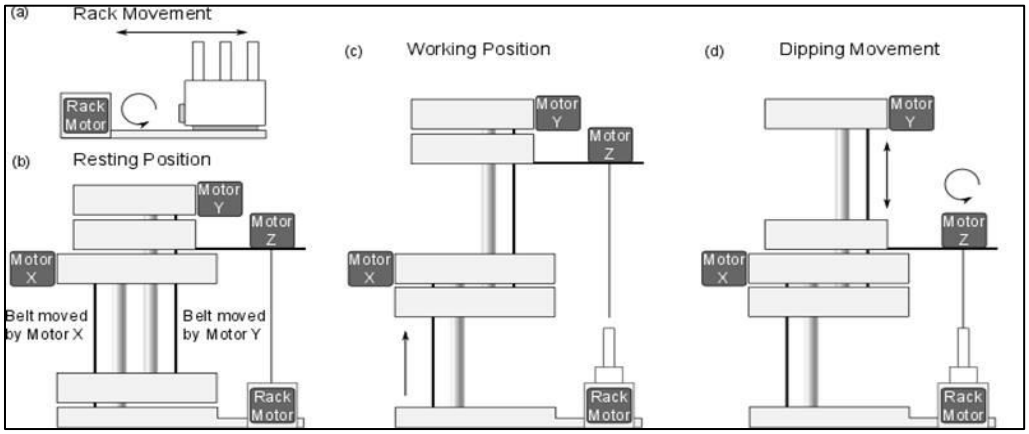

Figure 4-1: CNC machine. (a) Biomaterial switching; (b) resting position; (c) Working Position; (d) Dipping Movement (Wilkens et al., 2016).

Each motor is controlled by an electronic circuit using a gShield v.5 (1750, Adafruit) specially designed to allow easy control of the four bipolar stepper motors, simultaneously. The motion of the stepper motors is controlled by the Grbl firmware. G Code command inputs are streamed to the circuit using the Universal G-Code Sender.

4.2 Dipping-spinning

The dipping spinning technique consists on the controlled elevation and drop movement of the rod with a rotational movement simultaneously. The entire vascular graft fabrication was done with this technique. Different upward-speeds and rotational speed were used in the graft manufacturing.

4.3 Solution blow spinning (SBS)

The technique consist in the spun of polymer fibers using compressed air and a spraying apparatus (Figure 4-2a). The spraying apparatus consists of an inner and a concentric outer nozzle. (Figure 4-2b) A syringe pump injects and controls the polymer flow through the inner nozzle while compressed air at a certain pressure (P_1) flows through the outer nozzle. Because of the nozzle geometry, a region of low pressure around the inner nozzle (P_2) is created and a cone is formed by the polymer solution (Medeiros et al., 2009).

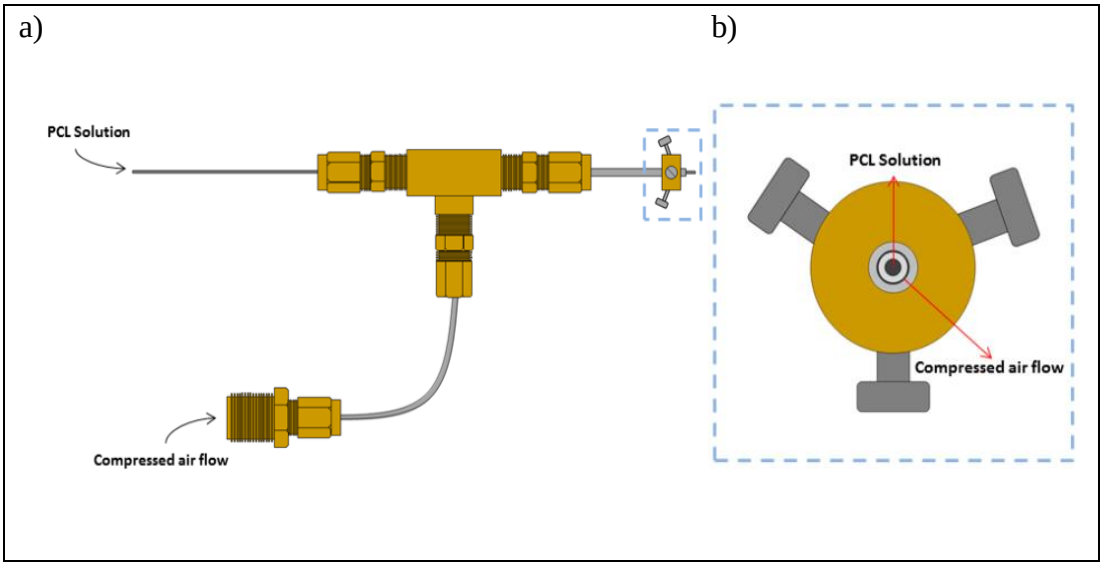

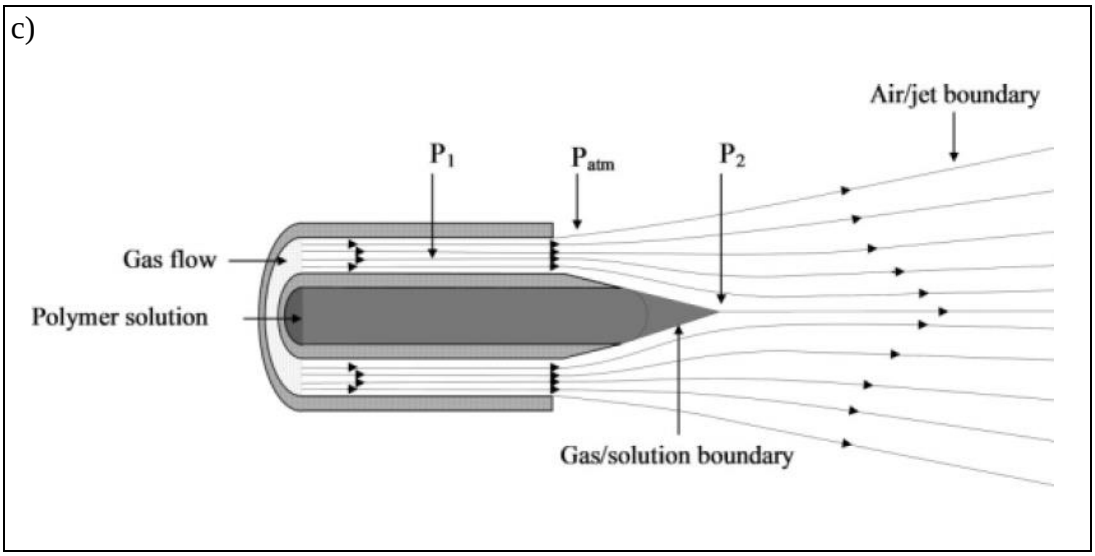

Figure 4-2: Solution blow spinning. (A) Spraying apparatus. (B) Concentric inner and outer nozzles. (C) Polymer and gas flow through inner and outer nozzle and fiber formation (Medeiros et al., 2009).

4.4 Lumen Fabrication

The inside and central space of blood vessels is called lumen and is where the blood flows through. In case of coronary arteries the lumen diameter ranges between 1.9 and 2.7 mm (Dodge 1992). For this purpose, a 1.8 mm diameter plastic rod was used for the vascular graft fabrication. Additionally, a sacrificial alginate layer was deposited by coating the plastic rod in order to achieve a soft lumen and easy mechanic extraction. The alginate scaffold was deposited by the dipping technique (Figure 4-3). The lumen fabrication consisted in two subsequent dippings in an alginate solution and then submerged during 15 s in $CaCl_2$ solution for crosslinking and finally immersed tree times in phosphate buffered saline (PBS) for 1 min for cleaning. The concentration of alginate solution, upward speed and number of dippings were defined by the standardization of luminal parameters experiment fund in Appendix 1. The parameter selection criterion was the one that allowed the most regular and smooth layer deposition. The most suitable parameters to obtain uniform structures were two dippings of 2% of alginate

concentration with 138 mm/s upward-speed is the most suitable parameters to obtain uniform structures.

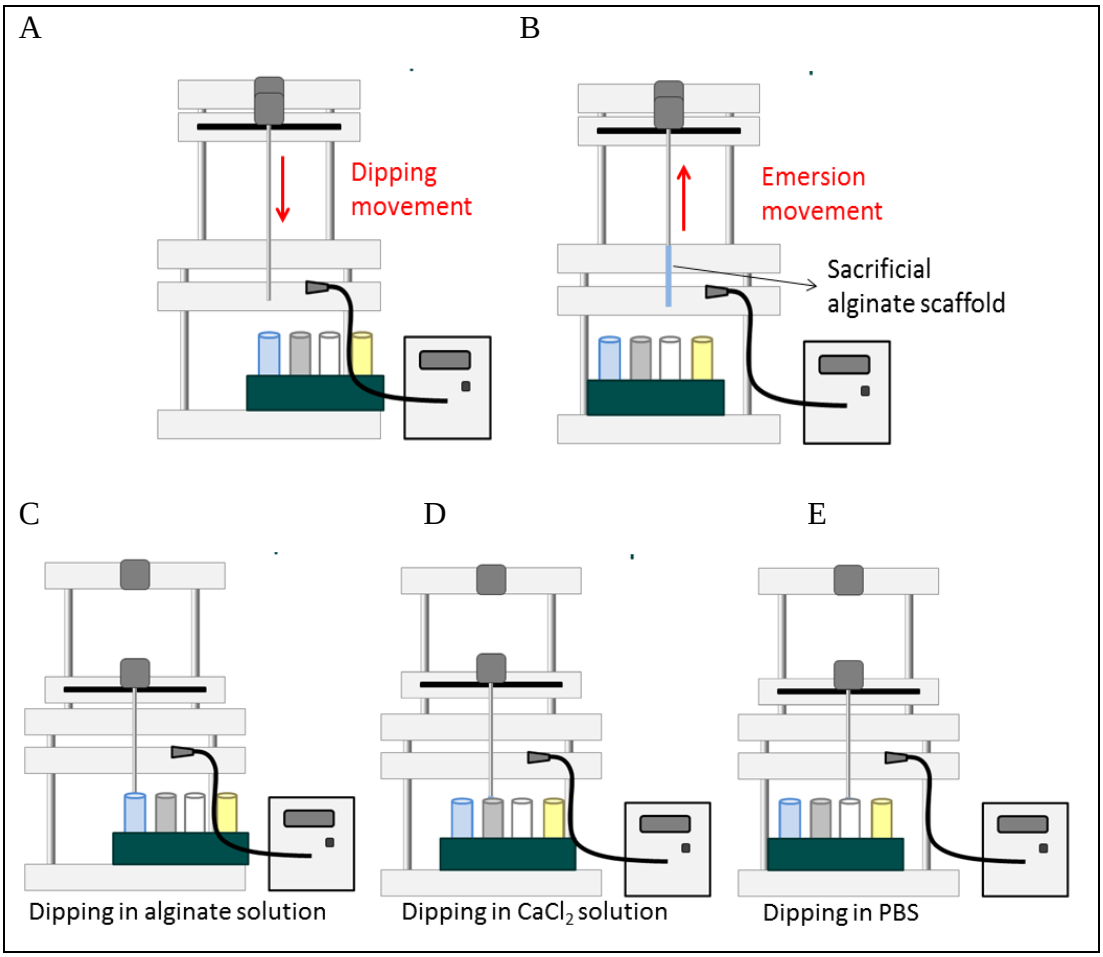

Figure 4-3: Lumen Fabrication. (A) Dipping movement of the robot device. (B) Emersion movement of the robot device and final sacrificial alginate scaffold. The alginate scaffold is fabricated in three steps: (C) two subsequent dippings into alginate solution; (D) one dipping into $CaCl_2$ solution of 15 s for crosslinking and (D) three dippings into PBS of 60 s for washing.

4.5 Hydrogel layers

Blood vessels basically consist on intercalated layers of cells with other extracellular matrix (ECM) components and fibers. To add the biological components to our vascular grafts, cells were encapsulated in the hydrogel layers.

Additionally, this cellularized hydrogel layers were deposited intercalated with the fiber layers. This hydrogel layer gives the versatility to add different cell types. In this way, the vascular graft can have the equivalent cell type of each artery layer. Moreover, the hydrogel layer fills the mechanical role of elastin fibers and has the potential to incorporate growth factors or drugs that allow the proliferation or differentiation of cells and to avoid thrombogenesis, hyperplasia or stenosis.

These layers are deposited with the dipping spinning technique as shown in Figure 4-4. Each layer is fabricated through several dippings of the rod into an encapsulation solution. Then, the rod is emerged with a rotational movement and polymerized by the UV light exposure (Figure 4-4c). The encapsulation solution is mixed with cells and kept in a water bath at 30°C to avoid the biomaterial gelation at room temperature.

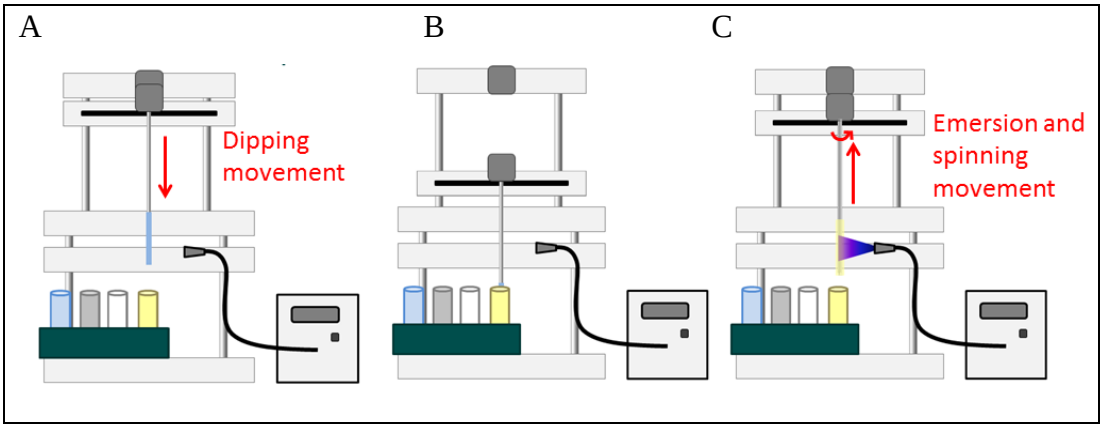

Figure 4-4: Hydrogel layer fabrication. (A-B) Dipping movement of the robot device into the encapsulation solution. (C) Emersion and spinning movement with a simultaneous UV exposure to allow the crosslinking and hydrogel formation of the encapsulation solution.

4.6 Fiber layers

Fiber layers were deposited to add the mechanical component to the vascular grafts. These layers mimic the distribution of collagen fibers in coronary arteries. In this way, because of the fibrous structure the graft can have similar mechanical properties to arteries such as compliance and J-shaped stress-strain curves.

The fiber layers were deposited by a combination of dipping-spinning and solution blow spinning (Figure 4-5). This technique has the versatility of easily depositing a large amount of fibers in a short time and at any angle of orientation. Each layer consists in fibers deposited in a certain angle and in the opposite angle to create a kind of mesh. In addition, a special forth-forward spinning movement was used. The fibers were deposited while the rod was subjected to down-and-up movement (Figure 4-5a) and a simultaneous unbalanced alternated spinning that consisted of cycles of 1 s right rotation followed by a 0.5 s left rotation (Figure 4-5b-d). The aim of this special rotation is to deposit wavy fibers such as the collagen fibers found in artery walls.

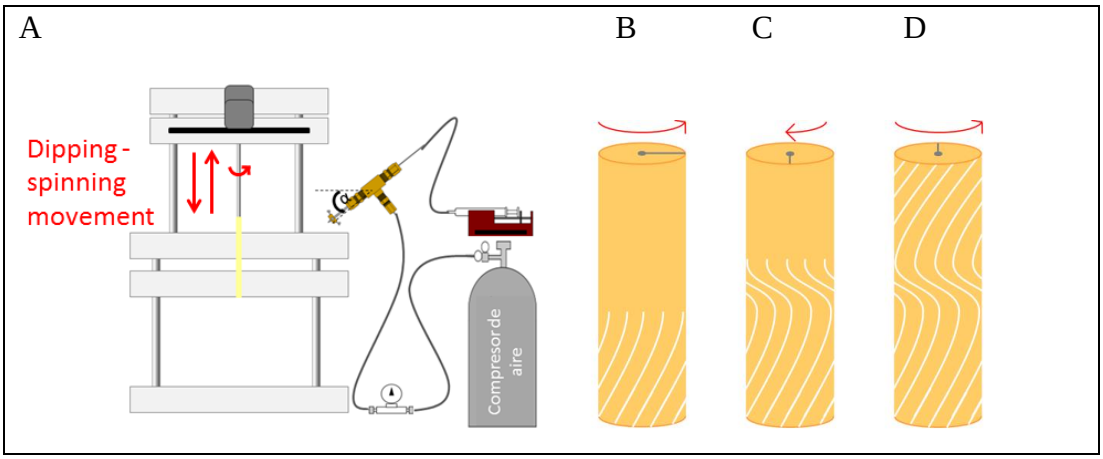

Figure 4-5: Wavy fiber deposition. (A) Combination of dipping-spinning and solution blow spinning technique. Representation of the forth-forward spinning movement. (B) Right movement for 1 s; (C) Left movement for 0.5 s; (D) Right movement for 1 s.

4.7 Fabrication materials

The biomaterials used in the fabrication of vascular grafts must be carefully selected in order to fulfill all the requirements for successful grafts mentioned in Chapter 1.6. For the lumen structure, sodium alginate was chosen. The materials for the encapsulation solution were a combination of bovine gelatin and sodium alginate. Finally, the polymer selected for the fibers was PCL. Each biomaterial

was selected because its characteristics allowing the mimicking of the vascular wall structure.

4.7.1 Alginate

Sodium alginate is a natural biomaterial obtained from brown seaweed. It has been widely investigated and used in biomedical applications due to its biocompatibility, low toxicity and relatively low cost (Lee and Mooney, 2012). Alginate can be dissolved in water or PBS. This biomaterial can be mildly gelled by the addition of divalent cations such as Ca^{2+} (Lee and Mooney, 2012). A common crosslinking method is the exposure to $CaCl_2$ (Lee and Mooney, 2012). Additionally, alginate hydrogel can be depolymerized using triphenyl phosphate (TPP).

For the lumen, a sacrificial alginate scaffold was chosen because of its simple crosslinking method, its biocompatibility and low toxicity to cells. The aqueous solution of alginate is easily and homogeneously deposited on the rod. Furthermore, alginate hydrogel can be easily mechanically removed or digested with TPP for chemical removal.

For the encapsulation solution, a low concentration of alginate was used to increase the solution density and viscosity. The reasons for choosing alginate were also the biocompatibility and low cellular toxicity. However, a low concentration is used because its low bioactivity (Sun and Tan, 2013).

4.7.2 Gelatin

Gelatin is a natural biomaterial obtained by the denaturation of collagen derived from a variety of sources; in this case we used bovine gelatin. Because of its natural precedence, it has characteristics such as biocompatibility, it has lower antigenicity that collagen, it is completely reabsorbable *in vivo* and it is bioactive (Van Den Bulcke et al. 2000). Bovine gelatin is soluble in warm water (>40°C) and cells can be added to the solution. Thermally gelation occurs when cooling

gelatin aqueous solutions. However, it is not stable at body temperature because its relatively low melting point (Van Den Bulcke et al., 2000).

A chemically stable material can be achieved by the reaction of gelatin with methacrylic anhydride. The product of this reaction is gelatin methacrylamide (GelMa); in our case it is bovine gelatin methacrylamide (GelBMa). The synthesis methodology used in this work was previously described in Nichol et al. (2010) and Van Den Bulcke et al. (2000). To form covalently crosslinked hydrogels, an aqueous solution of GelMa and photoinitiator has to be exposed to UV light. This process is called photoinitiated radical polymerization. The degradation time of polymerized GelMa hydrogels is among months (Chen et al., 2012, Visser et al. 2015).

For hydrogels layers GelBMa was chosen for two main reasons: its bioactive and biocompatible characteristics and its fabrication compatibility. Hydrogel layers contain cells that have to be able to proliferate, remodel the ECM, and even differentiate. GelMa has demonstrated to be a hydrogel platform that allows embedded cell matrix deposition (Visser et al., 2015). Moreover, the dipping-spinning technique requires an easy and rapid polymerization method. The crosslinking with UV light is compatible with these requirements achieving a GelBMa hydrogel after the emersion of the rod from the encapsulation solution.

4.7.3 Polycaprolactone

Polycaprolactone (PCL) is a synthetic biomaterial widely used in tissue engineering due to its biocompatibility, biodegradability, structural stability and mechanical properties (Patrício et al., 2013). However, it also has some disadvantages such as low bioactivity and high hydrophobicity (Patrício et al., 2013). PCL is soluble in N,N-dimethylformamide, 1-methyl-2-pyrrolidone, tetrahydrofuran, dichloromethane, dimethyl sulfoxide, acetone and chloroform. The last two are volatile solvents and therefore they quickly evaporate in air contact. This is very useful for fiber production since the solvent evaporates at the same time that the fiber is formed.

For fiber layer the selected biomaterial was PCL. First, because of its biocompatibility and biodegradability, which allow the incorporation of cells to the vascular graft and the ECM remodeling. Second, PCL mechanical properties are such that their fibers have similar resistance to collagen fibers in the arteries. Third, volatile solvents such as acetone and chloroform can be used to dissolve PCL. This is perfect for fiber deposition using the SBS technique. The compressed air evaporates the solvents forming the PCL fibers.

4.8 Determination of fabrication parameters

4.8.1 Hydrogel solution

As mentioned above, the hydrogel solution consists in a combination of GelBMa and sodium alginate. For the GelBMa polymerization a photoinitiatior (PI) called 2-Hydroxy-4′-(2-hydroxyethoxy)-2-methylpropiophenone (410896, Sigma, USA) was incorporated. In order to achieve a biomaterial that supports cell proliferation but also allow the deposition of the layers by dipping-spinning technique, parameters such as GelBMa, alginate and PI concentrations, UV intensity and cell concentration were determined.

a) GelBMa and alginate concentrations

For the hydrogel biomaterial concentrations we preferred a higher concentration of GelBMa compared to alginate because it is more bioactive. Previous studies in tissue engineering used GelBMa at 10% (w/v) concentration (Nichol et al., 2010; Visser et al., 2015).However; GelBMa at 10% concentration was not viscous enough for the deposition in the rod of dipping-spinning robot device. For this reason, alginate was added to increase the solution viscosity. By visual inspection, we determined that the lower concentration of alginate that allow the deposition and polymerization of a layer over the rod was 0.5% (w/v). Accordingly to this, a 10% of GelBMa (w/v) and 0.5% of Alginate (w/v) concentrations were suitable for the solution deposition and subsequent polymerization on the rod by dipping-spinning and exposure to UV light.

b) Cellular concentration

A cellular component was incorporated at a 10^7 cells/mL concentration for proliferation, distribution, immunogenicity and bioreactor assays, as other studies have shown for similar tests (Visser et al., 2015). Human Umbilical Vein Endothelial Cells (HUVEC) were used for the proliferation and distribution assays and Bone Marrow Cells (BMC) were used for immunogenicity and bioreactor assays.

c) PI concentration and UV light intensity

We observed that the PI concentration together with the UV light exposure could be toxic to cells. In order to reduce the encapsulation solution toxicity different PI concentrations and UV intensities were tested by the WST-1 Cell Proliferation Colorimetric Assay Kit (K302, Biovision, USA). This assay quantified the mitochondrial activity and therefor if cells are alive or dead.

i) Methodology

Hydrogel solution was made by dissolving GelBMa at 10% (w/v) and alginate at 0.5% (w/v) concentrations in PBS 1X until completely dissolved. A PI stock solution was prepared by dissolving PI at 2% (w/v) in PBS at 85°C and maintained at this temperature before used to avoid crystallization of the reagent. The PI stock solution was incorporated to the hydrogel solution up to five different concentrations: 0.05%, 0.1%, 0.2%, 0.5% and 1% (w/v).

HUVECs (ATCC® CRL1730™) were cultured and expanded in culture medium (high glucose Dulbecco's Modified Eagle's medium (DMEM) (16000-044, Gibco, USA) supplemented with 10%(v/v) fetal bovine serum (FBS) (16000-044, Gibco, USA), 2 mM glutamine (25030-081, Gibco, USA) and 1% (v/v) penicillin-streptomycin (15140-122, Gibco, USA)), and incubated at 37°C, 5% CO_2 and 96% of humidity.

HUVECs were mixed in the GelBMa-alginate solution at a concentration of 2 million cells mL^{-1}. In a 96 well plate 30 µL of the hydrogel mixture was deposited.

Three different intensities of UV light were tested: 121, 261, 323 mW cm^{-2}. Each well was exposed for 30 s to UV light. The proliferation was measured at day 1, 4, 7 and 14 after cell culture of the hydrogels in the same culture medium mentioned above. The assay consists on changing the medium to 100 µl, add 10 µl of WST reagent and incubate for 2.5 hrs. Finally, 100 µL of each well was measured by a microplate reader.

ii) Results and conclusions

Figure 4-6 shows the absorbance at 450 nm of hydrogels fabricated with different combinations of PI concentration and UV light intensity. Visual inspection of hydrogels with 0.1% (w/v) of PI determines that structures were weak and cells migrate to the bottom surface of the well. This implies that the fabrication with this concentration diminish the layer formation. On the other hand, when comparisons of time-dependent proliferation of cells samples crosslinked using the same UV irradiation but with different content of PI, significant differences were observed, revealing a dose dependent toxic effect of the PI. It is to say that 0.5% and 1% showed a toxic effect on cells in each UV light intensity. The best results were obtained with a 0.2% of PI concentration, however, by visual inspection crosslinking with 121 mW cm^{-2} generates also a weak scaffold that do not resist until day 14. Furthermore, for fabrication applicability the higher UV light intensity should be used. In conclusion, the most suitable parameters for hydrogel layer fabrication are a PI concentration of 0.2% (w/v) and exposure to UV light with 323 mW cm^{-2} of intensity.

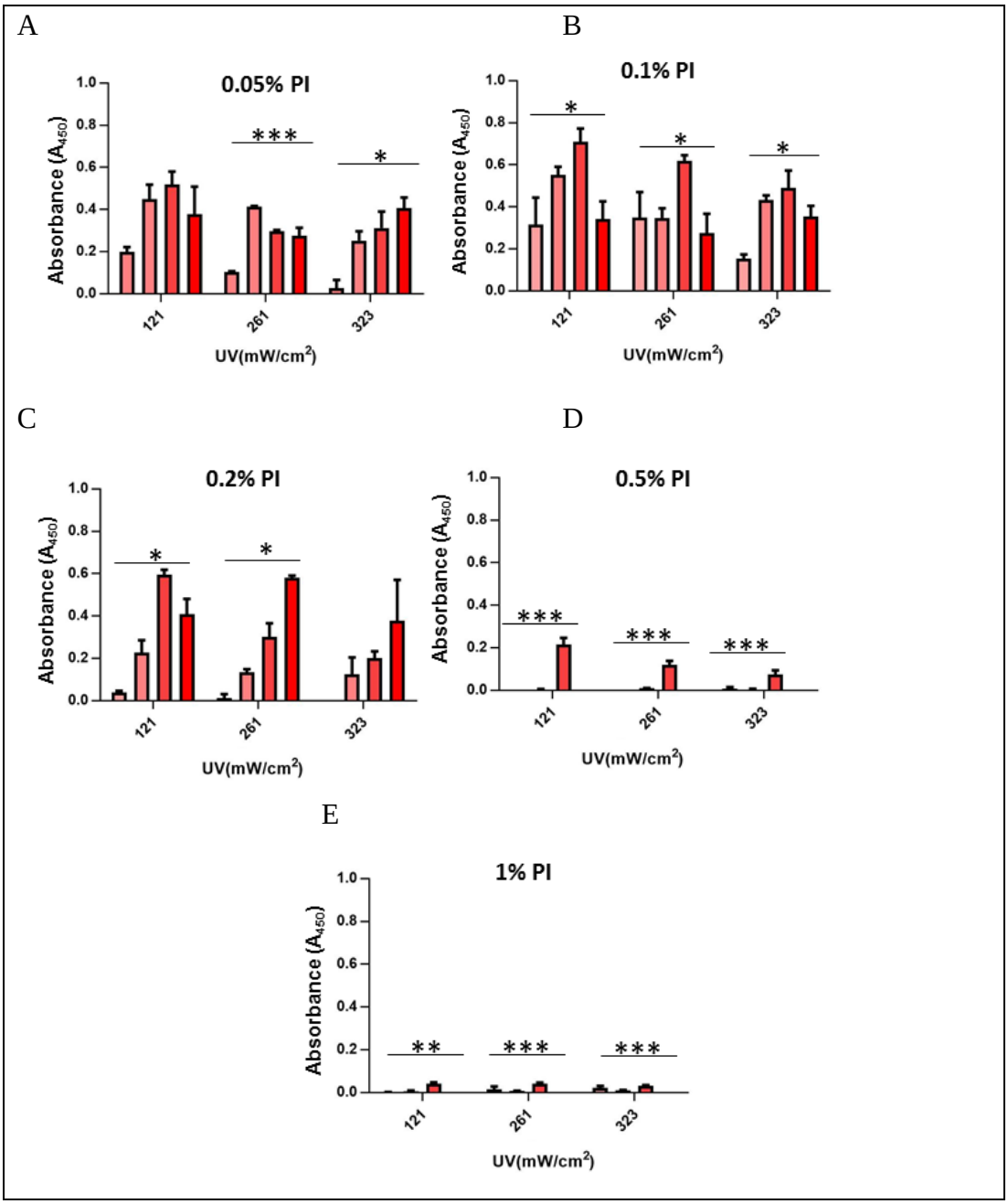

Figure 4-6: Effect of different PI concentrations on cell proliferation when using different UV irradiation. (A) 0.01%, (B) 0.05%, (C) 0.2%, (D) 0.5% and (E) 1% respectively. (Wilkens et al., 2016)

4.8.2 Fibers

Fibers to reinforce our vascular grafts were made from PCL using the SBS technique. In order to deposit fibers in the rod different parameters of the SBS technique were determined such as: PCL solution concentration, PCL flow rate, compressed air pressure, distance of the spraying apparatus, dipping-spinning speed, and angle of deposition of fibers.

a) PCL solution concentration

As mentioned before, for the fiber formation a volatile solvent is needed. Nevertheless, when too volatile it will evaporate before the fiber is formed. Because of this, a mixture of a very volatile solvent with a not too volatile solvent was used for the SBS fiber formation. Chloroform is more volatile that acetone. PCL dissolved only in chloroform does not allow the fiber formation, which is why it needs to be mixed with another solvent such as acetone. Three PCL solutions were tested in order to allow fiber formation: 100% (v/v) chloroform, 90% (v/v) chloroform and 10% (v/v) acetone and 80% (v/v) chloroform and 20% (v/v) acetone. By visual inspection of the amount of fiber deposited, and 80% (v/v) chloroform and 20% (v/v) acetone was chosen because it allows a higher amount of fiber deposition.

The PCL concentration used for the fiber deposition was 7% (w/v). This concentration was determined by trial and error, starting from a higher concentration (15% (w/v)) and decreasing until continuous and abundant fiber formation was observed. A similar concentration value was used in other study with PCL fibers produced with SBS but dissolved in dichloromethane (Oliveira et al., 2013). In that study they demonstrate that there are no residual solvents left after spinning, which is an important factor in applications for cell and tissue growth. Nevertheless, a very irregular structure with variable-sized fibers and network of beads was observed (Oliveira et al., 2013).

b) Flow rate

Three different flow rates for the syringe pump injection were used for fiber formation: 120, 200 and 300 µL/min. Using visual inspection of the fibers produced with the three values the flow rate was determined in 120 µL/min. This value is the same that other study use to produce PCL fibers with SBS (Oliveira et al., 2013).

c) Pressure

Three different pressures of compressed were used for fiber formation: 20, 40, 60 psi. Using visual inspection of the amount of fiber deposited with each pressure, the value of 60 psi was chosen because it allows a higher amount of fiber deposition.

d) Distance

Chloroform and acetone could damage the cells in the hydrogel layer. This is why when fibers are deposited in the vascular grafts the solvents must be completely evaporated. A distance of 30 cm from the SBS to the rod is used to achieve this issue.

e) Rod dipping-spinning speed

In order to deposit fibers in all the length of the rod, the dipping and emerging movements were controlled by the robot device. As mentioned before, the collagen fibers in arteries are in an undulated form and are not in a stretched form. To avoid a stressed deposition of fibers the rod up-down movement speed was decreased to 6.9 mm/s and spinning speed was speed also was decrease to 42 rpm. Furthermore, a forth-forward movement was performed simultaneously to the up-down movement in order to deposit the fibers in an undulated form. Specifically, the forth-forward movement consisted of cycles of 1 s right rotation followed by a 0.5 s left rotation at 42 rpm as explained before in Chapter 4.6.

f) Fiber angle deposition

Coronary artery has aligned and oriented collagen fibers to strengthen the vascular wall. It has been demonstrate that each artery layer has different fiber orientation and this can be translated into a direction of maximum strength and stiffness. For achieving similar mechanical properties in the vascular graft, our approximation was to resemble the collagen fiber organization in each layer. The fiber orientation was determined from a constitutive model of each human coronary artery layer (Holzapfel el al., 2005). For middle layer the angle deposition was 21° and for outer layer the angle deposition was 67° mimicking the media and adventitia orientation respectively. No fibers were deposited in the inner layer because its main role is the endothelial layer development and not the mechanical properties.

In this chapter we were able to determine and improve a manufacturing method for engineered tissues. On the one hand, the hydrogel solution parameters were determined to obtain layers that are able to deposit with the dipping-spinning technique, are resistant and with low cellular toxicity. On the other hand, the SBS manufacturing parameters were determined to deposit fibers with different orientations and with waviness in order to mimick the collagen fiber structure in arteries. The next chapter presents the Chapter 5 presents the manuscript submitted to the Journal Nature Communications where this manufacturing methodology is used to produce vascular grafts. The main objective of this work is to obtain mechanical properties that resemble the native behavior and at the same time incorporate cells to achieve biological function, and therefore be able to use it to as a replacement of human coronary arteries in a bypass surgery.

5. RAPID FABRICATION OF REINFORCED AND CELL-LADEN VASCULAR GRAFTS STRUCTURALLY INSPIRED BY THE HUMAN NATIVE CORONARY ARTERIES

Tamara L. Akentjew[1,2,3], Claudia F. Terraza[1,2], Camila A. Wilkens[1,2], Jonny J. Blaker[4], Jekaterina Maksimuck[5], Claudio M. García-Herrera[6], Javier I.Enrione[7], Loreto M. Valenzuela[3], Maroun Khoury[1,2,8] and Juan Pablo Acevedo[1,2,8,*]

[1]Laboratory of Nano-Regenerative Medicine, Faculty of Medicine, Universidad de los Andes, Santiago, Chile

[2]Cells for Cells, Santiago, Chile

[3]Department of Chemical and Bioprocess Engineering, School of Engineering, Pontificia Universidad Católica de Chile, Santiago, Chile

[4]Bio-Active Materials Group, School of Materials, MSS Tower, The University of Manchester, Manchester M13 9PL, UK

[5]School of Materials, MSS Tower, The University of Manchester, Manchester M13 9PL, UK

[6]Departmento de Ingeniería Mecánica, Universidad de Santiago de Chile, Santiago, Chile

[7]Biopolymer Research and Engineering Lab (BiopREL), Universidad de los Andes, Santiago, Chile

[8]Consorcio Regenero, Santiago, Chile

Affiliations Address: Centro de Investigación Biomédica, Universidad de los Andes, San Carlos de Apoquindo 2500, Santiago, Chile

*Corresponding author

Corresponding author, San Carlos de Apoquindo 2500, las Condes, 7620001, Santiago, Chile; Phone: +562 26181447; jpacevedo@uandes.cl

5.1 Abstract

Design strategies and fabrication of vascular grafts are converging from suboptimal synthetics prosthesis toward native-inspired tissue engineered grafts, especially for replacement of small diameter blood vessels (SDBV). In this work, a new automated technology is presented that combines a dipping-spinning methodology for the deposition of concentric cell-laden hydrogel layers, with an adapted solution blow spinning (SBS) device for intercalated placement of aligned reinforcing nanofibers between the cell-laden layers. This methodology allows the assembly of a natural structural inspired configuration of different concentric cell types with fibers in specific angles and arrangements. By adjusting the configuration of the middle and outer layers the production of a vascular graft with the typical J-shape mechanical response and compliance of the human coronary artery is achieved. Cellular content was successfully included in a concentric and homogenous distribution with no significant cytotoxic effect. This study demonstrates the wide versatility and scalability of this automated system to fabricate complex cellularized multilayer vascular grafts in less than 1 h. Interestingly, this combined dip-spinning-SBS technology was capable to generate a native-inspired distribution of extracellular matrix (ECM), enabling grafts to be obtained with native mechanical properties, of critical importance for bypass applications.

5.2 Introduction

Cardiovascular diseases are leading the global mortality and morbidity rates; representing 31% of all global deaths in 2015 (WHO, 2017). Only the coronary heart disease by itself was the cause of 7.4 million deaths, placing it as the main cardiovascular disease (WHO, 2017). These numbers are expected to increase due to the rapid demographic aging of the population (Mathers et al. 2006) and global cardiovascular deaths will reach 22.2 million in 2020 (WHO, 2013). This high medical need is largely unaddressed, as today's technologies are still unable to overturn this catastrophic scenario, yet.

Although autologous vessels (saphenous vein, arm vein, mammalian artery, or radial artery (Rathore et al. 2012) remain as the best alternative for the bypass of small diameter blood vessels, their application is limited by pre-existing vascular diseases, previous organ harvesting, amputations, limited length, low quality or considerable morbidity associated with autologous harvesting (Tien et al., 2006, L'Heureux et al. 2007, Rathore et al. 2012, Nemeno-Guanzon et al., 2012).

Vascular prostheses made of synthetic materials such as polytetrafluoroethylene (ePTFE) or polyethylene terephthalate (Dacron) have been widely used for large or medium diameter blood vessel replacement (Ercolani et al. 2013). However, when used as a small diameter vascular graft, synthetic prostheses have a tendency to occlude due to thrombosis and intimal hyperplasia, caused mainly by compliance mismatching between the natural blood vessels and the graft, leading to failure in the short term (Pashneh-Tala et al., 2015, Bustos et al., 2015). This makes synthetic prostheses unsuitable for the replacement of small diameter blood vessels such as coronary arteries (ID<6 mm).

Optimal vascular grafts must have comparable mechanical properties to native blood vessels. For this reason, strategies that incorporate a well-organized collagen-like matrix and an elastin network during the fabrication of vascular grafts are preferred to sustain physiological pressures and to provide the necessary compliance and recoil (Rathore et al. 2012). Additionally, optimal small diameter vascular grafts must resist thrombosis activation *in vivo*. Natural vessels inhibit actively the thrombus formation by the activity of the endothelial cells at the intima layers.

Tissue engineering emerged as an alternative inspired by the structure of blood vessels, seeking to replicate the biological and mechanical properties of native vessel tissue. Blood vessels are composed of three layers: the intima, media and adventitia. The intima layer consists of the endothelium, a monolayer of cells that provides a blood-compatible luminal interface. The media layer, largely responsible for the mechanical properties, is composed by smooth muscle cells,

elastin and collagen fibers. Finally, the adventitia layer is a protective coating of cells and ECM, is mainly composed by collagen and fibroblasts. Both, active (smooth cells) and passive (elastin and collagen fiber) components have roles in the mechanical response of arteries, with cyclical mechanical behavior governed by the elastin and collagen fibers. The variations in fiber orientation and composition in each layer are responsible for the different mechanical properties at the different branch hierarchy in the vascular tree. Furthermore, the amount of collagen fibers and their orientations varies depending on the vessel layer, type of vascular vessel, the species and the physiological stress or pressure to which it is naturally subjected (Holzapfel et al., 2005; Schriefl et al., 2011; Agianniotis et al., 2011). Studies in human coronary arteries concerned with numerically modeling the mechanical behavior of the vessel have determined that collagen fibers in the adventitia are oriented at an angle of 67° relative to the circumferential axis, while those in the media are oriented at 21° (Holzapfel et al., 2005). This is consistent with collagen fiber orientations observed in coronary artery layers through advanced microscopy techniques (Chen et al., 2011). Arteries under internal pressure present a non-linear elastic response, characterized by a deformation profile with a characteristic J-shape curve. High compliance of arteries at low or physiological pressures is conferred by the elastin membranes and intercalated elastin fibers in the media and adventitia. When the pressure increases beyond the elastic resistance of elastin fibers, wavy collagen fibers start stretching and govern the mechanical behavior at the final linear section of the J-shape curve (Dornhoffer, 1998).

Blood vessel grafts have been developed using various techniques such as decellularization (Amensag et al., 2012, Cho, et al. 2005), self-assembled cell sheets (Kelm et al., 2010, Bourget et al., 2012) and scaffold–based methods (Niklason et al., 1999, Boccafoschi et al., 2007, Thomas, et al. 2013). Electrospinning, coating and bioprinting are some of the manufacturing scaffold-based methods used to generate a variety of vascular grafts from natural, synthetic,

or both materials (Pashneh-Tala et al., 2016). Some studies have reported a vascular grafts with similar J-shaped stress-strain response curves, and compared them to native ovine carotid arteries (Peng et al., 2010), bovine arteries (Iwasaki et al., 2008), the rat abdominal aorta (Wu et al., 2012) and porcine carotid artery (Rapoport et al. 2012). Only few have developed grafts to replace human coronary arteries and compared their mechanical properties (Stankus et al. 2007, MacMahon et al. 2011, Montini-Ballarin et al., 2016; Peng et a., 2010; Iwasaki et al., 2008; Wu et al., 2012; Rapoport et al., 2012). Tubular constructs made from electrospun meshes of poly(ester urethane) urea (PEUU) (Stankus et al. 2007) in combination with poly(ethylene glycol)-fibrin hydrogels (MacMahon et al. 2011) have shown similar J-shape curve in the circumferential direction. Recently, an electrospun vascular graft of poly(ester urethane) (PEU) and poly(L-lactic acid) (PLLA) was able to resemble the mechanical behavior of collagen and elastin (Montini-Ballarin et al., 2016). For the achievement of immediate native-like mechanics, most of these techniques use synthetic polymers during manufacturing, usually requiring a further stage of cell seeding followed by long incubation times to incorporate the biological component (Peng et a., 2010; Iwasaki et al., 2008; MacMahon et al., 2011). Cell seeding is often ineffective for obtaining a homogeneous cell distributed throughout the scaffold. On the other hand, although mechanically appropriated, non-cellularized strategies (Wu et al., 2012; Rapoport et al., 2012; Montini-Ballarin et al., 2016) obscure the fulfillment of biological function and the benefits of having cells in the vascular graft. Long time maturation with pulsatile bioreactors of grafts fabricated with hybrid synthetic/natural material, with post cell-seeding, have shown beneficial effects in terms of final mechanical properties and improved cell infiltration and tissue formation (Iwasaki et al., 2008). A combination of fiber electrospinning and electrospraying of SMCs have proven useful in the fabrication of vascular grafts with homogeneous cells distribution, which as well exhibit J-shaped stress-strain curve and compliance values close to the native coronary arteries after three days in dynamic culture (Stankus et al., 2007). Nevertheless, none of these studies combine mimicry of the three layer

structure present in arteries, the orientation of collagen fibers in each layer and the distribution of different cells patterned across and throughout the different layers in the graft, recapitulating both mechanical properties (compliance) and biological function after implantation.

By reinforcing layers of cell-laden methacryloyl gelatin-alginate (GEAL) hydrogel with poly(ε-caprolactone) (PCL) fibers, the J-shape mechanical response and compliance of human coronary arteries were successfully reproduced. This resulted in an mimick of the observed orientation and waviness of collagen fibers similar to natural vessels. This strategy combines the cell-laden hydrogel with co-deposition of fibers to rapidly fabricate a ready to use and mechanically native-like vascular graft with the advantage of a controlled and customized distribution or patterning of cells across the different concentric layers. This advance will provide new effective tools for the treatment of coronary diseases.

5.3 Methods

5.3.1 Preparation of methacryloyl gelatin-alginate (GEAL) solution.

Methacryloyl gelatin-alginate (GEAL) was synthesized following a previously described protocol (Nichol et al. 2010; Van Den Bulcke et al. 2000). Briefly for Methacryloyl gelatin (GelMA) synthesis, a 10% (w/v) bovine gelatin (Bloom 220, Rousselot, Netherlands) solution in PBS 1x (pH 7.4) was prepared and maintained under agitation at 60°C. Methacrylic anhydride (Sigma, US) was added drop-wise to a final concentration of 8% (v/v), allowing the functionalization reaction to occurred for 3 hrs. Methacryloyl functionalization was stopped after adding 3 volumes of PBS 1X, and latter submitted to 7 days of dialysis (cut-off molecular weight of 8 kDa) to remove the non-reacted methacrylic anhydride. The solution was freeze-dried and stored at room temperature for later use. Three stock solutions were prepared. First, the GEAL stock solution was prepared by dissolving freeze dried GELMA in PBS 1X at 40°C at a concentration of 20% (w/v). Then, a 2% (w/v) alginate stock solution was prepared by dissolving medium viscosity sodium alginate (A2033, Sigma, USA) in PBS 1X under

continuous stirring at 60°C. For the preparation of a photoinitiator (PI) stock solution, 2-Hydroxy-4′-(2-hydroxyethoxy)-2-methylpropiophenone (410896, Sigma, USA) was fully dissolved in PBS 1X at 85°C to obtain a concentration of 2% (w/v), maintained at that temperature before used to avoid crystallization of the reagent. The GEAL solution was obtained after mixing the three stock solutions and the volume adjusted using PBS 1X to a final concentration of 10% (w/v) of GELMA, 0.5% (w/v) of alginate and 0.2% (w/v) of PI.

5.3.2 Deposition of PCL interlayers.

PCL interlayers were fabricated using PCL spun fibers using a combination of custom-made solution blow spinning (SBS) system (Medeiros et al. 2009; Mederios et al., 2016) and a dipping-spinning machine (Wilkens et al. 2016). PCL (440744, Sigma-Aldrich, USA) was dissolved in a mixture of 80/20 v/v ratio of chloroform/acetone to reach a final PCL concentration of 7% (w/v). The solution blow spinning configuration is illustrated in Figure 5-1a and Figure 5-1c. The system comprises an air compressor (Huracan 1520, Indura, Chile) equipped with a pressure regulator adjusted to 60 psi; additionally, a 10 mL hypodermic syringe is mounted in a syringe pump (NE-4002X, New Era Pump Systems, Inc. NY, USA) to control the injection rate of the PCL solution at 120 µL/min. Both, the compressed air and the flowing PCL solution are connected and converged into a spraying apparatus that consists of a concentric nozzle system with a central flow of PCL solution a peripheral flow of pressurized air (Figure 5-1c). The nozzle system could be placed at different positions and angles with respect to the dipping axis of the vascular graft. For fiber deposition, the system requires the dipping-spinning machine coupled to a deposition rod that moves downward and upward at a rate of 138 mm/min while spinning the same rod at 42 rpm (Figure 5-1a). This configuration allows a homogeneous fiber deposition along the spinning rod. A complete cycle of spinning down-and-up movement takes 30 sec and the distance between the SBS nozzle and the point of fiber deposition on the rod surface was kept constant at 30 cm.

For the fabrication of the adventitia layer, the SBS nozzle was orientated at 67° with respect to the circumferential axis of the graft, while for the media layer the orientation was 21°. This allowed the placement of aligned fibers in a specific orientation. The fibers were deposited while the rod was subjected to down-and-upward movement. A simultaneous alternated spinning that consisted of cycles of 1 s clockwise rotation at 42 rpm followed by a 0.5 s anti-clockwise rotation at 42 rpm allows the inclusion of waviness at the oriented PCL fibers (see Figure 5-S1 This particular approach was adapted in order to increase the waviness of fibers and imitate the natural configuration of collagen fiber (Chen et al., 2011,Rezakhaniha et al., 2012; Chen et al., 2013). To deposit a sequence of PCL fibers in opposite orientation in order to form an angled mesh comprising the PCL sublayer, the whole dipping-spinning device was switched from forward to backward position, and the spinning movement was changed to 1 s anti-clockwise rotation at 42 rpm followed by a 0.5 s clockwise rotation at 42 rpm (see Figure 5-1). One PCL fiber layer consists in one cycle in the positive angle and one cycle in the negative angle for achieving a meshed layer.

5.3.3 Deposition of individual GEAL sub-layers.

GEAL layers were generated with a custom-made CNC machine (Wilkens et al., 2017). Each layer is fabricated through several dippings of a rod previously covered with a PCL sublayer into the GEAL solution. The gelatin-based pre-crosslinked hydrogel solution was kept in a water bath at 30°C to avoid spontaneous gelation at room temperature. Crosslinking was achieved during emersion of the rod by exposing the temporally coated rod (gelatin solution is briefly stabilized before photo-crosslinking by cohesive forces) to UV light at 365 nm wavelength (1.21 W/cm^2) (OmniCure® S2000, Excelitas Technologies, USA). The UV source is place at a distance of 2 cm from the rod while the coated mandrel was rotating at 42 rpm and emerging at 138 mm/min upward-speed. (Figure 5-1b)

The middle and outer layer, which represent the media and adventitia layers of a natural artery, were fabricated intercalating GEAL and a PCL interlayers. For the middle and outer PCL interlayers, the SBS nozzle was oriented at ± 21° and ± 67° with respect to the circumferential axis (see Figure 5-S2). One graft sublayer/bilayer typically consists of one PCL fibre layer and one crosslinked GEAL layer. Different composition of sublayers and layers (see Figure 5-5) were tested in order to determine the best composition in terms of mechanical response. For this reason, the GEAL sublayers can be composed of 1, 2 or 3 cycles of dipping and UV-crosslinking. Additionally, the complete middle and outer layer can comprise series of 4, 5, 8, or 10 middle or outer graft sublayers respectively. The better mechanical performing middle layer was fabricated with 4 series of middle graft sublayer, consisted at the same time of a PCL interlayer and a GEAL interlayerlayer generated after 2 cycles of dipping and UV-crosslinking. The best outer layer consisted of 5 series of outer graft sublayers, in which the GEAL sublayer required 3 cycles of dipping with UV-crosslinking.

Transparency of alginate mandrel facilitates imaging of PCL fiber orientation of the middle and outer PCL layers, in which visualization was performed using a light microscope. Middle and outer PCL layers were imaged using a Scanning Electron Microscopy (SEM, LEO 1420 VP). The fiber orientation was measured with ImageJ software (National Institutes of Health, USA). Layer thickness was measured on each sample with a micrometer with 0.01 mm of accuracy.

5.3.4 Fabrication of a full vascular graft using GEAL layers reinforced with PCL fibers

A full bio-inspired vascular graft (BIVG) based on the reinforced GEAL hydrogel consists of three layers: inner, middle and outer, mimicking the tissue configuration of native coronary arteries (intima, media, and adventitia, respectively). For the inner layer, a GEAL sub-layer was fabricated after 9 cycles of dippings and UV-crosslinking using the alginate-coated rod (see Support Information) and the CNC machine. On top of the inner layer, an optimized

middle layer was manufactured as described above. Subsequently, the concentric optimized outer layer was fabricated around the middle one. Finally, the plastic rod and alginate coat were removed mechanically.

5.3.5 Micro and nano CT images

In order to analyze the macro/micro-structure of the full BIVG, some constructs were freeze-dried and images were acquired using a Micro-CT (SkyScan 1272, Bruker-microCT, Kontich, Belgium) operated at 40 kV and 250 µA. Additionally, a full fiber BIVG was fabricated, consisting only of PCL interlayers and images were obtained using high-resolution synchrotron X-ray tomography, performed at Diamond-Manchester branchline I13-2 at Diamond Light Source (Rau et al., 2011). A polychromatic filtered parallel-beam was used with a 0.33 µm effective pixel size. Over the 180° rotation, 3600 projections were collected at 0.05 s exposure time. The projections were tomographically reconstructed into a 3D volume using software developed at Diamond Light Source (Atwood et al., 2015). Visualization package Avizo was used to produce the 3D images.

5.3.6 Tensile test

a) Middle and outer layer tensile test

The middle and outer layer of the BIVGs were tested under uniaxial tension using a Texture analyzer (Stable Micro Systems, TA.XT.plus, Surrey, UK) with a 5 N load cell. For this end, rectangular samples of the graft oriented in the circumferential and longitudinal direction were cut, placed and maintained at 37° in PBS 1X (pH 7.4). For each layer, three samples were cut and tested in both directions, circumferential and longitudinal. Sample thickness and width were measured using a micrometer caliper with 10µm accuracy. For mechanical analysis, the sample length was considered as the distance between clamps in the texture analyzer after positioning the sample. Before the testing was carried out, five loading and unloading cycles at a constant rate of 10 mm/min were applied as the preconditioning step. The preconditioning loading/unloading cycles of the

outer layer in the longitudinal and circumferential direction did not exceed a 13% and 30% of strain, respectively. In the case of the middle layer, the strain during preconditioning did not exceed 35% and 30% in the circumferential and longitudinal direction, respectively. Uniaxial testing for both, circumferential and longitudinal samples, were performed at a constant rate of 10 mm/min (see Figure 5-S3a).

b) BIVG tensile test

BIVGs were tested under uniaxial (García-Herrera et al., 2012a) using a universal testing machine (Instron 3342, Norwood, MA, USA) with a 10 N load cell. Rectangular samples oriented circumferentially and longitudinally were cut, maintained and tested while being permanently immersed in phosphate buffered saline 1X (PBS) at 37° ± 0.5°C. For each BIVG, 5 samples were tested. Sample thickness, width and length were measured using image processing techniques. Before carrying out the tensile testing, five loading/unloading cycles were performed up to a 30% of strain at a constant rate of 10 mm/min. The uniaxial testing of samples was performed at a constant rate of 1 mm/min (see Figure 5-S3b).

Stress-strain curves for all tests were derived from axial load and clamps displacement recorded along the test. The stress was computed as F/A, where the F is the tensile load with a precision of 0.01N and A is the initial cross-sectional area. The strain was computed as $100*L/L_0$, with L and L_0 as the current and initial sample length, respectively.

c) Pressurization test

The pressurization test was used to study the response of the full BIVG under simulated conditions of human *in vivo* loading and pressure conditions (García-Herrera et al., 2012a). The test was performed in a customized set up using a universal testing machine (Instron 3342, Norwood, MA, USA), adapted with a plastic transparent chamber filled with PBS 1X at controlled temperature, 37° ±

0.5°C. The internal pressure was applied using an auxiliary line of PBS at 37°C connected to the internal graft lumen. The pressure was measured at the entrance of the chamber with a pressure transducer, whereas the graft diameter was measured using image processing techniques. Five samples with an average length of 5 mm were tested. Before testing, five loading/unloading cycles in the axial direction of the graft were applied, up to a 30% of strain, at a constant rate of 10 mm/min as preconditioning step. An additional preconditioning step in the circumferential direction was performed using 5 cycles of pressurization from 0 to 200 mmHg. Pressurization test of the full BIVGs were performed under three different constant axial strains, 10%, 20% and 25%.

The compliance value of full BIVGs (%C) was computed from the experimental data at three pressure ranges (50-90, 80-120, 110-150 mmHg), according to standard ISO 7198 (ANSI/AAMI/ 2010), and using following equation:

$$\%C = \frac{(R_{P_2} - R_{P_1})/R_{P_1}}{P_2 - P_1} * 10^4 \quad (1)$$

Where P_1 and P_2 correspond to the lower and higher range of pressure values in mmHg, and R_{P1} and R_{P2} are the external radiuses generated at those pressures, respectively.

5.3.7 Cell viability and Proliferation tests

a) Cell culture

Human Umbilical Cord Cells (HUVEC) (ATCC® CRL1730™) and Bone Marrow Mesenchymal Stem Cells (MSCs) were cultured and expanded in culture medium (high glucose Dulbecco's Modified Eagle's medium (DMEM) (16000-044, Gibco, USA) supplemented with 10%(v/v) fetal bovine serum (FBS) (16000-044, Gibco, USA), 2 mM glutamine (25030-081, Gibco, USA) and 1% (v/v) penicillin-streptomycin (15140-122, Gibco, USA)) and incubated at 37°C, 5% CO_2 and 96% of humidity. HUVECs or bone marrow MSCs were mixed in the GEAL solution at a concentration of 10 million cells mL^{-1}. BIVGs were fabricated as mentioned

before using a mixture of GEAL solution and cells in order to encapsulate the cells within the GEAL sublayers.

b) BIVG cell proliferation test

Cell proliferation tests were performed using a 5mm cylindrical section of the full BIVGs with HUVECs encapsulated using the WST-1 Cell Proliferation Colorimetric Assay Kit (K302, Biovision, USA). Briefly, this assay quantifies the metabolic cleavage of WST-1 to generate formazan by cellular mitochondrial dehydrogenases. The proliferation was measured at day 1 and day 7 after cell culture of the BIVG sections in culture medium supplemented with amphotericin b (15290-026, Gibco, USA). Cylindrical samples were afterward washed in PBS before including them into 200 µL of culture medium and 20 µL of WST reagent, and incubated for 2.5 hrs. A standard curve was done to estimate the number of cells in the BIVGs. For this, 5000, 10000, 20000 and 30000 cells were seeded and incubated with 200 µL of culture medium and 20 µL of WST reagent for 2.5 hrs. Number of metabolically active cells in the BIVG was obtained interpolating the absorbance values in the standard curve. Cell density was calculated dividing the number of active cells by the BIVG volume (≈30 mm^3).

c) Histological study

The same day of fabrication, BIVGs were embedded in O.C.T. Compound (Tissue-Tek, USA) and sectioned at 14 µm in transversal cuts using a cryostat (Microm, HM525, Walldorf, Germany). For the cell staining, the samples were incubated in Hoechst 33342 solution (Thermo Scientific, USA) following the provider's protocol. Transversal cuts were visualized using a fluorescent microscope (CKX41, Olympus, USA).

5.3.8 *In vivo* functionality of encapsulated cells in the fabricated BIVG

Six- to eight-week-old C57BL/6 wild-type mice and from the Jackson Laboratory (USA) were used in this study. Experiments were carried out at the Universidad de los Andes-Cells for Cells Animal Facility (Santiago, Chile) following the

institutional guidelines for care and experimentation with laboratory animals and approval the Institutional Ethical Committee.

Acellular BIVGs were fabricated using GEAL solution without cells. Cellularized BIVGs were fabricated mixing the GEAL solution with bone marrow MSCs in order to encapsulate the cells within the GEAL sublayers. Subcutaneous implantation of a cylindrical cut of the acellular and cellularized grafts was performed through a dorsal incision and suture of anesthetized mice with vaporized sevoflurane.

Skin grafting was performed as described previously (Campos-Morales et al., 2015), as rejection control. Briefly, tail skin (~ 1 cm^2) from C57BL/6 donors was transplanted onto the dorsal area of BALB/c. At day 14 post surgery, draining lymph nodes (dLNs) from graft recipients were obtained for further analysis. After 14 days, the BIVGs and draining lymph nodes (dLNs) from recipients were explanted for further analysis.

a) *In vivo* cell functionality of BIVGs flow cytometry analyses

dLNs obtained after surgery were processed and draining LN cells were quantified and stained using anti-mouse CD4, CD25, CD62L, CD44, Foxp3, CD19, MHC-II, CD86, CD11c, all from BioLegend (San Diego, CA) and conjugated with different fluorochromes. FACS data acquisition was performed with FACS Canto II cytometer by using the FACS Diva software (BD Biosciences, San Jose, CA). Data were analyzed using flowjo software (Tree Star, Canton, OH).

5.3.9 Statistical Analysis

Data are presented as mean ± SD. Statistical significance was determined using two-tailed T-student test in compliance and cell density of bioinspired BIVGs (Figure 5-7 and Figure 5-8). Two-tailed Mann-Whitney test was applied for the *in vivo* functionality experiments (Figure 5-9). For these conditions, 95% of confidence was used and significance was denoted as *$P \leq 0.05$, **$P \leq 0.01$ and ***$P \leq 0.001$.

5.4 Results

5.4.1 Combining two different fabrication technologies generates suitable vascular sublayers

In order to obtain mechanically suitable multilayer grafts, tubular GEAL sublayers reinforced with PCL fibers sublayers were fabricated combining two different techniques: dipping-spinning and a solution blow spinning (SBS) device positioned at specified angles (Figure 5-1 and Figure 5-2a). With the controlled movement of a computer numerical controlled (CNC) dipping-spinning device, a 3D printed rod out of MED610 Biocompatible resin (OBJ04057, Stratasys, USA) rod is immersed (dipped) in a GEAL solution and then lifted back into air with simultaneous rotational movement (spinning) for homogenous exposure to UV to crosslink the hydrogel using a lateral UV source (Figure 5-2b). Several cycles of dipping-spinning/crosslinking stabilized a concentric sublayer of GEAL around the rod, in which the layer thickness is control by changing the number of cycles. After GEAL crosslinking, a series of two cycles of fibers deposition at opposing angle orientations were applied to form a veil-like PCL sublayer using the SBS system (Figure 5-2). This process was repeated to build up multiple cell-laden hydrogel layers with interleaved fibers sprayed at prescribed angles.

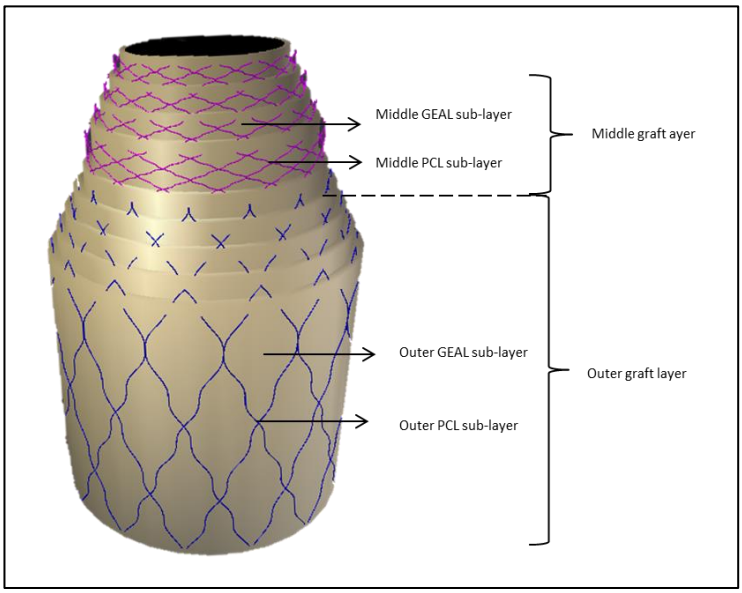

Figure 5-1: Scheme of middle and outer layers composition. Middle layer is composed of 4 series of a PCL sublayer with wavy fibers deposited at 21° and GEAL sublayer generated after 2 cycles of dipping and UV-crosslinking. Outer layer is composed of 5 series of a PCL sublayer with wavy fibers deposited at 67° and GEAL sublayer generated after 3 cycles of dipping and UV-crosslinking.

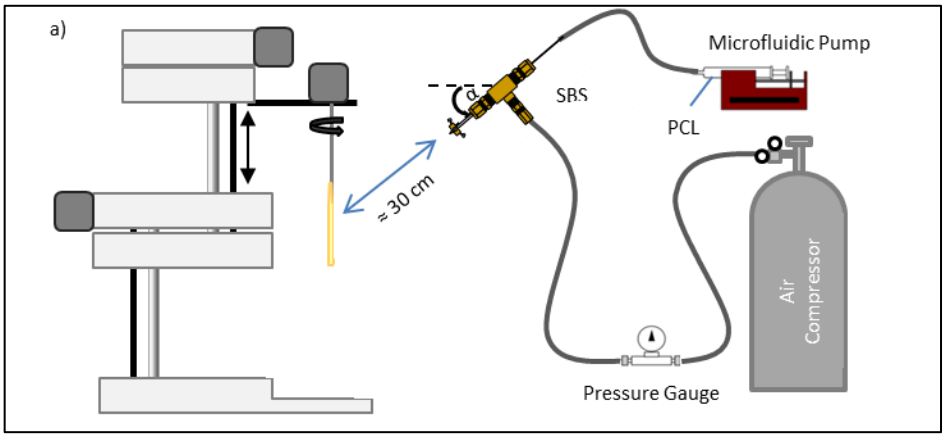

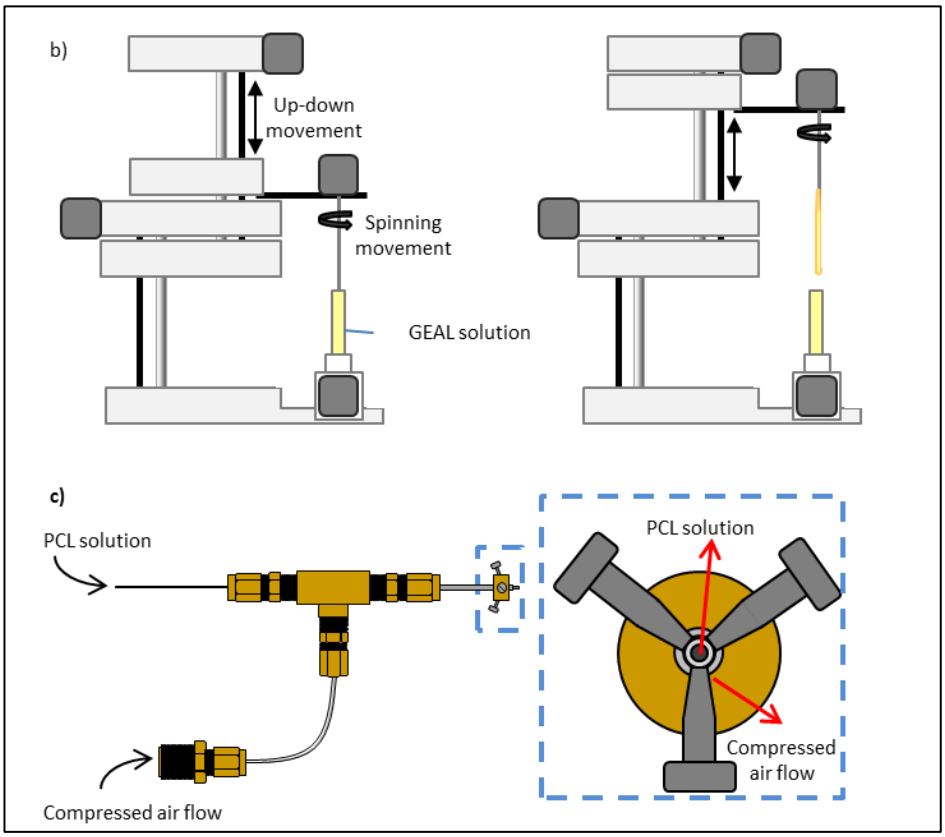

Figure 5-2: Fabrication method of bio-inspired vascular grafts through the deposition of GEAL and PCL fibers. a) Tubular scaffolds were fabricated combining the dipping-spinning technique and the SBS system. b) Fabrication of GEAL sub-layers through a dipping in pre-crosslinking GEAL solution and spinning for the exposure to UV light. c) Fabrication of PCL fiber interlayers through the deposition of fibers into a spinning rod using the solution blow spinning technique. The PCL solution is pumped through a thin, central and inner nozzle. The compressed air flows through the spraying apparatus and converge to an outer and concentric nozzle at a high pressure. The nozzle geometry and the airflow allow the PCL solution to form fibers after solvent evaporation.

During the fabrication of the PCL fiber interlayers, fiber orientation can be controlled by changing the nozzle angle and the direction of the rotational movement of the mandrel. Angles are defined with respect to the circumferential axis of the mandrel (Figure 5-2a). To reproduce the arrangement of collagen fibers

observed in natural blood vessels, and to understand the extent to which the fiber angles govern the mechanical behavior of the cylindrical multilayer constructs, veil-liked PCL sublayers were fabricated using the combination system described, adjusted for fiber deposition at angles of 21° (Figure 5-3a) and 67° (Figure 5-3b). For fiber interlayers fabricated at 21°, the resultant fiber angles had an average values of 31 ± 31° (Figure 5-3c) in one orientation and -28 ± 32° (Figure 5-3e) in the opposite orientation. For fiber interlayers fabricated at 67º, the resultant angles were measured to have an average value of 78 ± 22° (Figure 5-3d) while the oppositely oriented fibers were -77 ± 22° (Figure 5-3f). Major differences in mechanical response were observed for veil-like interlayers fabricated at 21° and 67° angle as evidenced in Figure 5-3g-h. A strikingly stiffer behavior is shown in the longitudinal tensile testing for interlayers with fibers deposited at an angle of 67° (Figure 5-3h) in comparison with fibers at 21° (Figure 5-3g). However, the characteristic J-shaped mechanical behavior was not attained even after varying the amount of deposited fibers (see Figure 5-3g-h). Two new approaches were done to overcome this.

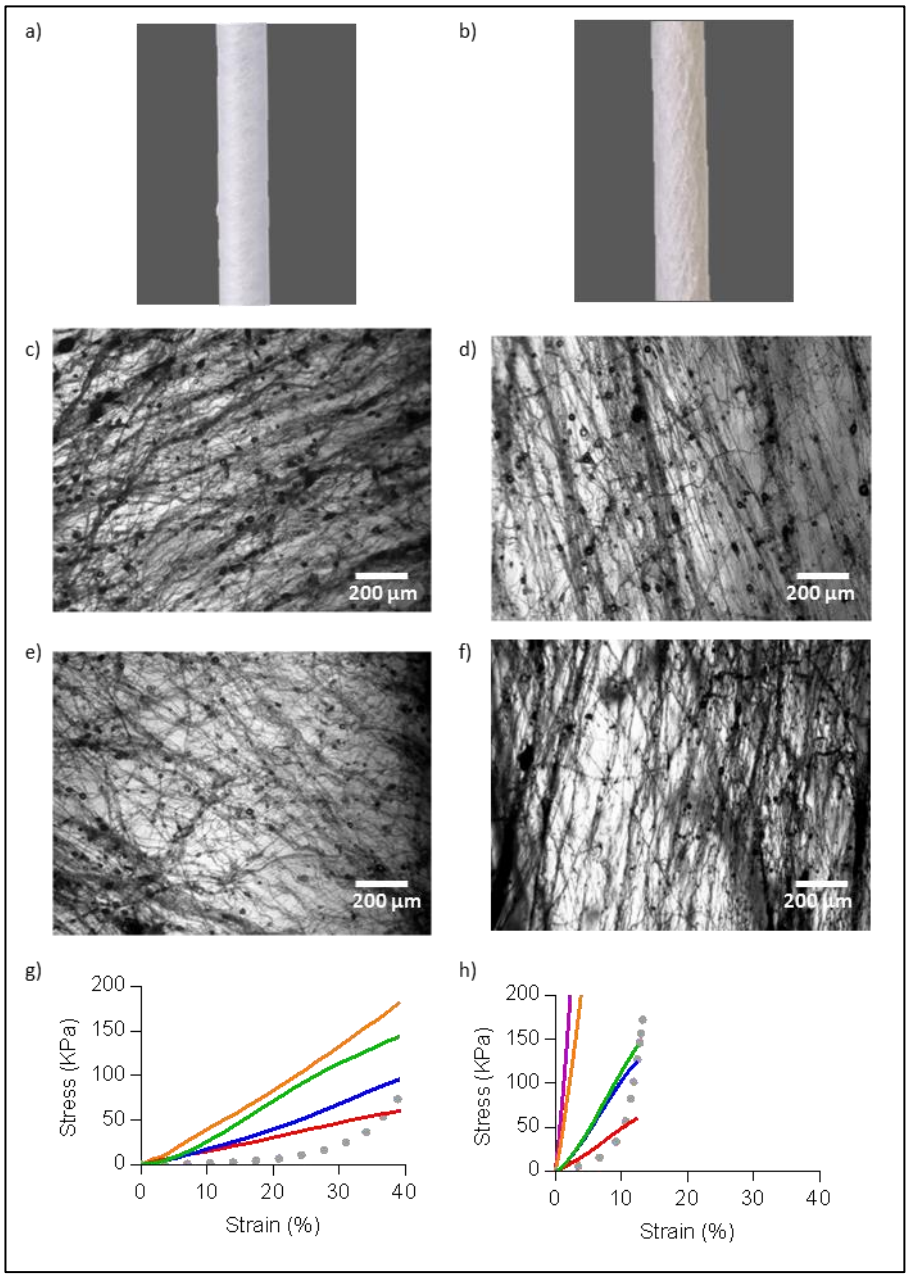

Figure 5-3: PCL inter-layers: (a) Co-deposition of PCL fibers at -21° and +21°. (b) Co-deposition of PCL fibers at -67° and +67°. (c-f) Fibers observation through optical microscopy was performed for fibers deposited at a single cycle around the alginate rod. Clockwise (c-d left) and anti-clockwise (e-f right) cycle deposition at 21° (c-e) and 67° (d-f) deposition angles were carried out for microscopy observation. Original magnifications 10X (c-f). (g-h) Strain-stress curves of PCL

sub-layers fabricated at a deposition angle of 21° (g) and 67° (h), and subjected to longitudinal tensile testing. PCL sub-layers were manufactured depositing 2 cycles (red), 4 cycles (blue), 8 cycles (green), 24 cycles (orange), 40 cycles (pink) of oriented PCL fibers. Every fiber deposition cycle takes 30 s and cycles alternate between clockwise and anti-clockwise deposition to create an angled mesh. 4 min of fiber deposition means 8 cycles of fibers deposition, 4 clockwise and 4 anticlockwise in an alternated manner.

5.4.2 Pre-stretching, wavy and intercalated distribution define J-shaped mechanical behavior

Stress-strain curves of the fabricated PCL interlayers described a linear relationship of variable (Figure 5-3c-d and Figure 5-4a), however natural blood vessels respond mechanically to stress in a non-linear manner, which has been previously described as a J-shape stress-strain curve (Claes et al., 2010). In the attempt to convert PCL sublayer stress-strain curves into J-shape curves, sublayers where conditioned by pre-stretching before mechanical testing. This treatment was capable to generate a more J-shaped curve, although not exactly faithful to the characteristic natural J-shape (see Figure 5-4b). At this point, and analogously to collagen and elastin fibers in natural vessels, the construct has an angled mesh arrangement of PCL fiber, however it lacks the characteristic rippled distribution of collagen and elastin fibers present in natural vascular vessels (Chen et al., 2011,Rezakhaniha et al., 2012; Chen et al., 2013). To include this additional feature in the constructs developed here, alternating clockwise and anti-clockwise rotations of the rod during cycles of PCL fiber deposition. Keeping an unbalanced ratio of clockwise and anti-clockwise rotation (e.g. 1 s in one direction and 0.5 s in the opposite direction), the system generated certain level of waviness capable to generate a more nature J-shape stress-strain curve (see Figure 5-4c, 5-4e and 5-4g).

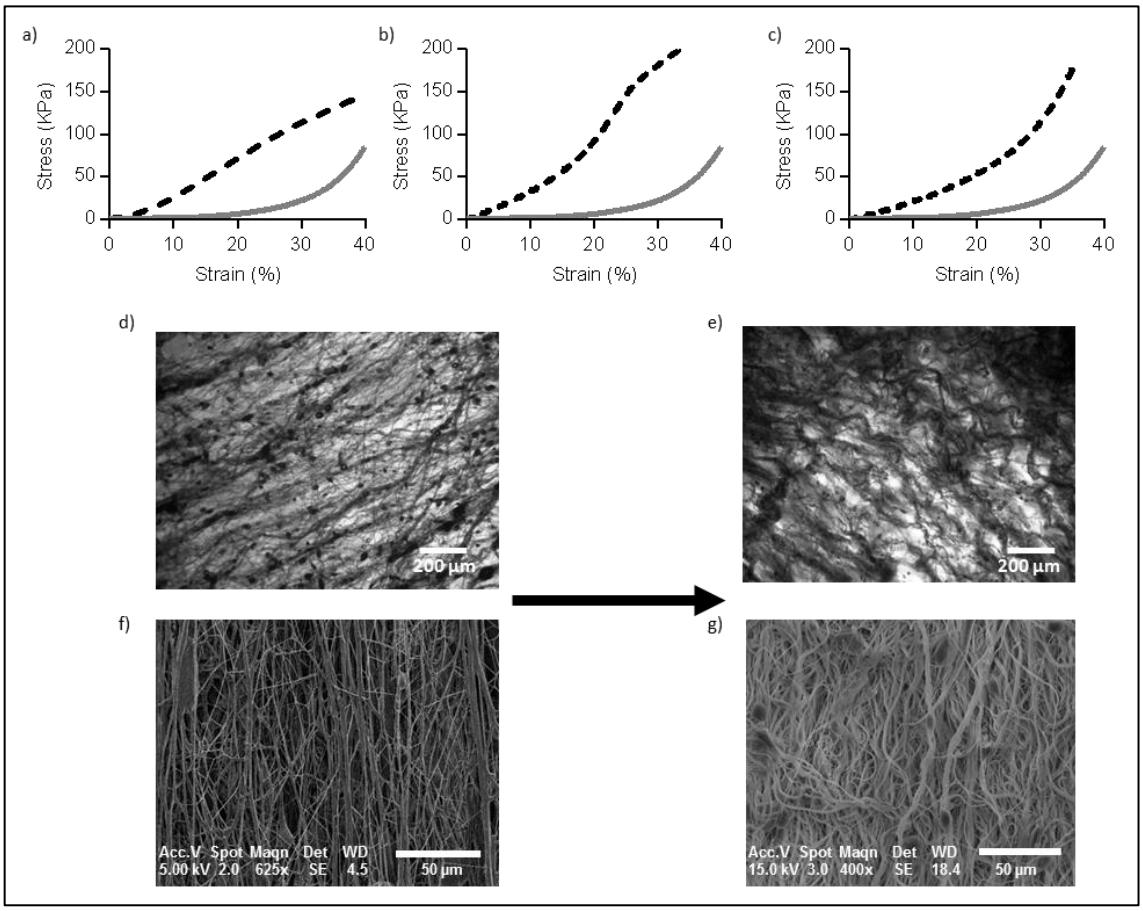

Figure 5-4: Iterative improvement for a J-shape stress-strain curve: (a) Strain-stress curve of a PCL sub-layer (grey) fabricated at a deposition angle of 21° and 48 cycles of alternated fiber deposition. (b) Strain-stress curves of PCL interlayer (grey) fabricated at a deposition angle of 21° and 48 cycles of alternated fiber deposition including a stretch pre-condition step. (c) Strain-stress curves of PCL interlayer (grey) fabricated at a deposition angle of 21°, 48 cycles of alternated fiber deposition and a stretch pre-condition step including alternated rod spinning consisted of cycles of 1 s rotation at 42 rpm followed by a 0.5 s rotation in the opposite direction at 42 rpm, allowing the inclusion of waviness at the oriented PCL fibers. (d) Microscopic image of PCL interlayer fabricated at a deposition angle of 21° and 1 cycle fiber deposition. (e) Microscopic image of PCL interlayer fabricated at a deposition angle of 21°, 1 cycle of fiber deposition with alternated rod spinning consisted of cycles of 1 s rotation at 42 rpm followed by a 0.5 s

rotation in the opposite direction at 42 rpm, allowing the inclusion of waviness at the oriented PCL fibers. (d) Scanning electronic microscopy image of PCL sub-layer fabricated at a deposition angle of 67° and 48 cycles of alternated fiber deposition. (e) Microscopic image of PCL interlayer fabricated at a deposition angle of 21°, 48 cycles of alternated fiber deposition with alternated rod spinning consisted of cycles of 1 s rotation at 42 rpm followed by a 0.5 s rotation in the opposite direction at 42 rpm, allowing the inclusion of waviness at the oriented PCL fibers.

5.4.3 Middle and outer layer mechanical improvement is defined by the composition and intercalated distribution

In order to define the structural configuration of the middle and outer layers of the new bio-inspired vascular graft (BIVG), iterative testing of layer formulations were performed toward resembling the average stress-strain curves of the media and adventitia layers of human coronary arteries (Holzapfel et al., 2005). Following J-shape achievement, it was necessary to adjust the number of graft interlayers in order to reach a close matching between the natural mechanical behavior of media and adventitia layers, and the middle and outer graft sublayer respectively. Each graft sublayer was composed of one PCL interlayer and one GEAL sub-layer (see Figure 5-1). Inspired by the natural distribution of intercalated collagen/elastin fibers and cells in human arteries, we proposed an intercalated configuration of PCL fiber interlayer and GEAL sublayer capable to include concentric patterns of encapsulated cells to incorporate biological function as previously developed in our group (Wilkens et al., 2016). Different numbers of graft interlayers constituted the media and outer layer. Stress-strain curves of the media and adventitia layers were plotted together with the different middle and outer graft interlayer formulations, in which the fiber reinforcement was done by PCL fibers deposition at angles of 21° and 67°, respectively (Figure 5-5a). Clearly, the layers with an orientation deposition of 67° showed a deformation profile (shape of the stress-strain curve), similar to the adventitia layer, whereas the layers

fabricated with fibers deposited at an angle of 21°, were capable to resemble the mechanical behavior of the media layer. Furthermore, the stiffness of layers is higher as the number of graft interlayers increases..

The layer formulation in which its mechanical response most closely approximates the native adventitia layer, hereafter called outer layer, is the one manufactured with 5 series of outer graft interlayers. On the other hand, for mimicking the media layer mechanics, the closest formulation was the one fabricated with four series of middle graft interlayers, hereafter called the middle layer. Inspired by the natural distribution of intercalated collagen/elastin fibers and cells in human arteries, an intercalated configuration of PCL fiber interlayer and GEAL deposition was chosen (Figure 5-5a and Figure 5-6).

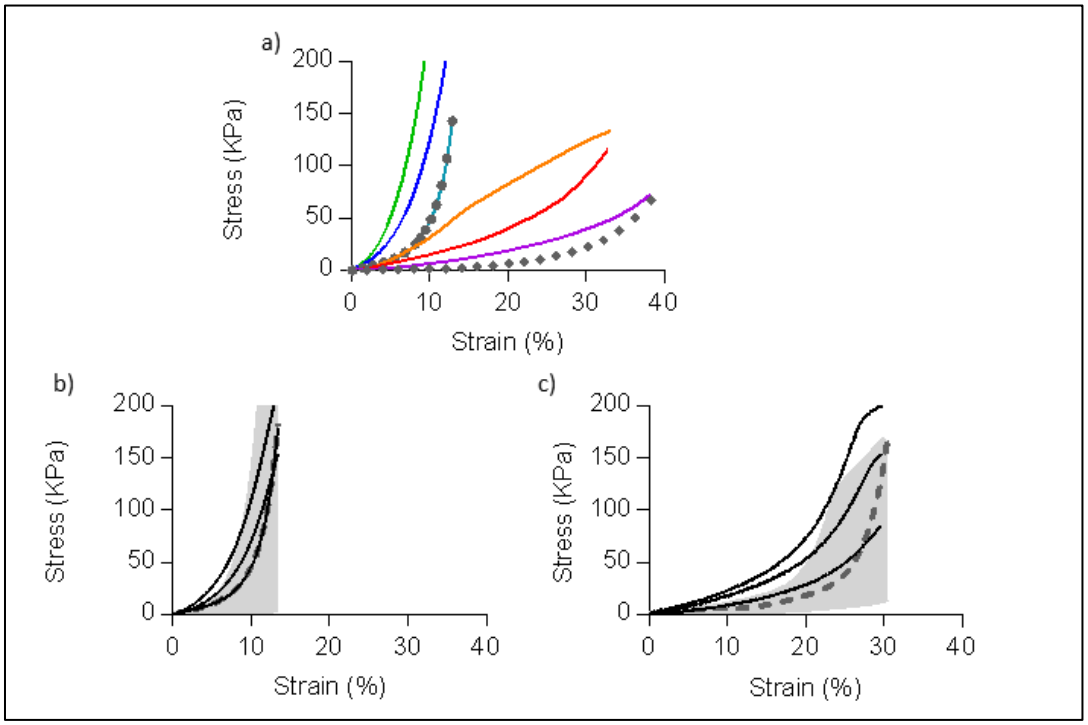

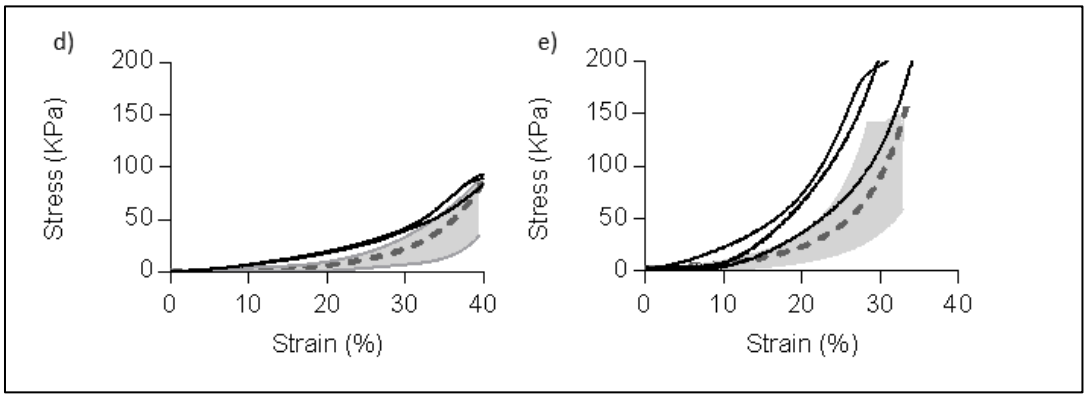

Figure 5-5: Stress-strain curves of the outer and middle layer based on GEAL hydrogel reinforced with PCL sublayers. a) Middle and outer layer iterative improvement: Testing of different compositions allowed us to approach the curve of native media (grey dotted line) and adventitia (grey line) of coronary arteries[12]. Fibers deposited at 67° using a manufacture processing composed of 10 cycles (solid circle), 8 cycles (solid square) and 5 cycles of graft sublayer (solid diamond). Fibers deposited at 21° with a total composition of 10 cycles (open circle), 8 cycles (open square) and 4 cycles (open diamond) of graft sublayer. Stress-strain curves of the (b-c) outer and (d-e) middle layers fabricated with the final composition. For outer layers the fibers were deposited at 67° with 5 cycles of PCL layers intercalated with 15 dipping/crosslinking in GEAL solution. The average model response of the adventitia layer in human coronary artery (grey dotted line) and its range (light grey) were plotted for b) longitudinal and c) circumferential testing, and compared to the iteratively improved outer layer of the BIVG. For middle layers the fibers were deposited at 21° with 4 cycles of PCL sublayer intercalated with 8 dipping/crosslinking in GEAL solution. The average model response of the media layer in human coronary artery (grey dotted line) and its range (light grey) were plotted for d) longitudinal and e) circumferential testing, and compared to the iteratively improved media layer of the BIVG. Every black line corresponds to individual experiments (n=3).

Middle and outer layers had thicknesses of 323 ± 41 and 298 ± 42 µm, respectively. Each layer showed an anisotropic and non-linear mechanical

response similar to the media and adventitia layers of human coronary arteries, respectively. The outer layer showed a stiffer behavior in the longitudinal direction compared to the circumferential direction (Figure 5-5b, 5-5c), whereas the middle layer is stiffer at the circumferential direction (Figure 5-5d, 5-5f). An opposite response is observed between the middle and outer layer in each direction. At the longitudinal direction, the middle layer is more compliant (Figure 5-5d); whereas at the circumferential direction middle layer tends to be slightly stiffer than the outer layer (Figure 5-5c and 5-5f).

In order to visualize the intercalated distribution of the outer and middle layer as a result of the combined fabrication using the dipping-spinning CNC machine and the SBS system, a full BIVS was fabricated, mimicking the three layers of native arteries: the inner (intima), middle (media) and outer (adventitia) layers. The inner layer was based on solely 15 cycles of dippings-spinning/crosslinking in GEAL solution, and the middle and the outer layer were fabricated as specified above (Figure 5-1). The wall thickness of the BIVS is 0.59 ± 0.17 mm and the inner diameter 3.59 ± 0.49 mm. Figure 5-6 shows structural details obtained from Micro and Nano CT data. The 9 graft sublayers can be clearly distinguished, in which the first four correspond to the inner and middle layer, and the last five to the outer layer. In the transversal cut of the structure and micro-CT visualization (Figure 5-6b), PCL-interlayers spaced by the GEAL hydrogel layers can be observed, which introduces the possibility of homogeneously distribute concentric layers of encapsulated cells in between PCL-interlayers. Close Nano-CT inspection at the PCL sublayer (Figure 5-6c), shows good porosity, possibly allowing good cell infiltration after graft implantation.

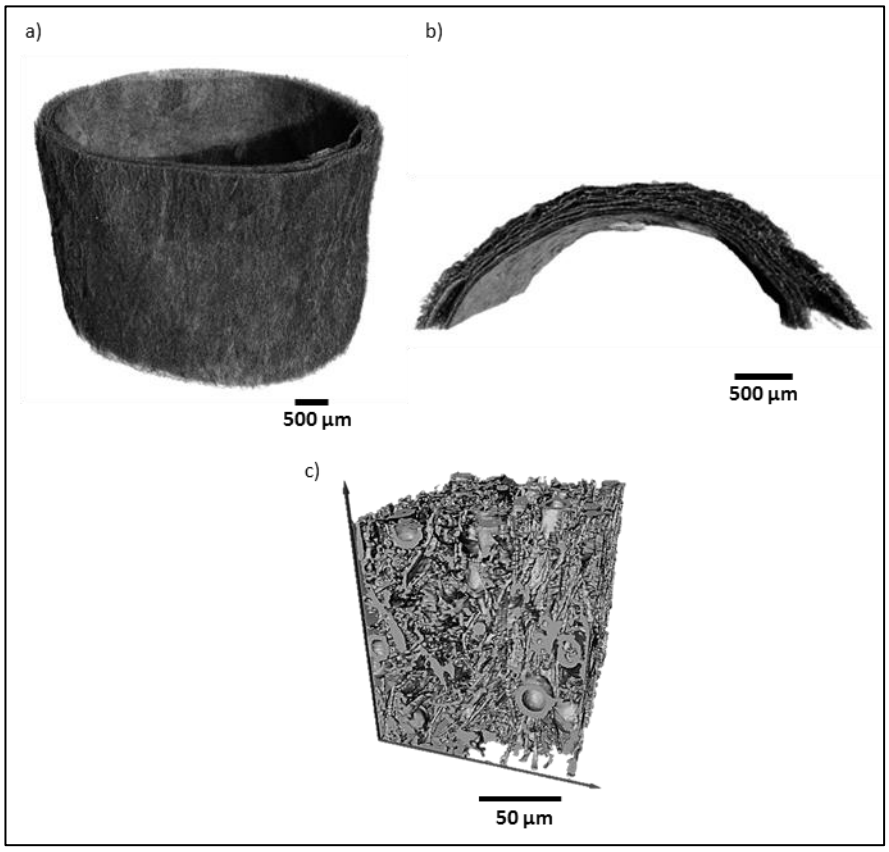

Figure 5-6: Structural images of the BIVS composed of successive GEAL and PCL sub-layers: (a) Micro CT of a lyophilized full BIVSs and (b) the transversal cut. (c) Fibrillar and porous inspection of one PCL sub-layer of the BIVSs in a Nano-CT system.

5.4.4 Mechanical properties of the bio-inspired vascular grafts (BIVG)

When inner, middle and outer layers are tested together in the configuration of a full BIVS, the nonlinear response and a clear anisotropy is maintained. In addition, a similar mechanical behavior to human coronary arteries is achieved in both directions in tensile testing, always inside the range of healthy natural coronary arteries (Figure 5-7a-b). To verify whether the mechanical properties of the bio-inspired BIVS change upon the application of repeated loading and unloading cycles, simulating the pulsatile flow under *in vivo* physiological conditions, 20 repetitions of circumferential stress were performed to a strip taken from the

fabricated BIVS (Figure 5-7c). A linear response is shown in the first cycle, which would correspond to the pre-condition stretching step. However, after the first cycle a non-linear and anisotropic behavior is observed, converging to a J-shaped stress-strain curve with small hysteresis.

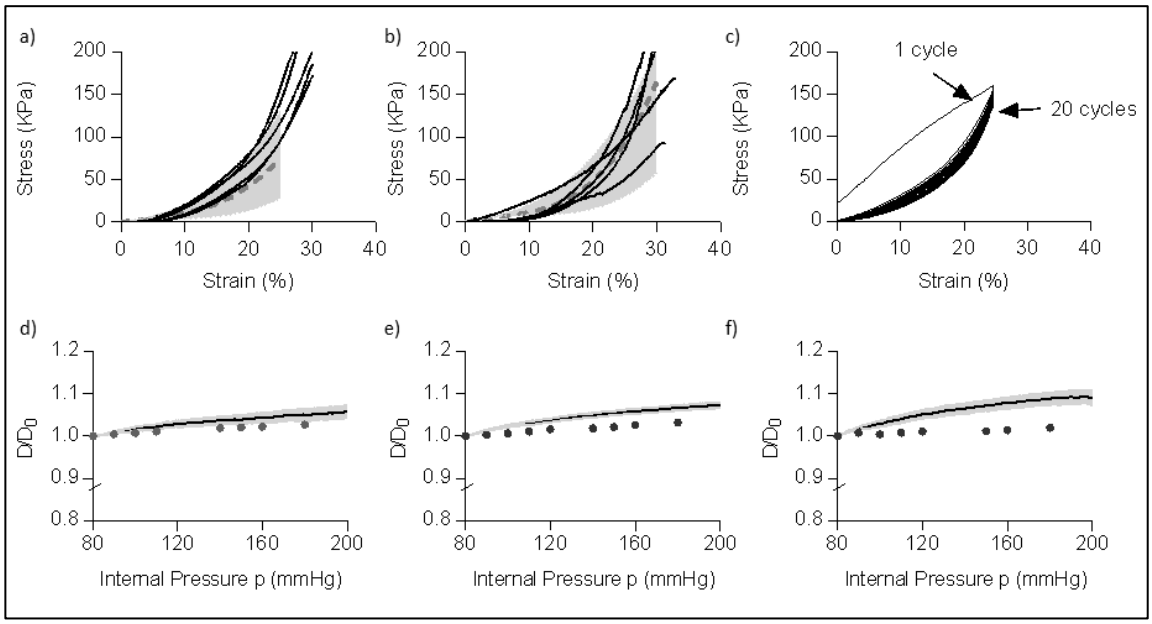

Figure 5-7: Mechanical characterization of the BIVG. a-b) Stress-strain curves of the BIVG (line) and the modelled human coronary artery (grey dotted line) with its respective range (light grey) in a) longitudinal and b) circumferential stretching directions. (c) Cyclic tensile testing in circumferential direction. d-f) D/D_0 vs pressure curves of the BIVS (line) compared with human coronary arteries (solid circle)[34,35] at three different values of axial pre-stretch. d) e_z=10% of axial pre-stretch.e) e_z=20% of axial pre-stretch. f) e_z =25% of axial pre-stretch.

Table 5.1: Bio-inspired vascular graft and human coronary artery compliance (%C) (10^{-2} mmHg) at different pressures ranges and longitudinal strains (e_z)

e_z	10%			20%			25%		
Pressure range (mmHg)	50-90	80-120	110-150	50-90	80-120	110-150	50-90	80-120	110-150
Vascular graft	29 ± 8.4	5.0 ± 2.1	4.0 ± 1.4	30 ± 7.8	9.3 ± 1.2	5.8 ± 0.4	25 ± 4.8	12.9 ± 2.6	7.5 ± 1
Coronary artery	6.3 ± 1.3	3.2 ± 0.04	2.5 ± 0.4	7.3 ± 2.2	3.6 ± 2.7	2.5 ± 2.1	7 ± 0.2*	2.7 ± 0.4*	1.2 ± 0.7**

*Statistical difference ($p<0.05$) compared with BIVS

**Statistical difference ($p<0.005$) compared with BIVS

Vascular constructs were then submitted to pressurized mechanical testing using a perfusion system with pulsatile changes of luminal pressure. Vascular constructs were subjected to three axial pre-stretching values prior to pressurized testing in order to test the behavior at physiological axial strain (10%) and at two axial stretching values that may occur during a clinical application where the safety value is 20% and the limit value is 25% (Van Andel et al., 2003). Comparisons with human coronary arteries were carried out in order to evaluate the similarity of fabricated grafts to natural vessels. A slightly J-shape response was obtained at the diameter-pressure curves and was not altered by higher axial pre-stretching deformation after preconditioning and prior to pressure testing (Figure 5-7d-f). In the approximated *in vivo* axial stretching of natural blood vessels (10 %), BIVSs showed a similar increase in external diameter under luminal pressurization compared with human coronary arteries (Figure 5-7.d). At 20% and 25% axial elongation during pressurized mechanical testing, larger changes of nominal diameter are observed for BIVSs compared to human coronary arteries (Figure 5-7.e and Figure 5-7.f)

Compliance values for BIVSs with 10% and 20% of axial stretching condition have no statistical difference with human coronary arteries. These results highlight the statistically similar compliant response that BIVSs have at pressures close to physiologic ranges (80-120 mmHg), making them specially prepared to response properly in a theoretical bypass situation. At higher values of axial elongation (25%) compliance values of human coronary arteries and BIVSs were statistically different (Table 5-1), hence axial stretching conditions during bypass surgery need to be considered.

5.4.5 Cell distribution and proliferation in BIVSs

Cells were mixed at a concentration of 10^7 cells mL^{-1} into the GEAL solution before starting graft manufacture, giving a solution with a cell density of 10^4 cells mm^{-3}. A 14 µm cryo-section of the BIVS was stained with nuclear dye to quantify the encapsulated cells and verify the cell distribution throughout the thickness of

the graft wall. Figure 5-8a shows the stained section where a higher cell density ($22x10^4$ cells mm^{-3}) than the density in the original GEAL solution is observed. A higher value in cell density can be associated to an adherence and accumulation of cells during the different cycles of dipping and UV-crosslinking or due to a content loss during the manufacturing process. BIVSs also showed homogeneous and concentric distribution of cells throughout the thickness of the graft wall and aligned distribution of cells following the concentric positioning of fabricated interlayers. Nevertheless, this staining displays the total number of encapsulated cells and does not represent the number of active cells post-fabrication. A cell proliferation assay was performed to evaluate the cell death generated during the manufacturing process. A 5 mm section of the BIVS was exposed to WST-1 reagent to measure the mitochondrial activity of encapsulated cells on day 1 and day 7. The amount metabolically active cells on day 1 was low in comparison with the amount of cells quantified in the cryo-section. However, a great increase in cell activity is observed at day 7, with significant difference with day 1 (Figure 5-8b). Additional considerations concerning the limited diffusion of nutrients and reagents of the proliferation kit within the graft must be taken, possibly resulting in an underestimation of the proliferative activity, hence cell survival.

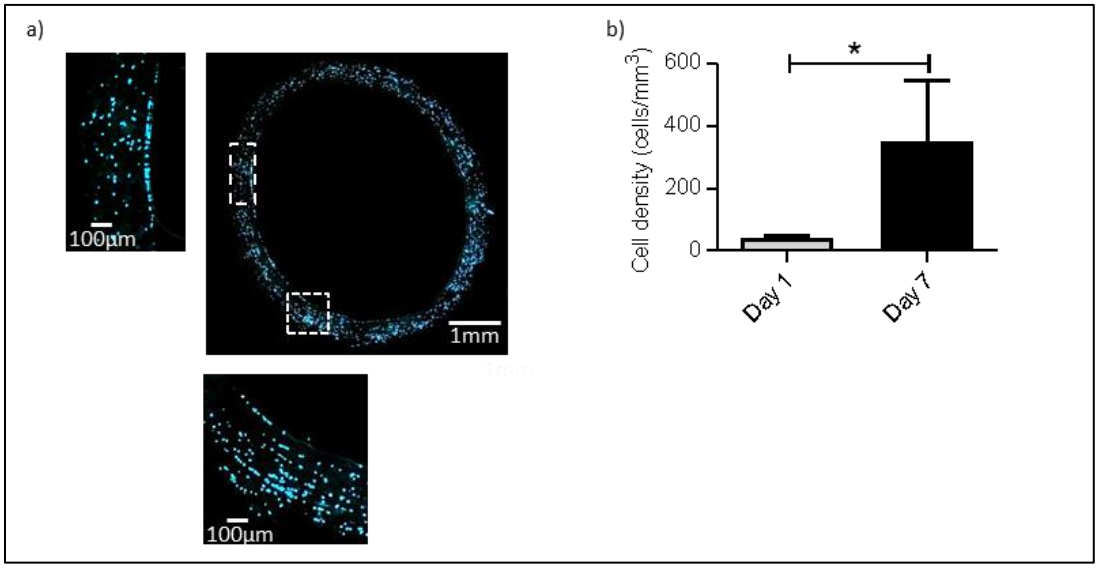

Figure 5-8: **Cell density and distribution in GEAL reinforced with PCL fibers BIVSs.** a) Fluorescence microscopy image of a transversal cut of a BIVS on day of manufacturing. b) Cell density at 1 and 7 days of encapsulated cells (n=4). c) Microscopy image of a H&E stained transversal cut of a BIVS after 1 month in cell culture

5.4.6 Engraftment potential of the encapsulated cells in an immunocompetent animal model

An *in vivo* experiment was performed to determine if SIVG with and without bone marrow MSCs (BM-MSC) were rejected when implanted subcutaneously and to evaluate if encapsulated cells remained functional after the fabrication process. It is known that alginate contains endotoxins (Dusseault et al., 2006), therefore it was important to assess the immunological activation in response to grafts with alginate (or LPS-loaded grafts). Nevertheless, BM-MSCs are known to have immunomodulatory activity; therefore, it is expected that immunoreaction in presence of this type of cells would be controlled and the effect of endotoxins ameliorated. Additionally, because the assay enables cell functionality evaluation it can also asses indirectly cell survival in the vascular graft which could be compromised while cells show viability.

Regarding graft rejection, an overall analysis indicates that SIVG with encapsulated endotoxins and without BM-MSCs induced graft rejection when implanted subcutaneously, characterized by the lack of graft incision healing (see Figure 5-S4a) and increased number of cells in the dLN, $CD4^+$ T cells, $CD8^+$ T cells, antigen presenting cells and B cells (Figure 5-9 a, b, c, d and e respectively). Whereas, under the same conditions with encapsulated BM-MSCs, no signs of rejection were observed. After implantation the incision healed correctly, (Figure 5-S4b) and a decreased number of cells in the dLNs, $CD4^+$ T cells, $CD8^+$ T cells, antigen presenting cells and B cells (Figure 5-9 a, b, c, d and e respectively). This result suggests that an immunomodulation is being carried out by the viable and

functional encapsulated BM-MSCs. therefore proving also that cells maintain viability and functionality after being subjected to the manufacturing process.

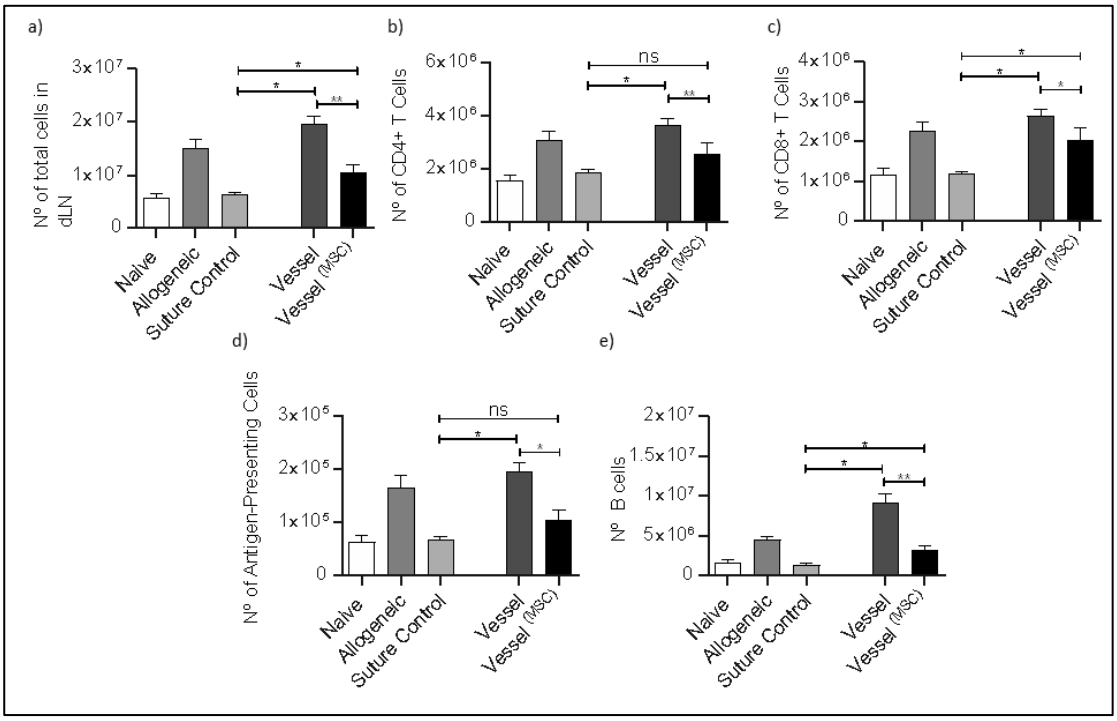

Figure 5-9: Descriptions of immune results. (a) Number of cells in dNL. (b) Number of CD4+CD8- cells in dNL. (c) Number of CD4-CD8+ cells in dNL. (d) Number of of activated antigen presenting cells in dNL. (e) Number of B lymphocytes in dNL. (n=5)

5.5 Discussion

In this study, vascular grafts resembling the mechanical behavior of human coronary arteries were successfully fabricated by combining the dipping-spinning method (Wilkens et al., 2016) and adapted solution blow spinning device for angled fiber spinning. This manufacturing method allows the reinforcement of the cellularized GEAL layers with PCL fibers by intercalating GEAL and PCL sub-layers. The compositions of these grafts were iteratively improved to present the mechanical properties and behavior of a human coronary artery. However, it can be easily customized to mimic any native blood vessel as required. On the one

hand, mechanical properties can be customized by changing the number of dippings, quantity of PCL fiber deposited during fabrication and the angle of fibers deposition. Further, different cell types can be encapsulated in the GEAL sub-layers for the biological functionality of grafts.

Vascular grafts have previously been fabricated for the replacement of small diameter blood vessels (SDBV) (Amensag et al., 2012, Cho, et al. 2005, Niklason et al., 1999, Boccafoschi et al., 2007, Thomas, et al. 2013, Kelm et al., 2010, Bourget et al., 2012). Most of the studies of vascular grafts for replacement of coronary arteries have failed in reaching a similar J-shape mechanical response and achieving compliance close to the one shown by the coronary arteries at physiological elongation. To overcome these issues, middle and outer layer were fabricated mimicking the structural configurations of the media and adventitia layer of coronary arteries respectively. First, the PCL fibers were deposited at an angle of 21° and 67° for the middle and outer layers, inspired by the collagen fiber angles observed in the media and adventitia layers in coronary arteries (Holzapfel et al., 2005, Chen et al., 2011). Second, the elastin and collagen fibers are known to exert their action at different pressure ranges, meaning that at low pressures the artery deformation is controlled by the elastin, meanwhile, at high pressures, collagen fibers start to align and govern the mechanical response (Armentano et al,1991). Due to this, fibers were deposited using a continuous rod rotation sequence of 1 movement forward and half a turn backward; thereby the fibers are not fully stretched during the fabrication, showing certain degree of waviness, similar to collagen fibers in natural vessels under unloaded pressure conditions (Chen et al., 2011,Rezakhaniha et al., 2012; Chen et al., 2013). PCL fibers can then be aligned and start controlling mechanical behavior under higher pressure conditions by extending their resistance after strain changes. Thirdly, blood vessels are in constant loading-unloading cycles, contributing to the J-shape mechanical behavior of the natural extracellular matrix and cells (Thomas et al., 2013; Seliktar et al., 2000). In our vascular graft, the contribution of loading-unloading cycles in

the J-shape mechanics is included by the preconditioning step before the tensile and pressurization test are performed. This preconditioning comprises five cycles of loading-unloading, thus the fibers can re-adapt and align within the scaffold.

With the final objective of manufacturing BIVSs with similar stress-strain curve and compliance to human coronary arteries, each layer was iteratively designed separately to match the mechanical properties of the respective native layers. As we supposed, the best fitting stress-strain curves for the middle and outer layers were in fact capable to resemble the media and adventitia layer. The thickness and fiber angle of each layer were comparable to the coronary arteries, and the anisotropy at the circumferential and longitudinal directions, and the different behavior between middle and outer layers can be explained by the quantity of fibers, thickness of the layer and angle of the deposited fibers. The effect of the angle of deposited fibers appears as one of the key elements to customize and achieve similar mechanical properties to native arteries.

BIVSs based on GEAL reinforced with PCL fibers were fabricated combining the inner, middle and outer layers. The last two layers were previously optimized to obtain similar mechanical response and the existence of an inner layer has the perspective to work as an endothelial monolayer after *in vitro* or *in vivo* maturation. The stress-strain curves shown for the BIVS fabricated from the combination of the three layers fits perfectly within the curve range of human coronary artery in circumferential and longitudinal tests. The inner diameter and thickness are also comparable with the human coronary arteries, which have been reported to range from 3.7 to 1.9 mm (JT Dodge 1992), and 0.55 to 1 mm, respectively (Perry, 2013).

Low patency of BIVS is associated with intima hyperplasia and thrombus formation. The development of intimal hyperplasia in BIVSs is mainly related to mechanical mismatching, provoking compliance differences between the BIVS and the native vessel; changes in the flow vectors at the anastomosis; difference in luminal diameter at the anastomosis section; vessel wall damage; and suture

defects (Sarkar et al., 2006). Moreover, compliance mismatch with the native artery is detrimental to the patency of the BIVS by causing occlusion in general (Abbot et al, 1986, Weston et al 1996, Salacinski et al 2001). The replacement of blood vessel with a BIVS that have luminal diameter and mechanical behavior identical to the contiguous vessel will theoretically significantly reduce the possibility of intimal hyperplasia formation by decreasing the flow and tension variations caused by the compliance or diameter mismatch. This manufacturing method allows the production of BIVSs with similar diameter variation in response to blood pressure. At physiological pressures and elongations, BIVS's compliance was comparable to the human coronary arteries. On one hand, this proves the effectiveness of optimizing each layer separately to achieve the production of BIVSs with suitable mechanical properties. Moreover, these results highlight the importance of the effect of fiber angle deposition on mechanical properties. The mechanical similarity with human coronary arteries demonstrates the potential of our BIVS as a replacement with low risk of producing thrombus or intima hyperplasia and therefore allowing longer patency.

The technique used in this work, intercalated layers of PCL fibers within a cell compatible GEAL hydrogel, allows the controlled and homogenous incorporation of cells all along and across the BIVS, which is otherwise difficult to achieve using steps of post-fabrication cell seeding of scaffolds. The cells were capable not only to survive the fabrication method, they also proliferate in the BIVS and stay functional. Furthermore, the immune reaction assays demonstrate that the encapsulation of UC-MSCs lower the rejection of the BIVS. These results prove the importance of fabricating cellularized grafts to prevent rejection and enhance the functionality of the implant. In our previous work, we demonstrate that with this methodology cells can be encapsulated in specific patterns (Wilkens et al., 2016). Therefore, inner, middle and outer layers can encapsulate different cell types for mimicking the biological function of arteries. Furthermore, the inner layer is displayed as a thin layer of concentric cells that can work as the

endothelial monolayer to avoid the thrombogenic phenomenon. The PCL fibers present in the BIVSs have a degradation profile of years (Bölgen et al., 2005), while the GEAL component will degrade within months (Chen et al., 2012). This biomaterial combination enables the continuous tissue regeneration by hydrogel remodeling while keeping proper mechanical resistance possibly avoiding aneurismal like-dilation. As the cell-laden hydrogel layers are degrading, the fiber layers act as a structural support for new cells to migrate to the scaffold and fabricate extracellular matrix. Additionally, mesenchymal stem cells (MSCs) can be encapsulated as a pluripotent source of the biological component with the ability to differentiate to the desired tissues, or assist the migration of patients cells by different means and possess anti-thrombogenic properties (Hashi et al., 2007).

The manufacturing method has several advantages and potentialities. Solution blow spinning (SBS) has great advantages over other manufacturing method usually used for the fabrication of this type of scaffold as electrospinning, melt electrospinning or writing mode (Xie et al., 2010; Farrugia et al., 2013; Su et al., 2014; Mohtaram et al., 2014; Visser et al., 2015). SBS is applicable over a wide range of materials, including sol-gel hybrids and bioactive composites. In this method, SBS is shown to easily deposit fibers at relatively defined angles, to created mesh- and veil-like structures and with a higher rate of fiber deposition that the other mentioned methods. Moreover, this technique does not need a high voltages and changing parameters for each layers, which makes easier and fastest the fabrication of multilayer cell-laden tubular constructs. The whole manufacturing method has been automatized using a programmable microprocessor. The software can generate specific instructions in order to control the dipping process, including: rotation movement, robot device direction, spray apparatus, angle orientation, PCL solution injection, and compressed air supply. The complete fabrication of a BIVS takes approximately 1 h and does not require specialized workers to operate the equipment. Furthermore, this manufacturing equipment can be scaled to fabricate more than one vascular graft at a time. These

advantages increase the feasibility of this manufacturing method to end up in a lower cost and accessible technology with better commercialization prospective and clinical practice.

In conclusion, this study shows the fabrication of vascular grafts using the combination of the dipping-spinning technique and solution blow spinning device that is capable to deliver fiber interlayers at defined angles. The mechanical and biological functionality of the scaffold is allowed by the presence of fibers and cells throughout the thickness and length of the graft. The mechanical improvement of each layer by mimicking the fiber angle, layer and vessel thickness enable close resemblance to the deformation profile and compliance of human coronary arteries. Specific types of cells can be encapsulated to fulfill the biological function of each layer, with a homogeneous distribution guaranteed. Finally, this study shows a good potential of usability of the vascular grafts based on GEAL layers reinforced with PCL fibers for the replacement of small diameter blood vessel with long patency perspectives.

6. FURTHER DISCUSSIONS AND CONCLUSIONS

6.1 Summary and further discussion

In this thesis vascular grafts for the replacement of human coronary arteries were fabricated. A manufacturing method was developed using a combination of two techniques: dipping-spinning and solution blow spinning. The mechanical behavior of the fabricated vascular grafts was studied through mechanical tests and was compared with human coronary artery mechanical response. The biological component was incorporated and studied through proliferation assays and staining of transversal slices.

Two different tissue engineering techniques were selected for the vascular graft manufacture. Hydrogel consisting in a GelBMa-alginate scaffold with cells encapsulated were deposit in a concentric tubular layer structure using the dipping-spinning technique with UV light exposure for simultaneous crosslinking. PCL fibers for the reinforcement of vascular graft were deposited at different orientations with the solution blow spinning technique.

These techniques were selected because of various characteristics. In first place, the combination of both techniques allows the deposition of intercalated layers of hydrogel and fibers. In this way the distribution of fibers and cells is homogeneous throughout the thickness and length of the vascular graft. In second place, the dipping-spinning technique enables the deposition of regular hydrogel layer with cells encapsulated. In third place, solution blow spinning gives the versatility to deposit fiber in different orientations creating a mesh of angled fibers. In addition to this, each layer can have its own fiber orientation. Finally, several advantages of solution blow spinning over other spun techniques as electrospinning are demonstrated such as high rate of fiber deposition, elimination of high voltages, no need to change parameters for each layer and easy deposition of fibers in a mesh and tubular shape with defined angles.

Fabrication materials and parameters were determined in order to obtain biological and mechanical properties resembling the coronary arteries. The hydrogel layers were constructed with two biocompatible natural polymers that provide a bioactive support to cell proliferation, differentiation and remodeling. Hydrogel solution parameters such as GelBMa, alginate, PI and cellular concentrations and UV intensity were determined for the production of hydrogel layers resistant to dipping-spinning manufacture and with low cellular toxicity. The reinforcing fibers were made with PCL, a synthetic polymer that provides the strength needed to resist blood pressure and implantation and present a similar compliance. Moreover, fiber fabrication parameters were selected in order to be deposit in a way that resembles the collagen fibers in coronary arteries. Parameters such as: PCL concentration and solvent mixture, PCL flow rate, compressed air pressure, distance of the spraying apparatus, dipping and spinning speed and angle of fiber deposition.

The improvement of mechanical properties approach used in this work was to structurally mimic the media and adventitia layers. Moreover, the separately improvement of each layer leads to an entire vascular grafts improvement. Thus, middle and adventitia layer were fabricated with different parameter combinations for the selection of the best parameters for the manufacturing of each layer. Tensile test were performed to each parameter combination. The selection criterion was the combination that allows the most similar j-shape strain-stress curve to coronary arteries. A key effect of the angle of fiber deposition was observed in the generation of anisotropic, non-linear and hyperelastic tissue behavior. Outer layer with fibers deposited in 67° showed a stiffer response than middle layer with fibers deposited in 21° at the longitudinal direction. An opposite effect is shown at the circumferential direction. Parameters such as number of hydrogel and fiber layers were changed until similar thickness was obtained. Once improved middle and outer layer were achieved a complete vascular graft was

manufactured with three concentric layers: inner hydrogel layer improved middle layer and improved outer layer.

Two mechanical tests were used to study the mechanical properties of our vascular grafts. Both tests were done in a special chamber that resembles physiological conditions of temperature and humidity. Uniaxial tensile test was performed to obtain the stress-strain response of vascular graft under longitudinal and circumferential elongations and pressurization test was performed to obtain the diameter variations with pressure. Compliance was calculated from these pressurization test data.

A similar mechanical behavior to coronary arteries was shown by vascular grafts. The stress-stain response has a clear J-shape and anisotropy was demonstrated at the comparison between longitudinal and circumferential directions.

The anisotropic and nonlinear response is mainly produced by the collagen fibers. These fibers are organized in a wavy, not fully stretched, oriented and semi-aligned form. In this work, structure was manufactured imitating the collagen fibers by three methods. First, the fibers were deposited at an angle of 21° and 67° for middle and outer layer creating a mesh, which was inspired by the collagen angles in media and adventitia layers respectively. Second, the fibers were deposited with a forth-forward spinning movement that allows the deposition of undulated fibers. Third, a preconditioning comprising five cycles of loading-unloading was done previous to uniaxial tensile test and pressurization test.

To verify if the manufacturing method is detrimental to the encapsulated cells a proliferation assay was performed. In addition, to demonstrate the homogeneous distribution of cells of the manufacturing method transversal slices were stained.

6.2 Conclusions

This work demonstrates that vascular grafts with biological and mechanical properties resembling human coronary arteries can be produced with a combination of dipping-spinning and solution blow spinning technique. This

methodology allows obtaining more similar mechanical and biological characteristics in less fabrication time. The main reasons why it has better characteristics lies in the deposition of oriented and wavy fibers and co-deposition of cells.

The angle in which the fibers are deposited has a clear effect in the mechanical response. Therefore, the graft layers with fibers deposited in the same angles found in the collagen fibers of native layers resulted similar mechanical properties to those native layers.

The success in achieving the mechanical properties of coronary arteries in vascular grafts is associated to the fabrication method and the precondition done to samples. Specifically, three steps are essential for achieving a non-linear, anisotropic, hyperelastic and J-shaped response: depositing the fibers in angle, the forth-forward spinning movement for the wavy fiber deposition and the sample preconditioning.

Our approach method of optimizing each layer separately allows the production of improved vascular grafts without further readjustments. The stress-strain and diameter versus pressure curves fits the human coronary artery range and similar statistically compliance values were obtained at similar at physiological strain and pressures demonstrating our optimizing approach and fabrication methodology.

Cells were successfully incorporated and distributed homogeneously in concentric layers throughout the thickness of the vascular grafts. Cells were not only capable to survive to the manufacturing method but also proliferate in the vascular graft. Furthermore, different cell type can be incorporated in each layer, for example, hydrogel layers of endothelial cells encapsulated at the inner layer, SMCs at the middle layer and fibroblast in the outer layer mimicking the cell distribution in arteries. However, for a faster fabrication that not require previous differentiation BMCs can be encapsulated in the three layers and *in vivo* differentiation can happen.

Finally, the major achievement of this work is the fulfillment of part of the requirements for coronary vascular grafts. Vascular grafts fabricated with this methodology were proved to be non-cytotoxic and have similar dimensions and compliance. Because grafts have similar mechanical properties they should withstand blood pressure and resist implantation, but further test must be performed. Although this fabrication method was designed for the production of coronary vascular grafts, it can be applied to a variety of soft tissues such as other arteries or veins, skin, cartilage, ligaments and tendons among others. Furthermore, this fabrication method can be completely automatized and scaled which imply high viability in marketability and clinical practice.

6.3 Major contribution of this work

The major contributions done by this thesis work are four:

1) This work is the first manufacturing method that combines the dipping-spinning and solution blow spinning to produce vascular graft structurally inspired in human coronary arteries with intercalated layers of cell-laden hydrogel and oriented fibers

2) Layer optimization for the production of optimized tissue. The adjusting of each layer enable the production of improved vascular grafts without need of any further adjusts. This approach can be extended to any tissue with sections of different compositions.

3) Study of the fiber effect in the mechanical response. The mimicking of fiber orientation allows obtaining similar mechanical properties of vascular grafts. Furthermore, the deposition of fibers with waviness and orientation allow resembling the mechanical properties of soft tissues. Like the previous contribution, this knowledge can be extended to any tissue with collagen fibers oriented and aligned at a certain angle.

4) Study of the importance of preconditioning in vascular grafts as a way of simulating of cyclic tension received by the native tissue. Also this can be extended to almost every tissue in the body.

6.4 Future projections

As future work, the following studies should be performed:

- Optimize the solution blow spinning parameters: PCL concentration, flow rate and compressed air pressure. The aim of this optimization is to obtain more aligned fibers and ensure fiber deposition without beads or solvent traces for the improvement of mechanical properties and guarantee a non-cytotoxic implant.
- Perform all mechanical assays according to standard ISO 7198 (ANSI/AAMI/ 2010) such as: burst pressure, suture strength resistance and kink diameter/radius among others. The importance of these assays is to ensure a good performance of the vascular grafts when implanted in the body and the FDA approval of this tissue engineered vascular graft.
- Study the immunogenic response in mouse to identify if the vascular graft has any adverse immunogenic reaction. This is essential to evaluate if the body will produce rejection to the graft implant.
- Perform differentiation of cells encapsulated in layers to endothelial cells, SMC and fibroblast in inner, middle and outer layer respectively. The aim of the differentiation of cells is to customize each layer to perform the biological function that inner, media and adventitia layer has. In this way, the vascular graft not only will resemble the mechanical properties of arteries, but will perform the same function.
- Perform thrombogenesis assays to the vascular graft to ensure that the materials and fabrication formulation is not thrombogenic. This is one of the most important test that certify that the grafts could be used as a replace of blood vessels.
- Perform *in vivo* assays in suitable animal model such as porcine or goat. The purpose of this testing is to evaluate the response of the host tissues following the implantation in the vascular site and to assess the short-term response and patency of the prosthesis. Furthermore, the degradation time, invasion of cells and remodeling of the vascular graft could be determined with this assay.

REFERENCES

Abbott, W. M., Megerman, J., Hasson, J. E., L'Italien, G., & Warnock, D. F. (1987). Effect of compliance mismatch on vascular graft patency. *Journal of Vascular Surgery*, *5*(2), 376-382.

Adamian, M., Colombo, A., Briguori, C., Nishida, T., Marsico, F., Di Mario, C., ... & Moses, J. W. (2001). Cutting balloon angioplasty for the treatment of in-stent restenosis: a matched comparison with rotational atherectomy, additional stent implantation and balloon angioplasty. *Journal of the American College of Cardiology*, *38*(3), 672-679.

Agianniotis, A., Rezakhaniha, R., & Stergiopulos, N. (2011). A structural constitutive model considering angular dispersion and waviness of collagen fibres of rabbit facial veins. *Biomedical engineering online*, *10*(1), 18.

Alberts, B., Johnson, A., Lewis, J., Raff, M., Roberts, K., Walter, P. (2002). Blood vessels and endothelial cells. *Molecular biology of the cell (4th ed.)*, Garland Science, pp. 1279-1283.

Amensag, S., & McFetridge, P. S. (2012). Rolling the human amnion to engineer laminated vascular tissues. *Tissue Engineering Part C: Methods*, *18*(11), 903-912.

Armentano, R. L., Levenson, J., Barra, J. G., Fischer, E. I., Breitbart, G. J., Pichel, R. H., & Simon, A. (1991). Assessment of elastin and collagen contribution to aortic elasticity in conscious dogs. *American Journal of Physiology-Heart and Circulatory Physiology*, *260*(6), H1870-H1877.

Association for the Advancement of Medical Instrumentation. (2004). Cardiovascular implants—Tubular vascular prostheses. *American National Standard*.

Atwood, R. C., Bodey, A. J., Price, S. W., Basham, M., & Drakopoulos, M. (2015). A high-throughput system for high-quality tomographic reconstruction of large datasets at Diamond Light Source. *Philosophical Transactions of the Royal Society of London A: Mathematical, Physical and Engineering Sciences*, *373*(2043), 20140398.

Blausen.com staff. (2014). Medical gallery of Blausen Medical 2014. *WikiJournal Medicine* **1** (2). DOI:10.15347/WIN/2014.010.ISS 2002-4436

Bloom, D.E., Cafiero, E.T., Jané-Llopis, E., Abrahams-Gessel, S., Bloom, L.R., Fathima, S., Feigl, A.B., Gaziano, T., Mowafi, M., Pandya, A., Prettner, K., Rosenberg, L., Seligman, B., Stein, A.Z., & Weinstein, C. (2011). The Global Economic Burden of Noncommunicable Diseases. Geneva: World Economic Forum.

Boccafoschi, F., Rajan, N., Habermehl, J., & Mantovani, D. (2007). Preparation and Characterization of a Scaffold for Vascular Tissue Engineering by Direct-Assembling of Collagen and Cells in a Cylindrical Geometry. *Macromolecular bioscience*, *7*(5), 719-726.

Bölgen, N., Menceloğlu, Y. Z., Acatay, K., Vargel, I., & Pişkin, E. (2005). In vitro and in vivo degradation of non-woven materials made of poly (ε-caprolactone) nanofibers prepared by electrospinning under different conditions. *Journal of Biomaterials Science, Polymer Edition*, *16*(12), 1537-1555.

Bourget, J. M., Gauvin, R., Larouche, D., Lavoie, A., Labbé, R., Auger, F. A., & Germain, L. (2012). Human fibroblast-derived ECM as a scaffold for vascular tissue engineering. *Biomaterials*, *33*(36), 9205-9213.

Bramucci, E., Angoli, L., Merlini, P. A., Barberis, P., Laudisa, M. L., Colombi, E., ... & Ardissino, D. (1998). Adjunctive stent implantation following directional coronary atherectomy in patients with coronary artery disease. *Journal of the American College of Cardiology*, *32*(7), 1855-1860.

Bustos, C. A., García-Herrera, C. M., & Celentano, D. J. (2016). Mechanical characterisation of Dacron graft: Experiments and numerical simulation. *Journal of biomechanics*, *49*(1), 13-18.

Byrom, M. J., Ng, M. K., & Bannon, P. G. (2013). Biomechanics and biocompatibility of the perfect conduit—can we build one?. *Annals of Cardiothoracic Surgery*, *2*(4), 435-443.

Campos-Mora, M., Morales, R. A., Pérez, F., Gajardo, T., Campos, J., Catalan, D., ... & Pino-Lagos, K. (2015). Neuropilin-1+ regulatory T cells promote skin allograft survival and modulate effector CD4+ T cells phenotypic signature. *Immunology and cell biology*, *93*(2), 113-119.

Catto, V., Farè, S., Cattaneo, I., Figliuzzi, M., Alessandrino, A., Freddi, G., ... & Tanzi, M. C. (2015). Small diameter electrospun silk fibroin vascular grafts: Mechanical properties, in vitro biodegradability, and in vivo biocompatibility. *Materials Science and Engineering: C*, *54*, 101-111.

Chen, H., Liu, Y., Slipchenko, M. N., Zhao, X., Cheng, J. X., & Kassab, G. S. (2011). The layered structure of coronary adventitia under mechanical load. *Biophysical journal*, *101*(11), 2555-2562.

Chen, H., Slipchenko, M. N., Liu, Y., Zhao, X., Cheng, J. X., Lanir, Y., & Kassab, G. S. (2013). Biaxial deformation of collagen and elastin fibers in coronary adventitia. *Journal of Applied Physiology*, *115*(11), 1683-1693.

Chen, Y. C., Lin, R. Z., Qi, H., Yang, Y., Bae, H., Melero-Martin, J. M., & Khademhosseini, A. (2012). Functional human vascular network generated in photocrosslinkable gelatin methacrylate hydrogels. *Advanced functional materials*, *22*(10), 2027-2039.

Cho, S. W., Lim, S. H., Kim, I. K., Hong, Y. S., Kim, S. S., Yoo, K. J., ... & Hwang, K. C. (2005). Small-diameter blood vessels engineered with bone marrow–derived cells. *Annals of surgery*, *241*(3), 506-515.

Claes, E. (2010). *Estudio mecánico de las arterias coronarias humanas y sus sustitutos vasculares* (Doctoral dissertation, Caminos).

Claes, E., Atienza, J. M., Guinea, G. V., Rojo, F. J., Bernal, J. M., Revuelta, J. M., & Elices, M. (2010, August). Mechanical properties of human coronary arteries. In *Engineering in Medicine and Biology Society (EMBC), 2010 Annual International Conference of the IEEE* (pp. 3792-3795). IEEE.

Collagen [Online image]. (n.d.) Retrieved March 27, 2017 from http:/www.sigmaaldrich.com/life-science/metabolomics/enzyme-explorer/learning-center/structural-proteins/collagen.html#collagen

de Souza, M. D. F. M., Gawryszewski, V. P., Ordunez, P., Sanhueza, A., & Espinal, M. A. (2012). Cardiovascular disease mortality in the Americas: current trends and disparities. *Heart*, *98*(16), 1207-1212.

Dodge, J. T., Brown, B. G., Bolson, E. L., & Dodge, H. T. (1992). Lumen diameter of normal human coronary arteries. Influence of age, sex, anatomic variation, and left ventricular hypertrophy or dilation. *Circulation*, *86*(1), 232-246.

Dornhoffer, John L. Hearing results with the Dornhoffer ossicular replacement prostheses. *The Laryngoscope* 108.4, 531-536 (1998)

Dusseault, J., Tam, S. K., Ménard, M., Polizu, S., Jourdan, G., Yahia, L. H., & Hallé, J. P. (2006). Evaluation of alginate purification methods: effect on polyphenol, endotoxin, and protein contamination. *Journal of Biomedical Materials Research Part A*, *76*(2), 243-251.

Elastic fibers are made of elastine, one type of structural protein found in the ECM of animal cells [Online image]. (2012). Retrieved March 27, 2017 from https://biology-forums.com/index.php?action=gallery;sa=view;id=282

Epstein, A. J., Polsky, D., Yang, F., Yang, L., & Groeneveld, P. W. (2011). Coronary revascularization trends in the United States, 2001-2008. *Jama*, *305*(17), 1769-1776.

Ercolani, E., Del Gaudio, C., & Bianco, A. (2013). Vascular tissue engineering of small-diameter blood vessels: reviewing the electrospinning approach. *Journal of tissue engineering and regenerative medicine*.

Farrugia, B. L., Brown, T. D., Upton, Z., Hutmacher, D. W., Dalton, P. D., & Dargaville, T. R. (2013). Dermal fibroblast infiltration of poly (ε-caprolactone) scaffolds fabricated by melt electrospinning in a direct writing mode. *Biofabrication*, *5*(2), 025001.

Fischer, E. I. C. (2008). La adventicia: estado actual del conocimiento. *Rev Argent Cardiol*, *76*, 58-63.

Fischer, G. M., & Llaurado, J. G. (1966). Collagen and elastin content in canine arteries selected from functionally different vascular beds. *Circulation research*, *19*(2), 394-399.

Foerst, J., Vorpahl, M., Engelhardt, M., Koehler, T., Tiroch, K., & Wessely, R. (2013). Evolution of coronary stents: From bare-metal stents to fully biodegradable, drug-eluting stents. *Combination Products in Therapy*, *3*(1-2), 9-24.

García-Herrera, C. M., Atienza, J. M., Rojo, F. J., Claes, E., Guinea, G. V., Celentano, D. J., ... & Burgos, R. L. (2012). Mechanical behaviour and rupture of normal and pathological human ascending aortic wall. *Medical & biological engineering & computing*, *50*(6), 559-566.

García-Herrera, C. M., Celentano, D. J., & Cruchaga, M. A. (2013). Bending and pressurisation test of the human aortic arch: experiments, modelling and simulation of a patient-specific case. *Computer methods in biomechanics and biomedical engineering*, *16*(8), 830-839.Garg, S., & Serruys, P. W. (2010). Coronary stents: current status. *Journal of the American College of Cardiology*, *56*(10), S1-S42.

Grech, E. D. (2003). Percutaneous coronary intervention. I: History and development. *BMJ: British Medical Journal*, *326*(7398), 1080.

Hamid, H., & Coltart, J. (2007). 'Miracle stents'-a future without restenosis. *McGill Journal of Medicine: MJM*, *10*(2), 105.

Hare, J. M., & Chaparro, S. V. (2008). Cardiac regeneration and stem cell therapy. *Current opinion in organ transplantation*, *13*(5), 536.

Hashi, C. K., Zhu, Y., Yang, G. Y., Young, W. L., Hsiao, B. S., Wang, K., ... & Li, S. (2007). Antithrombogenic property of bone marrow mesenchymal stem cells in nanofibrous vascular grafts. *Proceedings of the National Academy of Sciences*, *104*(29), 11915-11920.

Healthwise Staff (2015a). Angioplasty. Retrieved from: http://www.webmd.com/heart-disease/angioplasty

Healthwise Staff (2015b). Coronary Stent. Retrieved from: http://www.webmd.com/heart-disease/coronary-stent

Henrikson R.C., & Mazurkiewics. J.E. (1997). *Histology*. Volumen 518. New York: National Medical Series for Independent Study (NMS), 1997.

Hess, C. N., Lopes, R. D., Gibson, C. M., Hager, R., Wojdyla, D. M., Englum, B. R., ... & Alexander, J. H. (2014). Saphenous vein graft failure after coronary artery bypass surgery: insights from PREVENT IV. *Circulation*, CIRCULATIONAHA-113.

Hinohara, T., Selmon, M. R., Robertson, G. C., Braden, L., & Simpson, J. S. (1990). Directional atherectomy. New approaches for treatment of obstructive coronary and peripheral vascular disease. *Circulation*, *81*(3 Suppl), IV79-91.

Hoffmann, R., Mintz, G. S., Kent, K. M., Pichard, A. D., Satler, L. F., Popma, J. J., ... & Leon, M. B. (1998). Comparative early and nine-month results of rotational atherectomy, stents, and the combination of both for calcified lesions in large coronary arteries. *The American journal of cardiology*, *81*(5), 552-557.

Holmes, D. R., Leon, M. B., Moses, J. W., Popma, J. J., Cutlip, D., Fitzgerald, P. J., ... & Snead, D. (2004). Analysis of 1-year clinical outcomes in the SIRIUS trial a randomized trial of a sirolimus-eluting stent versus a standard stent in patients at high risk for coronary restenosis. *Circulation*, *109*(5), 634-640.

Holzapfel, G. A., Sommer, G., Gasser, C. T., & Regitnig, P. (2005). Determination of layer-specific mechanical properties of human coronary arteries with nonatherosclerotic intimal thickening and related constitutive modeling. *American Journal of Physiology-Heart and Circulatory Physiology*, *289*(5), H2048-H2058.

Holroyd Heart Centre (2016). Rotational Atherectomy. Retrieved from: http://www.holroydheart.com.au/coronary_procedures.html

Hundley, W. G., Lange, R. A., Clarke, G. D., Meshack, B. M., Payne, J., Landau, C., ... & Hillis, L. D. (1996). Assessment of coronary arterial flow and flow reserve in humans with magnetic resonance imaging. *Circulation*, *93*(8), 1502-1508.

Iwasaki, K., Kojima, K., Kodama, S., Paz, A. C., Chambers, M., Umezu, M., & Vacanti, C. A. (2008). Bioengineered three-layered robust and elastic artery using hemodynamically-equivalent pulsatile bioreactor. *Circulation*, *118*(14 suppl 1), S52-S57.

Jang, K. I., Chung, H. U., Xu, S., Lee, C. H., Luan, H., Jeong, J., ... & Kim, J. (2015). Soft network composite materials with deterministic and bio-inspired designs. *Nature communications*, *6*.

Kelm, J. M., Lorber, V., Snedeker, J. G., Schmidt, D., Broggini-Tenzer, A., Weisstanner, M., ... & Hoerstrup, S. P. (2010). A novel concept for scaffold-free vessel tissue engineering: self-assembly of microtissue building blocks. *Journal of biotechnology*, *148*(1), 46-55.

Kielty, C. M., Sherratt, M. J., & Shuttleworth, C. A. (2002). Elastic fibres. *Journal of cell science*, *115*(14), 2817-2828.

Lanas, F., Serón, P., & Lanas, A. (2013). Coronary heart disease and risk factors in Latin America. *Global heart*, *8*(4), 341-348.

Lee, K. Y., & Mooney, D. J. (2012). Alginate: properties and biomedical applications. *Progress in polymer science*, *37*(1), 106-126.

L'heureux, N., Dusserre, N., Marini, A., Garrido, S., De La Fuente, L., & McAllister, T. (2007). Technology insight: the evolution of tissue-engineered vascular grafts—from research to clinical practice. *Nature Clinical Practice Cardiovascular Medicine*, *4*(7), 389-395.

Li, D. Y., Brooke, B., Davis, E. C., Mecham, R. P., Sorensen, L. K., Boak, B. B., ... & Keating, M. T. (1998). Elastin is an essential determinant of arterial morphogenesis. *Nature*, *393*(6682), 276-280.

Li, S., & Li, J. J. (2015). PCSK9: A key factor modulating atherosclerosis. *Journal of atherosclerosis and thrombosis*, *22*(3), 221-230.

Lodish, H., Berk, A., Zipursky, S. L., Matsudaira, P., Baltimore, D., & Darnell, J. (2000). Collagen: the fibrous proteins of the matrix. *Molecular cell biology*, *4*.

Ma, Q., Cheng, H., Jang, K. I., Luan, H., Hwang, K. C., Rogers, J. A., ... & Zhang, Y. (2016). A nonlinear mechanics model of bio-inspired hierarchical lattice materials consisting of horseshoe microstructures. *Journal of the Mechanics and Physics of Solids*, *90*, 179-202.

Mathers, C. D., & Loncar, D. (2006). Projections of global mortality and burden of disease from 2002 to 2030. *Plos med*, *3*(11), e442.

McAllister, T. N., Maruszewski, M., Garrido, S. A., Wystrychowski, W., Dusserre, N., Marini, A., ... & Antonelli, J. (2009). Effectiveness of haemodialysis access with an autologous tissue-engineered vascular graft: a multicentre cohort study. *The Lancet*, *373*(9673), 1440-1446.

McMahon, R. E., Qu, X., Jimenez-Vergara, A. C., Bashur, C. A., Guelcher, S. A., Goldstein, A. S., & Hahn, M. S. (2011). Hydrogel–electrospun mesh composites for coronary artery bypass grafts. *Tissue Engineering Part C: Methods*, *17*(4), 451-461.

Medeiros, E. S., Glenn, G. M., Klamczynski, A. P., Orts, W. J., & Mattoso, L. H. (2009). Solution blow spinning: A new method to produce micro-and nanofibers from polymer solutions. *Journal of Applied Polymer Science*, *113*(4), 2322-2330.

Medeiros, E. L. G., Braz, A. L., Porto, I. J., Menner, A., Bismarck, A., Boccaccini, A. R., ... & Blaker, J. J. (2016). Porous Bioactive Nanofibers via Cryogenic Solution Blow Spinning and Their Formation into 3D Macroporous Scaffolds. *ACS Biomaterials Science & Engineering*, *2*(9), 1442-1449.

Ministerio de Salud, Gobierno de Chile (MINSAL) (2014). Indicadores Básicos de Salud Chile 2014. Retrived from: http://www.deis.cl/wp-content/uploads/2015/04/IBS-2014.pdf

Mitra, A. K., & Agrawal, D. K. (2006). In stent restenosis: bane of the stent era. *Journal of clinical pathology*, *59*(3), 232-239.

Mohan, S., & Dhall, A. (2010). A comparative study of restenosis rates in bare metal and drug-eluting stents. *International Journal of Angiology*, *19*(02), e66-e72.

Mohtaram, N. K., Ko, J., King, C., Montgomery, A., Sun, L., Vasandani, R., ... & Willerth, S. M. (2014). NEURONAL DIFFERENTIATION OF HUMAN INDUCED PLURIPOTENT STEM CELLS SEEDED ON MELT ELECTROSPUN MICROFIBERS.

Montini-Ballarin, F., Calvo, D., Caracciolo, P. C., Rojo, F., Frontini, P. M., Abraham, G. A., & Guinea, G. V. (2016). Mechanical behavior of bilayered small-diameter nanofibrous structures as biomimetic vascular grafts. *Journal of the mechanical behavior of biomedical materials*, *60*, 220-233.

National Heart, Lung, and Blood Institute (NIH) (2012). What is Coronary Artery Bypass Grafting, Retrieved from: https://www.nhlbi.nih.gov/health/health-topics/topics/cabg

Nemeno-Guanzon, J. G., Lee, S., Berg, J. R., Jo, Y. H., Yeo, J. E., Nam, B. M., ... & Lee, J. I. (2012). Trends in tissue engineering for blood vessels. *BioMed Research International*, *2012*.

Nichol, J. W., Koshy, S. T., Bae, H., Hwang, C. M., Yamanlar, S., & Khademhosseini, A. (2010). Cell-laden microengineered gelatin methacrylate hydrogels. *Biomaterials*, *31*(21), 5536-5544.

Niklason, L. E., Gao, J., Abbott, W. M., Hirschi, K. K., Houser, S., Marini, R., & Langer, R. (1999). Functional arteries grown in vitro. *Science*, *284*(5413), 489-493.

Oliveira, J. E., Mattoso, L. H., Orts, W. J., & Medeiros, E. S. (2013). Structural and morphological characterization of micro and nanofibers produced by electrospinning and solution blow spinning: a comparative study. *Advances in Materials Science and Engineering*, *2013*.

Ottani, V., Raspanti, M., & Ruggeri, A. (2001). Collagen structure and functional implications. *Micron*, *32*(3), 251-260.

Pashneh-Tala, S., MacNeil, S., & Claeyssens, F. (2015). The Tissue-Engineered Vascular Graft—Past, Present, and Future. *Tissue Engineering Part B: Reviews*, *22*(1), 68-100.

Pan American Health Organization (PAHO) (2014a). Death due to Noncommunicable Diseases, Countries of the Americas. Retrieved from: http://www.paho.org/hq/index.php?option=com_content&view=article&id=10169&Itemid=41167&lang=en

Pan American Health Organization (PAHO) (2014b). NMH Database, Noncommunicable Diseases, & Mental Heald (NMH). Retrieved from: http://www.paho.org/hq/index.php?option=com_content&view=article&id=10168&Itemid=41162&lang=en

Pan American Health Organization (PAHO/WHO) (2016). Registered death, Regional Mortality Information System. Retrieved from: http://www.paho.org/hq/index.php?option=com_content&view=article&id=10169&Itemid=41167&lang=en

Patrício, T., Domingos, M., Gloria, A., & Bártolo, P. (2013). Characterisation of PCL and PCL/PLA scaffolds for tissue engineering. *Procedia CIRP*, *5*, 110-114.

Peng, H. F., Liu, J. Y., Andreadis, S. T., & Swartz, D. D. (2011). Hair follicle-derived smooth muscle cells and small intestinal submucosa for engineering mechanically robust and vasoreactive vascular media. *Tissue Engineering Part A*, *17*(7-8), 981-990.

Perry, R. A., Seth, A., Singh, A., & Shiu, M. F. (1988). Success and complication rates of coronary angioplasty in patients with and without previous myocardial infarction. *European heart journal*, *9*(1), 37-42.

Perry, R., Joseph, M. X., Chew, D. P., Aylward, P. E., & De Pasquale, C. G. (2013). Coronary artery wall thickness of the left anterior descending artery using high

resolution transthoracic echocardiography–normal range of values. *Echocardiography*, *30*(7), 759-764.

Rajendran, P., Rengarajan, T., Thangavel, J., Nishigaki, Y., Sakthisekaran, D., Sethi, G., & Nishigaki, I. (2013). The vascular endothelium and human diseases. *Int J Biol Sci*, *9*(10), 1057-69.

Rapoport, H. S., Fish, J., Basu, J., Campbell, J., Genheimer, C., Payne, R., & Jain, D. (2012). Construction of a tubular scaffold that mimics J-shaped stress/strain mechanics using an innovative electrospinning technique. *Tissue Engineering Part C: Methods*, *18*(8), 567-574.

Rathore, A., Cleary, M., Naito, Y., Rocco, K., & Breuer, C. (2012). Development of tissue engineered vascular grafts and application of nanomedicine. *Wiley Interdisciplinary Reviews: Nanomedicine and Nanobiotechnology*, *4*(3), 257-272.

Rau, C., Wagner, U., Pešić, Z., & De Fanis, A. (2011). Coherent imaging at the Diamond beamline I13. *physica status solidi (a)*, *208*(11), 2522-2525.

Rezakhaniha, R., Agianniotis, A., Schrauwen, J. T. C., Griffa, A., Sage, D., Bouten, C. V. C., ... & Stergiopulos, N. (2012). Experimental investigation of collagen waviness and orientation in the arterial adventitia using confocal laser scanning microscopy. *Biomechanics and modeling in mechanobiology*, *11*(3-4), 461-473.

Roach, M. R., & Burton, A. C. (1957). The reason for the shape of the distensibility curves of arteries. *Canadian journal of biochemistry and physiology*, *35*(8), 681-690.

Safar, M. E. (2010). Arterial aging—hemodynamic changes and therapeutic options. *Nature Reviews Cardiology*, *7*(8), 442-449.

Salacinski, H. J., Goldner, S., Giudiceandrea, A., Hamilton, G., Seifalian, A. M., Edwards, A., & Carson, R. J. (2001). The mechanical behavior of vascular grafts: a review. *Journal of biomaterials applications*, *15*(3), 241-278.

Sarkar, S., Salacinski, H. J., Hamilton, G., & Seifalian, A. M. (2006). The mechanical properties of infrainguinal vascular bypass grafts: their role in influencing patency. *European journal of vascular and endovascular surgery*, *31*(6), 627-636.

Schriefl, A. J., Zeindlinger, G., Pierce, D. M., Regitnig, P., & Holzapfel, G. A. (2011). Determination of the layer-specific distributed collagen fibre orientations in human thoracic and abdominal aortas and common iliac arteries. *Journal of the Royal Society Interface*, rsif20110727.

Schwartz, R. S. (1994). Neointima and arterial injury: dogs, rats, pigs, and more. *Laboratory investigation; a journal of technical methods and pathology*, *71*(6), 789-791.

Seliktar, D., Black, R. A., Vito, R. P., & Nerem, R. M. (2000). Dynamic mechanical conditioning of collagen-gel blood vessel constructs induces remodeling in vitro. *Annals of biomedical engineering*, *28*(4), 351-362.

Shoulders, M. D., & Raines, R. T. (2009). Collagen structure and stability. *Annual review of biochemistry*, *78*, 929-958.

Smith, S. C., Dove, J. T., Jacobs, A. K., Kennedy, J. W., Kereiakes, D., Kern, M. J., ... & Gibbons, R. J. (2001). ACC/AHA Guidelines for Percutaneous Coronary Intervention (Revision of the 1993 PTCA Guidelines)—Executive Summary A Report of the American College of Cardiology/American Heart Association Task Force on Practice Guidelines (Committee to Revise the 1993 Guidelines for Percutaneous Transluminal Coronary Angioplasty) Endorsed by the Society for Cardiac Angiography and Interventions. *Circulation*, *103*(24), 3019-3041.

Stankus, J. J., Soletti, L., Fujimoto, K., Hong, Y., Vorp, D. A., & Wagner, W. R. (2007). Fabrication of cell microintegrated blood vessel constructs through electrohydrodynamic atomization. *Biomaterials*, *28*(17), 2738-2746.

Stenmark, K. R., Yeager, M. E., El Kasmi, K. C., Nozik-Grayck, E., Gerasimovskaya, E. V., Li, M., ... & Frid, M. G. (2013). The adventitia: essential regulator of vascular wall structure and function. *Annual review of physiology*, *75*, 23.

Su, Z., Li, J., Ouyang, Z., Arras, M. M., Wei, G., & Jandt, K. D. (2014). Biomimetic 3D hydroxyapatite architectures with interconnected pores based on electrospun biaxially orientated PCL nanofibers. *RSC Advances*, *4*(29), 14833-14839.

Sullivan S., Brockbank K. (2000) Small-diameter vascular grafts. In: Lanza R, Langer R, Vacanti J. eds. *Principles of tissue engineering*. 2nd ed Academic press, 447-54

Sun, J., & Tan, H. (2013). Alginate-based biomaterials for regenerative medicine applications. *Materials*, *6*(4), 1285-1309.

Thomas, L. V., & Nair, P. D. (2013). The effect of pulsatile loading and scaffold structure for the generation of a medial equivalent tissue engineered vascular graft. *BioResearch open access*, *2*(3), 227-239.

Tien, J., Golden, A. P., & Tang, M. D. (2006). Engineering of Blood Vessels.

van Andel, C. J., Pistecky, P. V., & Borst, C. (2003). Mechanical properties of porcine and human arteries: implications for coronary anastomotic connectors. *The Annals of thoracic surgery*, *76*(1), 58-64.

Van Den Bulcke, A. I., Bogdanov, B., De Rooze, N., Schacht, E. H., Cornelissen, M., & Berghmans, H. (2000). Structural and rheological properties of methacrylamide modified gelatin hydrogels. *Biomacromolecules*, *1*(1), 31-38.

Visser, J., Melchels, F. P., Jeon, J. E., van Bussel, E. M., Kimpton, L. S., Byrne, H. M., ... & Malda, J. (2015). Reinforcement of hydrogels using three-dimensionally printed microfibres. *Nature communications*, *6*.

Wasiak, J., Law, J., Watson, P., & Spinks, A. (2012). Percutaneous transluminal rotational atherectomy for coronary artery disease. *The Cochrane Library*.

Wagenseil, J. E., & Mecham, R. P. (2009). Vascular extracellular matrix and arterial mechanics. *Physiological reviews*, *89*(3), 957-989.

Weldon, S. (n.d.). Coronary Artery Disease and Coronary Bypass Surgery, Cardiac vessel anatomy. Retrieved from: https://www.bcm.edu/healthcare/care-centers/cardiothoracic/procedures/coronary-artery-disease-coronary-bypass

Weston, M. W., Rhee, K., & Tarbell, J. M. (1996). Compliance and diameter mismatch affect the wall shear rate distribution near an end-to-end anastomosis. *Journal of biomechanics*, *29*(2), 187-198.

Wilkens, C. A., Rivet, C. J., Akentjew, T. L., Alverio, J., Khoury, M., & Acevedo, J. P. (2016). Layer-by-layer approach for a uniformed fabrication of a cell patterned vessel-like construct. *Biofabrication*, *9*(1), 015001.

World Heart Federation. (2016). Cost of heart disease in Latin America tops $30BN. Retrieved from: http://www.world-heart-federation.org/press/releases/detail/article/cost-of-heart-disease-in-latin-america-tops-30bn/

World Heart Federation. (2017) Champions Advocate Programme. The cost of CVD. Retrieved from: http://www.championadvocates.org/en/champion-advocates-programme/the-costs-of-cvd.

World Health Organization (WHO) (2017a). Cardiovascular diseases (CVDs) fact sheet. Retrieved from: https://www.who.int/mediacenter/factsheet/fs317/en/

World Health Organization (WHO) (2017b). Cardiovascular diseases (CVDs). The Atlas of Heart Disease and Stroke: The Future. Retrieved from: https://www.who.int/cardiovascular_diseases/en/cvd_atlas_25_future.pdf?ua=1

Wu, W., Allen, R. A., & Wang, Y. (2012). Fast-degrading elastomer enables rapid remodeling of a cell-free synthetic graft into a neoartery. *Nature medicine*, *18*(7), 1148-1153.

Wystrychowski, W., McAllister, T. N., Zagalski, K., Dusserre, N., Cierpka, L., & L'Heureux, N. (2014). First human use of an allogeneic tissue-engineered vascular graft for hemodialysis access. *Journal of vascular surgery*, *60*(5), 1353-1357.

Xie, J., MacEwan, M. R., Schwartz, A. G., & Xia, Y. (2010). Electrospun nanofibers for neural tissue engineering. *Nanoscale*, *2*(1), 35-44.

ATTACHMENTS

ATTACHMENTS A: Lumen structure

Determination of most suitable parameters was made to standardize luminal dimensional uniformity of vascular grafts using a rod covered with sacrificial alginate. The parameters evaluated were alginate concentration and rod upward-speed during the emersion from the pre-polymerized alginate solution.

8.1 Methodology

Four alginate concentration 1%, 2%, 2.5% and 3% (w/v) were prepared by dissolving medium viscosity sodium alginate (A2033, Sigma, USA) in PBS 1X under continuous stirring at 60°C, which gives a range of 73 ± 5 – 245 ± 15 cP in viscosity. For the crosslinking of alginate scaffold, $CaCl_2$ was dissolved in ddH_2O at a concentration of 5% (w/v) and maintained at 4°C. The sacrificial alginate scaffold was built after two subsequent dippings before polymerization. Four values of upward-speed were studied: 4.6 mm/s; 11.5 mm/s; 23 mm/s; 46 mm/s; 52 mm/s; 138 mm/s and 184 mm/s. The alginate scaffold was deposited in a 0.33 mm metal rod.

Luminal dimensional analysis was made from images of lumen structure. Diameter of lumen fabricated with each combination of parameters was measured with the Image J software. Seven measures were made at four sections of the lumen for 3 replicates. These are representative of the lumen and are classified as head, front, mid and tail.

8.2 Results

Figure A1 shows the lumen structure diameter fabricated with four different alginate concentrations and seven different upward-speeds. Structures fabricated with alginate concentrations below 2% (w/v) (165 ± 11 cP) at any upward-speed below 23 mm/s were highly irregular and not suitable for analysis. Visual inspection of these constructs indicates that while working under those parameters, the slight vibration of the CNC machine has a negative effect on the structural regularity inducing a rippled pattern. Structures fabricated with 2% (w/v) alginate, which has a viscosity of 165 ± 11 cP are the most uniform, characterized by similar diameter values among front, mid and tail sections, with no significant difference between those values at any speed. In addition,

lumen fabricated with 2% of alginate and 138 mm/s upward-speed present the most uniform structures.

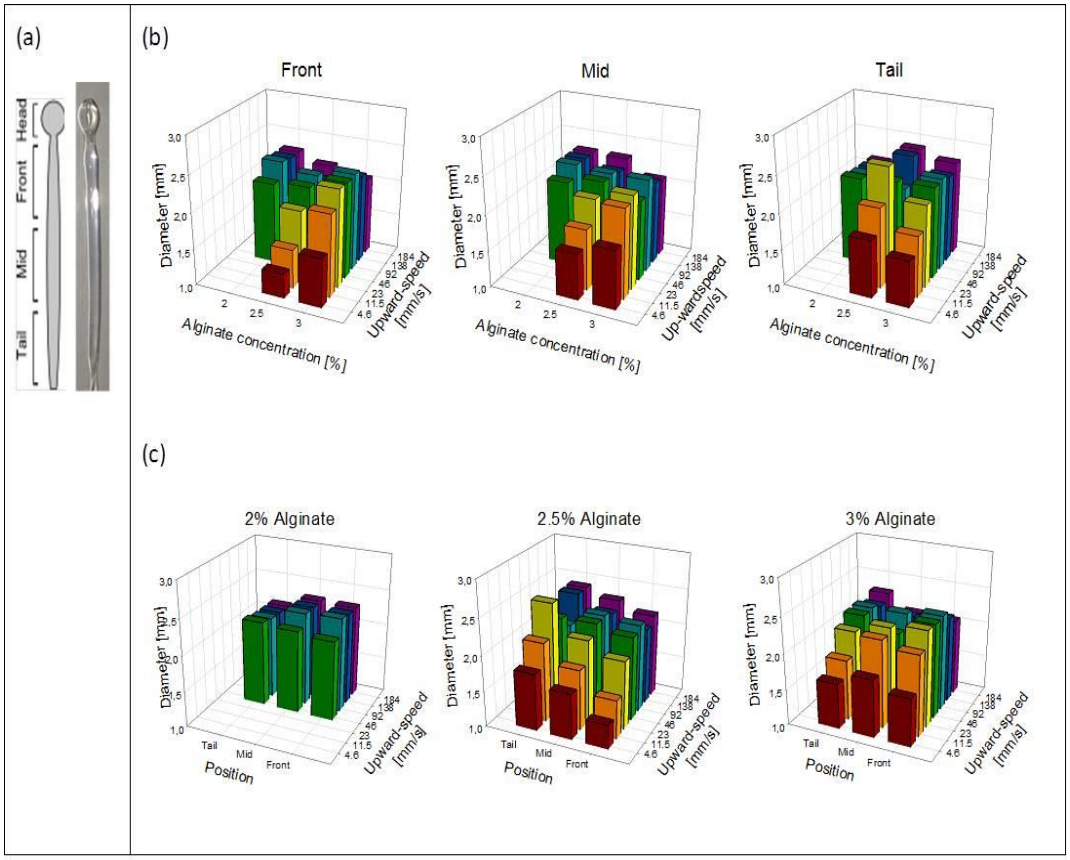

Figure A-1: Lumen structure diameter with respect to alginate concentration and upward-speed identifying its head, front, mid and tail. b) Lumen structures diameters, at front, mid and tail, constructed with four different alginate solutions and seven different upward-speeds. c) Lumen structures diameters at different concentrations of alginate. Representation focuses on comparisons of lumen or alginate mandrel dimensions at the different sections (front, mid and tail) (Wilkens et al., 2016).